Mechanical Behavior of Tough Hydrogels for Structural Applications

Mechanical Behavior of Tough Hydrogels for Structural Applications

A dissertation presented

by

Widusha Ruwangi Kaushalya Illeperuma

to

The School of Engineering and Applied Sciences

in partial fulfillment of the requirements

for the degree of

Doctor of Philosophy

in the subject of

Engineering Sciences

Harvard University

Cambridge, Massachusetts

April, 2015

Thesis Advisors
Zhigang Suo, Joost J. Vlassak

Author
Widusha Ruwangi Kaushalya Illeperuma

Mechanical Behavior of Tough Hydrogels for Structural Applications

Abstract

Hydrogels are widely used in many commercial products including Jell-O, contact lenses, and superabsorbent diapers. In recent decades, hydrogels have been under intense development for biomedical applications, such as scaffolds in tissue engineering, carriers for drug delivery, and valves in microfluidic systems. But the scope is severely limited as conventional hydrogels are weak and brittle and are not very stretchable. This thesis investigates the approaches that enhance the mechanical properties of hydrogels and their structural applications.

We discovered a class of exceptionally stretchable and tough hydrogels made from polymers that form networks via ionic and covalent crosslinks. Although such a hydrogel contains ~90% water, it can be stretched beyond 20 times its initial length, and has a fracture energy of ~9000 J/m^2. The combination of large stretchability, remarkable toughness, and recoverability of stiffness and toughness, along with easy synthesis makes this material much superior over existing hydrogels. Extreme stretchability and blunted crack tips of these hydrogels question the validity of traditional fracture testing methods. We re-examine a widely used pure shear test method to measure the fracture energy. With the experimental and simulation results, we conclude that the pure shear test method can be used to measure

fracture energy of extremely stretchable materials.

Even though polyacrylamide-alginate hydrogels have an extremely high toughness, it has a relatively low stiffness and strength. We improved the stiffness and strength by embedding fibers. Most hydrogels are brittle, allowing the fibers to cut through the hydrogel when the composite is loaded. But tough hydrogel composites do not fail by the fibers cutting the hydrogel; instead, it undergoes large deforming by fibers sliding through the matrix.

Hydrogels were not considered as materials for structural applications. But with enhanced mechanical properties, they have opened up novel applications. This thesis aims to investigate the broader applications, well beyond those investigated so far. We show fiber reinforced tough hydrogels can dissipate a significant amount of energy at a tunable level of stress, making them suitable for energy absorbing applications such as inner layer of helmets. We develop inexpensive fire-retarding materials using tough hydrogels that provide superior protection from burn injuries. We also study hydrogels as actuators that can be used in soft robotics. Hydrogels contain mostly water and they freeze when the temperature drops below $0^{o}C$ and lose its functions. We demonstrate a new class of hydrogels that do not freeze and hydrogels that partially freeze below water freezing temperature. Partially freezing hydrogels are ideal for cooling applications such as gel packs and non-freezing hydrogels are useful in all the structural applications at low temperatures.

This thesis will enable the use of inexpensive hydrogels in a new class of non-traditional structural applications where the mechanical behavior of the hydrogel is of prime importance.

Table of Contents

Acknowledgements

First and foremost, I would like to thank my advisors Prof. Zhigang Suo and Prof. Joost Vlassak for their extreme support throughout the years at Harvard. I'm very fortunate for having two advisors to guide me and enormously benefited from working with them. They both provided me tremendous advice on both research as well as on my career and guided me to become the researcher I am today.

Prof. Zhigang Suo is a remarkable teacher and a very enthusiastic and energetic mentor. It has been such a pleasure to listen to his lectures and conversations as he has an amazing ability of simplifying any difficult concept. His deep understanding of mechanics of materials has helped me to learn this field and make progress in my research. He has allowed me so much freedom in exploring different areas. I am constantly inspired by his creative way of thinking and motivation to explore new ideas.

I am fortunate to have been a student of Prof. Joost Vlassak. He has always been a very supportive and encouraging mentor. His vast knowledge in mechanics of materials and critical way of thinking has shaped up my research in many ways. He is very patient with all the details in my experiments and has suggested coolest experiments I can perform. His creativity and thoroughness in designing experiments has hugely benefited my research. With his guidance I have realized how joyful it is to conduct creative experiments.

I also want to thank my committee members Prof. Katia Bertoldi and Prof. Jennifer Lewis. Prof. Bertoldi is my mentor in Harvard Graduate Women in Sciences and Engineering (HGWISE) program. I have regularly discussed all my concerns and issues with her about

research, career and life and it has immensely benefited me. She is an expert in finite element analysis and I learned a lot from her class on the finite element method. I'm thankful to Prof. Lewis for accepting to serve in my committee despite her busy schedule. She is a remarkable scholar and an expert in the field of 3D printing and I have learned a lot by reading her papers.

I'm deeply grateful for Dr. Ravindra Herath, Dr. Shobha Herath and Prof. Munidasa Ranaweera of University of Peradeniya in Sri Lanka for encouraging me towards graduate studies in mechanics and materials. Their continuous advice gave me incredible impetus through out the years. I wish to bring my gratitude to Prof. Rohan Abeyaratne at Massachusetts Institute of Technology for encouraging and supporting me to apply for graduate studies in USA universities.

It was an incredible privilege to be a part of both Suo and Vlassak groups. I am deeply grateful to Prof Jeong-Yun Sun who was a visiting student and postdoc, for mentoring and collaborating with me during my first few years in graduate school. Working with him has motivated me to become an experimentalist. I also want to thank Jianyu Li for all the discussions and collaborations we had and sharing similar thesis topics.

It was joyful to work with all the members in Suo and Vlassak groups. I would like to thank all of them and especially Prof. Yuhang hu, Prof. Shengqiang Cai, Prof. Kejie Zhao, Dr.Matt Pharr, Dr. Lihua Jin, Qihan Liu, Philipp Rothemund, Chao Chen, Ruobing Bai, Yechen Wang, Jiawei Yang, Zhengjin Wang, Jingda Tang, Dr. Gidong Sim, Dongwoo Lee, Dr. Gayatri Cuddelorepatta, Mingyu Li, Kechao Xiao, Dr. Kamyar Devoudi and Kevin Tian. I thank them for all the discussions and suggestions we had throughout these years.

I also want to extend my gratitude to my good friends Gongjie Li, Tori Steinmeier, Teja Reddi, Hyungsuk Tak, Hiro Yoshie, Chathurika Abeyratna, Prabha Pathirana and Sewwandi Wijeratna for all the support and encouragement. I want to express my gratitude to Strod family for been there as my host family and making Boston feel like home. I would bring my deepest gratitude to my parents, my sister, brother-in-law and my relatives for their unconditional love, support and encouragement for make this journey fruitful for me. This thesis is dedicated to my beloved father and mother. It is your shining examples that I try to emulate in all that I do. Thank you for everything.

Chapter 1

Introduction

Engineering structures are made with hard materials such as metal, concrete, glass and ceramic. In contrast soft materials are the major components of natural systems including humans, animals and plants [1,2]. Natural tissues such as cartilage, spinal disc, tendons and ligaments are all soft materials. They contain mostly water but they are tough and strong and can protect the human body from all the impacts in life. There is a long driven search to develop soft and wet materials to match with the mechanical properties of natural tissues [3, 4]. Researchers believe hydrogels are the closest materials to natural tissues.

Hydrogels are aggregations of hydrophilic polymer networks and water. Typical hydrogels contain more than 90% water and less that 10% polymer network by weight. Hydrogels have two salient attributes: the polymer network enables elasticity, making the hydrogels solid-like; and the permeating water enables mass transport, making the hydrogels liquid-like. Hydrogels differ from conventional solids in their mechanical properties and their response to external stimuli [4]. Hydrogels can change the volume dramatically by absorbing or releasing water, which can result in changes of properties. Even though conventional hydrogels are soft and wet similar to natural tissues, they are weak and brittle and exhibit much poor mechanical properties compared to natural tissues.

Hydrogels are widely used in many commercial products such as Jell-O, contact lenses, superabsorbent diapers, medical creams, cosmetics, gel packs and so on. Many of these applications do not require hydrogels for bearing a significant load. But some commercial

applications of hydrogels are limited by the poor strength and toughness of hydrogels. The durability of contact lenses, for instance, is limited by the low toughness of the hydrogel used to make them [5]. In recent decades, hydrogels have been under intense development for biomedical applications, such as scaffolds in tissue engineering [6], carriers for drug delivery [7], and extracellular matrices for biological studies [8]. Hydrogels are also studied as valves in microfluidic systems [9] sensors and actuators [10], antifouling gel coatings [11] and packers in oilfields [12]. The scope of applications, however, is often severely limited by the mechanical behavior of hydrogels [3, 4].

1.1 Motivation of the thesis

Most existing hydrogels are weak, brittle, and not very stretchable. Thus hydrogels are not considered as materials for load bearing structural applications [4]. Hydrogels with enhanced mechanical properties not only improve the scope of the developing applications but also will lead to novel and large-scale applications that researchers have not investigated so far. This thesis investigates scientific issues that arise in the development of stretchable, tough and strong hydrogels. Large-scale use of hydrogels is attractive for a number of reasons. Many kinds of polymers can form hydrogels; this diversity enables suitable polymers to be selected to achieve specific functions. Hydrogels consist mostly of water; many hydrogels are inexpensive and environmentally friendly. Hydrogels based on alginates are a case in point. Alginates are extracted from seaweeds (e.g. rockweed and giant kelp) that are naturally abundant in the oceans throughout the world. The annual production of alginates is estimated to be less than 10% of that available in the algae crops [13]. The

sources of alginates are regarded as unlimited even for a steadily growing industry: it is conceivable that algae will be cultivated if large-scale applications emerge. Although the cost of hydrogels is low, examples of massive use of hydrogels are few. A notable exception is their use in superabsorbent disposable diapers [14]. The main obstacle to widespread use of hydrogels is the poor mechanical properties.

Most existing hydrogels are soft and brittle, with strength on the order of 10 kPa, and fracture energy on the order of 10 Jm^{-2} [4, 15]. This value of fracture energy is compared with the values for several other materials. For instance, the fracture energy is on the order of 10 Jm^{-2} for tofu and Jell-O, 100 Jm^{-2} for contact lenses, 1000 Jm^{-2} for cartilage, and 10,000 Jm^{-2} for natural rubber. In the recent decade, several strategies have emerged to synthesize tough hydrogels, including double network hydrogels [16], nano- and micro-composite hydrogels [17,18], tri-block copolymers and hydrophobic associated hydrogels [19,20]. The double network hydrogel, perhaps the best-known tough gel emerged in the last decade, has a fracture energy of 100-1000J m^{-2} [16]. Hydrogels of much improved mechanical behavior have raised the hope that they might substitute traditional soft materials such as natural rubber in some existing applications. Here we investigate possible structural applications where mechanical behavior is critical.

1.2 Outline of the thesis

The goal of this thesis is to discover, understand and exploit hydrogels with superior mechanical properties for non-traditional structural applications. The thesis is organized as follows. Chapter 2 investigates a new class of exceptionally stretchable and tough hydrogels

made from polymers that form networks via ionic and covalent crosslinks [21]. Although such a hydrogel contains ~90% water, it can be stretched beyond 20 times its initial length and has a fracture energy of ~9000J/m^2. Extreme stretchability and blunted crack tips of these hydrogels question the validity of traditional fracture testing methods. In chapter 3 we propose to use the classical pure shear test method to measure fracture toughness [22]. Both experimental and simulation results show that pure shear test method can still be used for extremely stretchable materials beyond the pure shear test conditions.

Whereas the stretchability and fracture energy of the polyacrylamide-alginate hydrogels are exceptional, its stiffness and strength are modest. Chapter 4 explores fiber-reinforced hydrogel composites with improved stiffness and strength [23]. Development of tough, strong and stretchable hydrogels has allowed us to investigate novel structural applications for hydrogels. Fiber reinforced hydrogels are ideal for absorbing energy and can be used as inner layers of helmets to avoid head injuries as shown in chapter 4. Chapter 5 investigates hydrogels as fire-retarding materials [24]. Tough hydrogels contain mostly water and can absorb a large amount of heat from a fire. By combining with a low thermal conductive fabric, we prepare laminates that can save peoples lives from burn injuries. Chapter 6 characterizes the force-stroke behavior for hydrogel actuators using ideal elastomeric gel theory and with experiments [25]. In chapter 7 we develop a new class of hydrogels that partially freeze and hydrogels that do not freeze. Partially frozen hydrogels are ideal for cooling applications. Non-freezing hydrogels are suitable for all the above-mentioned applications.

Chapter 2

Highly stretchable and tough hydrogels

2.1 Introduction

Most hydrogels do not exhibit high stretchability and toughness. For example, an alginate hydrogel ruptures when stretched to about 1.2 times its original length. Some synthetic elastic hydrogels [26, 27] have achieved stretches in the range of 10-20, but elastic gels are known to reduce achievable stretches markedly when samples contain notches. Most hydrogels are brittle, having fracture energy on the order of 10 J/m^2 [28]. By comparison, the fracture energy is ~1000 J/m^2 for cartilage [29] and ~10,000 J/m^2 for natural rubbers [30]. Intense efforts are devoted to synthesizing hydrogels of enhanced mechanical properties [16-20, 31-36]; certain synthetic hydrogels have reached fracture energy in the range 100-1000 J/m^2 [16,32,35]. Despite the exciting achievements, much of the property space of hydrogels remains uncharted.

Here we report extremely stretchable and tough hydrogels made of polymers forming networks via ionic and covalent crosslinks. Although such a gel contains ~ 90% water, it can be stretched beyond 20 times its initial length, and has fracture energy of ~9000 J/m^2. Even for samples containing notches, a stretch of 17 is demonstrated. The extremely high fracture energy is attributed to the synergy of two toughening mechanisms: crack bringing by the network of covalent crosslinks, and hysteresis by unzipping the network of ionic crosslinks over a large region of the gel. Furthermore, the network of covalent crosslinks preserves the memory of the initial state, so that much of the large deformation is removed when the load is removed. The unzipped ionic crosslinks cause internal damage, which heals as ionic

crosslinks re-zip. We envision that these hydrogels will serve as model systems to explore mechanisms of deformation and energy dissipation, and that hydrogels with enhanced mechanical properties will considerably expand the scope of their applications.

2.2 Hydrogels with improved mechanical properties

Certain synthetic hydrogels have achieved exceptional mechanical behavior. A hydrogel containing slide-ring polymers can be stretched more than 10 times its initial length [26]; a tetra-poly (ethylene glycol) gel exhibits strength of ~2.6 MPa [27]. These gels deform elastically. An elastic gel is known to be brittle and notch-sensitive—that is, the high stretchability and strength drop markedly when samples contain notches, or any other features that cause inhomogeneous deformation [37]. A gel can be made tough and notch-insensitive by introducing energy-dissipating mechanisms. For example, fracture energy of ~1000 J/m^2 is achieved with a double-network gel, in which two networks are separately crosslinked by covalent bonds, one network having short chains, and the other having long chains [16]. When the gel is stretched, the short-chain network ruptures and dissipates energy [38]. The rupture of the short-chain network, however, causes permanent damage. After the first loading the gel does not recover from the damage; on subsequent loadings the fracture energy is much reduced [39]. To enable recoverable energy-dissipating mechanisms, several recent works have replaced the sacrificial covalent bonds with noncovalent bonds. In a gel with a copolymer of triblock chains, for example, the end blocks of different chains form glassy domains, and the midblocks of different chains form ionic crosslinks [40]. When the gel is stretched, the glassy domains remain intact, while the ionic crosslinks break and

dissipate energy. The ionic crosslinks reform during a period of time after the first loading [40]. Recoverable energy dissipation can also be effected by hydrophobic associations [35, 36]. When a gel made with hydrophobic bilayers in a hydrophilic polymer network is stretched, the bilayers dissociate and dissipate energy; upon unloading, the bilayers re-assemble, leading to recovery [35]. The existing works, however, have demonstrated fracture energy comparable to, or lower than, that of the double-network gels.

2.3 Extremely stretchable and tough polyacrylamide-alginate hydrogels

Here we demonstrate extremely stretchable and tough hydrogels by mixing two types of crosslinked polymers: ionically crosslinked alginate and covalently crosslinked polyacrylamide (Figure 2.1). An alginate chain consists of mannuronic acid (M unit) and guluronic acid (G unit), arranged in blocks rich in G units, blocks rich in M units, and blocks of alternating G and M units. In an aqueous solution, the G blocks on different alginate chains form ionic crosslinks through divalent cations (e.g., Ca^{2+}), resulting in a network in water—an alginate hydrogel. By contrast, in a polyacrylamide hydrogel, the polyacrylamide chains form a network by covalent crosslinks.

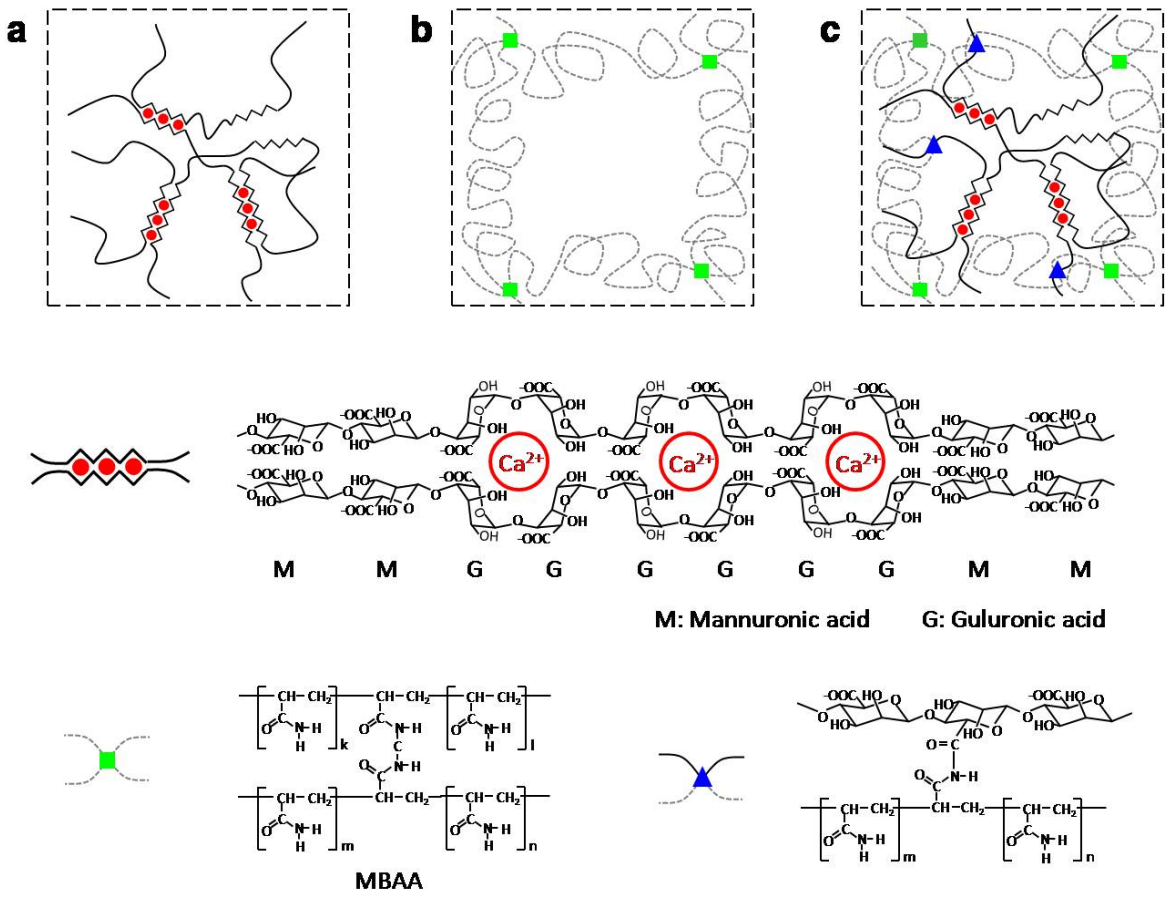

Figure 2.1 Schematics of three types of hydrogels. (a) In an alginate gel, the G blocks on different polymer chains form ionic crosslinks through Ca^{2+}. (b) In a polyacrylamide gel, the polymer chains form covalent crosslinks through MBAA. (c) In an alginate-polyacrylamide hybrid gel, the two types of polymer networks are intertwined.

2.4 Experimental procedure

Powders of alginate (FMC Biopolymer, LF 20/40) and acrylamide (Sigma, A8887) were dissolved in deionized water. Unless otherwise stated, the water content was fixed at 86 wt%. Ammonium persulfate (AP; Sigma, A9164) was added as a photo initiator for polyacrylamide, and N,N-methylenebisacrylamide (MBAA; Sigma, M7279) was added as the crosslinker for polyacrylamide. After degassing the solution in a vacuum chamber, N,N,N',N'-

tetramethylethylenediamine (TEMED; Sigma, T7024), 0.0025 the weight of acrylamide, was added as the crosslinking accelerator for polyacrylamide. Calcium sulfate slurry ($CaSO_4 \cdot 2H_2O$; Sigma, 31221) was added as the ionic crosslinker for alginate. The solution was poured into a glass mold, 75.0 x 150.0 x 3.0 mm^3, covered with a 3-mm thick glass plate. The gel was cured in one step with ultraviolet light (Hoefer, UVC 500) for 1 hour, with 8 W power and 254 nm wavelength at 50 °C. The gel was then left in a humid box for 1 day to stabilize the reactions. After curing, the gel was taken out of the humid box, and water on the surfaces of the gel was removed with N_2 gas for 1 minute.

The gel was glued to two clamps made of polystyrene, resulting in specimens of 75.0 x 5.0 x 3.0 mm^3. All mechanical tests were performed in air, at room temperature, using a tensile machine (Instron model 3342) with a 500-N load cell. In both loading and unloading, the rate of stretch was kept constant at 2 per minute. We stretched an alginate-polyacrylamide hybrid gel over 20 times its original length without rupture (Figure 2.2 (a),(b)). The hybrid gel was also extremely notch-insensitive. When we cut a notch into the gel (Figure 2.2(c)) and then pulled the gel to a stretch of 17, the notch was dramatically blunted and remained stable (Figure 2.2(d)). At a critical applied stretch, a crack initiated at the root of the notch, and ran rapidly through the entire sample.

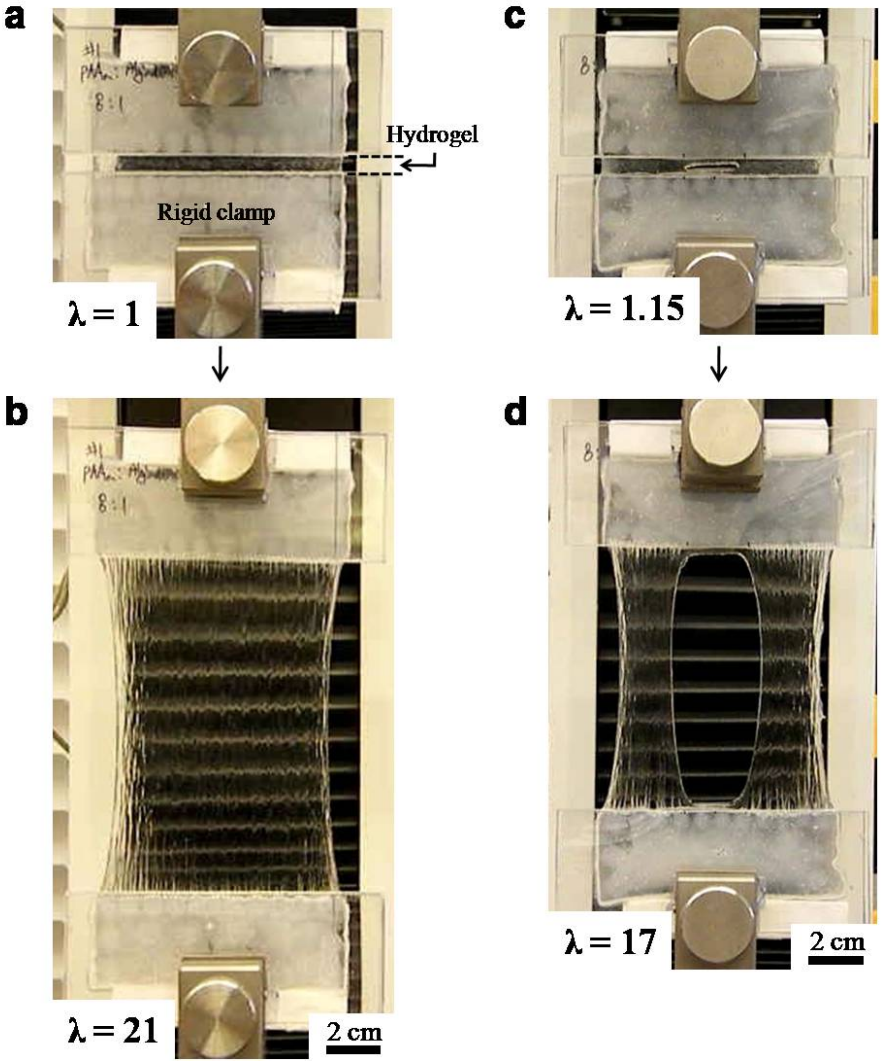

Figure 2.2 The hybrid gel is highly stretchable and notch-insensitive. (a) A strip of the undeformed gel was glued to two rigid clamps. (b) The gel was stretched 21 times its initial length. The stretch λ is defined by the distance between the two clamps when the gel is deformed divided by the distance when the gel is undeformed. (c) A notch was cut into the gel by using a razor blade; a small stretch of 1.15 was used to make the notch clearly visible. (d) The gel containing the notch was stretched 17 times its initial length. The alginate-to-acrylamide ratio was 1:8. The covalent crosslinker, MBAA, was fixed at 0.0006 the weight of acrylamide. The ionic crosslinker, $CaSO_4$, was fixed at 0.1328 the weight of alginate.

2.5 Mechanical tests of polyacrylamide-alginate hydrogels

The extremely stretchable hybrid gels are even more remarkable when compared with their parents: the alginate gel and the polyacrylamide gel (Figure 2.3(a)). The amounts of alginate and acrylamide in the hybrid gels were kept the same as those in the alginate gel and polyacrylamide gel, respectively. When the stretch was small, the elastic modulus of the hybrid gel was 29 kPa, which was close to the sum of the elastic modulus of the alginate gel (17kPa) and that of the polyacrylamide gel (8kPa). The stress and the stretch at rupture were, respectively, 156 kPa and 23 for the hybrid gel, 3.7 kPa and 1.2 for the alginate gel, and 11 kPa and 6.6 for the polyacrylamide gel. That is, the properties at rupture of the hybrid gel far exceeded those of either of its parents.

Hybrid gels dissipate energy effectively, as shown by pronounced hysteresis. The area between the loading and unloading curves of a gel gave the energy dissipated per unit volume (Figure 2.3(b)). The alginate gel exhibited pronounced hysteresis and retained significant permanent deformation after unloading. In contrast, the polyacrylamide gel showed negligible hysteresis, and the sample fully recovered its original length after unloading. The hybrid gel also showed pronounced hysteresis, but the permanent deformation after unloading was significantly smaller than that of the alginate gel. The pronounced hysteresis and relatively small permanent deformation of the hybrid gel were further demonstrated by loading several samples to large values of stretch before unloading (Figure 2.3(c)).

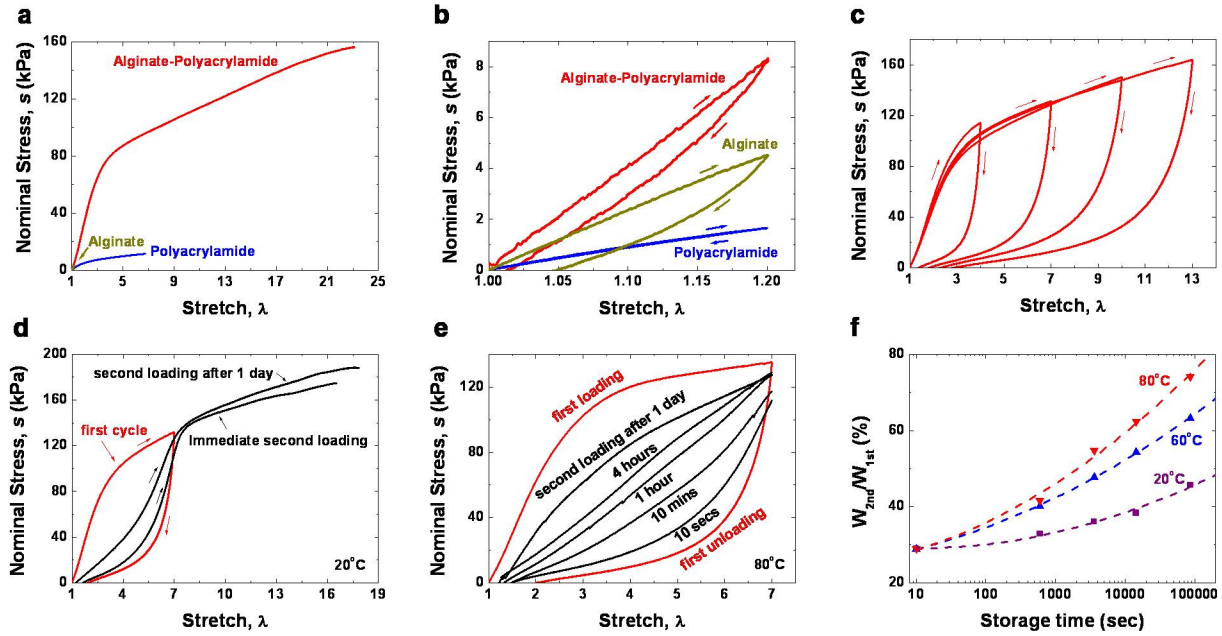

Figure 2.3 Mechanical tests under various conditions. (a) Stress-stretch curves of the three types of gels, each stretched to rupture. The nominal stress s is defined by the force applied on the deformed gel divided by the cross-sectional area of the undeformed gel. (b) The gels were each loaded to a stretch of 1.2, just below the value that would rupture the alginate gel, and were then unloaded. (c) Samples of the hybrid gel were subject to a cycle of loading and unloading of varying maximum stretch. (d) After the first loading and unloading, one sample was reloaded immediately, and the other sample was reloaded after 1 day. (e) Recovery of samples stored at 80°C for different durations of time. (f) The work of the second loading W_{2nd} normalized by that of the first loading W_{1st} was measured for samples stored for different periods of time at different temperatures. The alginate-to-acrylamide ratio was 1:8 for a and b, and was 1:6 for c-f. The covalent crosslinker, MBAA, was fixed at 0.0006 the weight of acrylamide for polyacrylamide gel and hybrid gel. The ionic crosslinker, $CaSO_4$, was fixed at 0.1328 the weight of alginate for alginate gel and hybrid gel.

After the first loading and unloading, the hybrid gel was much weaker if the second loading was applied immediately, and recovered somewhat if the second loading was applied 1 day later (Figure 2.3(d)). We loaded a sample of the hybrid gel to a stretch of 7, and then

unloaded the gel to zero force. The sample was then sealed in a polyethylene bag and submerged in mineral oil to prevent water from evaporation, and stored in a bath of a fixed temperature for a certain period of time. The sample was taken out of the storage and its stress-stretch curve was measured again at room temperature. The internal damage was much better healed by storing the gel at an elevated temperature for some time before reloading (Figure 2.3(e)). After storing at 80 °C for 1 day, the work on reloading was recovered to 74 % of that of the first loading (Figure 2.3(f)).

2.6 Effect of polymer ratio on the mechanical behavior

Gels of various proportions of alginate and acrylamide were prepared to study why the hybrids were much more stretchable and stronger than either of their parents. When the proportion of acrylamide was increased, the elastic modulus of the hybrid gel was reduced (Figure 2.4(a)). However, the critical stretch at rupture reached the maximum when acrylamide was 89 wt.-%. A similar trend was observed for samples with notches (Figure 2.4(c)). The fracture energy reached a maximum value of 8700 J/m^2 when acrylamide was 86 wt.-% (Figure 2.4(d)). The densities of ionic and covalent crosslinks also strongly affect the mechanical behavior of the hybrid gels as well as that of pure alginate gels and pure polyacrylamide gels.

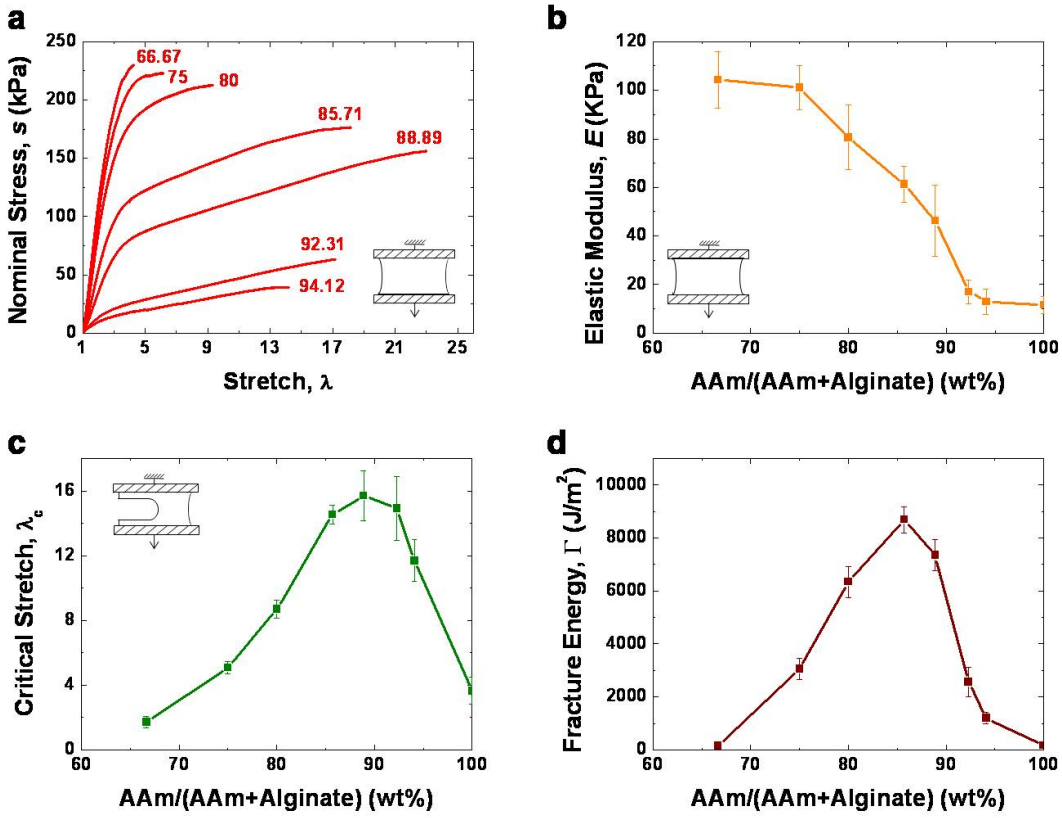

Figure 2.4 The composition greatly affects the behavior of the hybrid gel. (a) Stress-strain curves of gels of various weight ratios of acrylamide and alginate. Each test was conducted by pulling an unnotched sample to rupture. (b) Elastic moduli were calculated from stress-strain curves. (c) Notched gels of various acrylamide-to-alginate ratios were pulled to rupture to measure the critical stretches. (d) Fracture energy was plotted as a function of the acrylamide-to-alginate ratio. The covalent crosslinker, MBAA, was fixed at 0.0006 the weight of acrylamide. The ionic crosslinker, $CaSO_4$, was fixed at 0.1328 the weight of alginate. (Error bars, S.D.; n=4)

2.7 Energy dissipation mechanism

On the basis of our experimental findings, we discuss mechanisms of deformation and energy dissipation. When an unnotched hybrid gel is subject to a small stretch, the elastic modulus of the hybrid gel is nearly the sum of that of the alginate gel and that of the polyacrylamide gel. Thus, in the hybrid gel the alginate and the polyacrylamide chains both

bear loads. The load sharing of the two networks may be achieved by entanglements of the polymers, and by possible covalent crosslinks formed between the amine groups on polyacrylamide chains and the carboxyl groups on alginate chains [21]. As the stretch increases, the alginate network unzips progressively [41], while the polyacrylamide network remains intact, so that the hybrid gel exhibits pronounced hysteresis and little permanent deformation. Since only the ionic crosslinks are broken, and the alginate chains themselves remain intact, the ionic crosslinks can reform, leading to the healing of the internal damage. The giant fracture energy of the hybrid gel is remarkable, considering that its parents—the alginate gel and polyacrylamide gel—have fracture energies in the range of 10-250 J/m^2 [21].

The relatively low fracture energy of a hydrogel of a single network with covalent crosslinks is understood in terms of the Lake-Thomas model [28]. When the gel contains a notch and is stretched, the deformation is inhomogeneous: the network directly ahead the notch is stretched more than elsewhere (Figure 2.5 (a)). For the notch to turn into a running crack, only the chains directly ahead the notch needs to break. Once a chain breaks, the energy stored in the entire chain is dissipated. In the ionically crosslinked alginate, fracture proceeds by unzipping ionic crosslinks and pulling out chains [42]. After one pair of G blocks unzip, the high stress shifts to the neighboring pair of G blocks and causes them to unzip also (Figure 2.5 (b)). For the notch in the alginate gel to turn into a running crack, only the alginate chains crossing the crack plane need to unzip, leaving the network elsewhere intact. In both polyacrylamide gel and alginate gel, rupture results from localized damage, leading to small fracture energies.

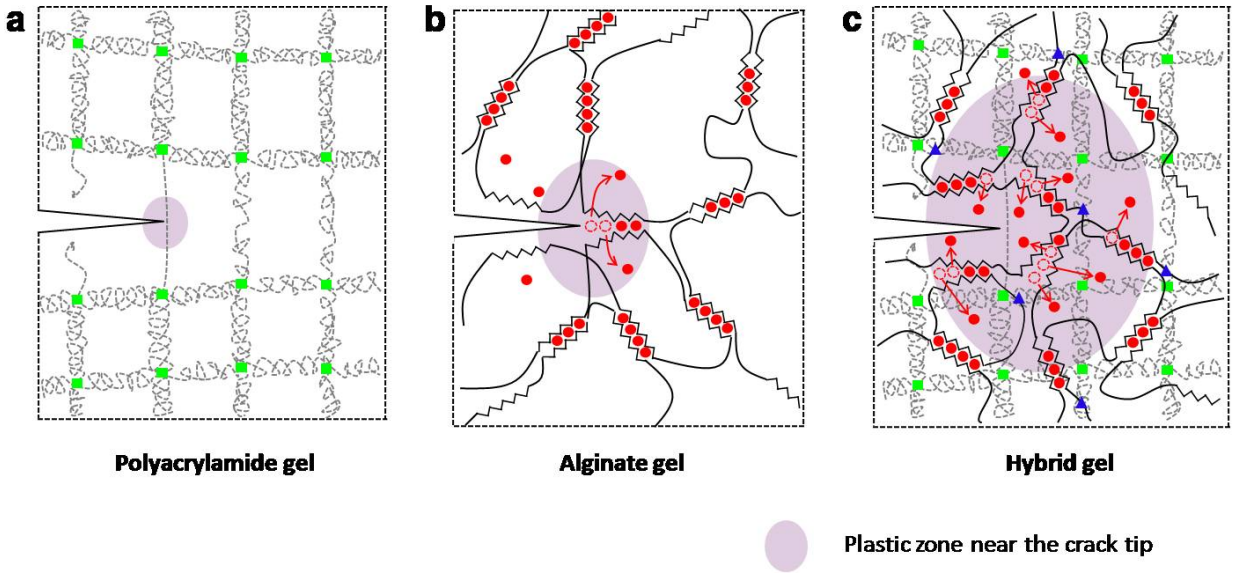

Figure 2.5 Synergy between alginate and polyacrylamide. (a) In the polyacrylamide gel, for the notch to turn into a running crack, only the polyacrylamide chains crossing the crack plane need to break, and chains elsewhere remain intact. (b) In the alginate gel, for the notch to turn into a running crack, only the ionic crosslinks for the chains crossing the crack need to break, and ionic crosslinks elsewhere remain intact. (c) In the hybrid gel, the polyacrylamide chains bridge the crack and stabilize deformation in the background, the chemical interactions between the networks transfer the load over a large zone, and the ionic crosslinks between alginate chains break and provide inelastic deformation over this large zone around the root of the notch.

That a tough material can be made of brittle constituents is reminiscent of transformation-toughening ceramics and composites made of ceramic fibers and ceramic matrices. The toughness of the hybrid gel can be understood by adapting a model well studied for toughened ceramics [43], as well as for gels of double networks of covalent crosslinks [44, 45]. When a notched hybrid gel is stretched, the polyacrylamide network bridges the crack and stabilizes deformation, enabling the alginate network to unzip over a large region of the gel (Figure 2.5(c)). The unzipping of the alginate network, in its turn,

reduces the stress concentration of the polyacrylamide network ahead the notch. The model highlights the synergy of the two toughening mechanisms: crack bridging and background hysteresis.

The idea that gels can be toughened by mixing weak and strong bonds has been exploited in several ways, including hydrophobic associations [36], particle filled gels [27,33] and supramolecular chemistry [35,40]. The fracture energy of the alginate-polyacrylamide hybrid gel, however, is much larger than previously reported values of tough synthetic gels (100-1000 J/m^2) [32,35,38,46], a finding which we attribute to how the alginate network unzips. Each alginate chain contains a large number of G blocks, many of which form ionic crosslinks with G blocks on other chains when enough Ca^{++} ions are present [6]. When the hybrid gel is stretched, the polyacrylamide network remains intact and stabilizes the deformation, while the alginate network unzips progressively, with closely spaced ionic crosslinks unzipping at a small stretch, followed by more and more widely spaced ionic crosslinks unzipping as the stretch increases.

2.8 Summary

Our data suggest that the fracture energy of hydrogels can be dramatically enhanced by combining weak and strong crosslinks. The combination of relatively high stiffness, high toughness and recoverability of stiffness and toughness along with an easy method of synthesis, make these materials an ideal candidate for further investigation. Further development is needed to relate macroscopically observed mechanical behavior to microscopic parameters. The diversity of weak and strong molecular integrations makes

hybrid gels of various kinds a fertile area of research. In many applications, such as tissue engineering, cell encapsulation, contact lenses and actuators, the use of hydrogels is often severely limited by their mechanical properties. For example, the poor mechanical stability of hydrogels used for cell encapsulation often leads to unintended cell release and death [47], and low toughness limits the durability of contact lenses [5]. Hydrogels of superior stiffness, toughness, stretchability and recoverability will improve the performance in these applications, and likely open up new areas of application for this class of materials.

Chapter 3

A method to measure fracture toughness of extremely stretchable hydrogels

3.1 Introduction

Fracture of hydrogels has become an interesting research area in recent years [48-52]. Conventional hydrogels are weak, brittle and fracture easily. Along with recent innovations in synthetic chemistry, hydrogels with enhanced mechanical properties are developed [16-20, 31-36]. These hydrogels have high mechanical properties compared to conventional hydrogels.

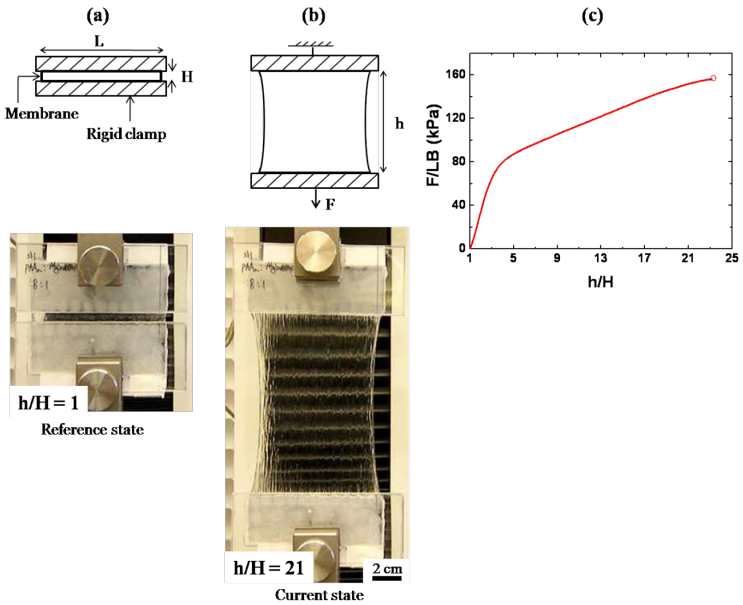

Figure 3.1 (a) Reference state of polyacrylamide-alginate hydrogel with sample length H, sample width L and sample thickness B, attached to two rigid clamps. Schematic of the reference state is shown at the top and the experimental figure is shown at the bottom. For this case, H=5mm, L=75mm, B=3mm and stretch rate=2/min. (b) Current state of the polyacrylamide-alginate hydrogel with an extremely large stretch of 21. (c) The corresponding stress-stretch curve of the tensile test, the circle denotes the rupture of the specimen.

We have recently discovered polyacrylamide-alginate hydrogel [21], which is an extremely stretchable material, as illustrated in figure 3.1.

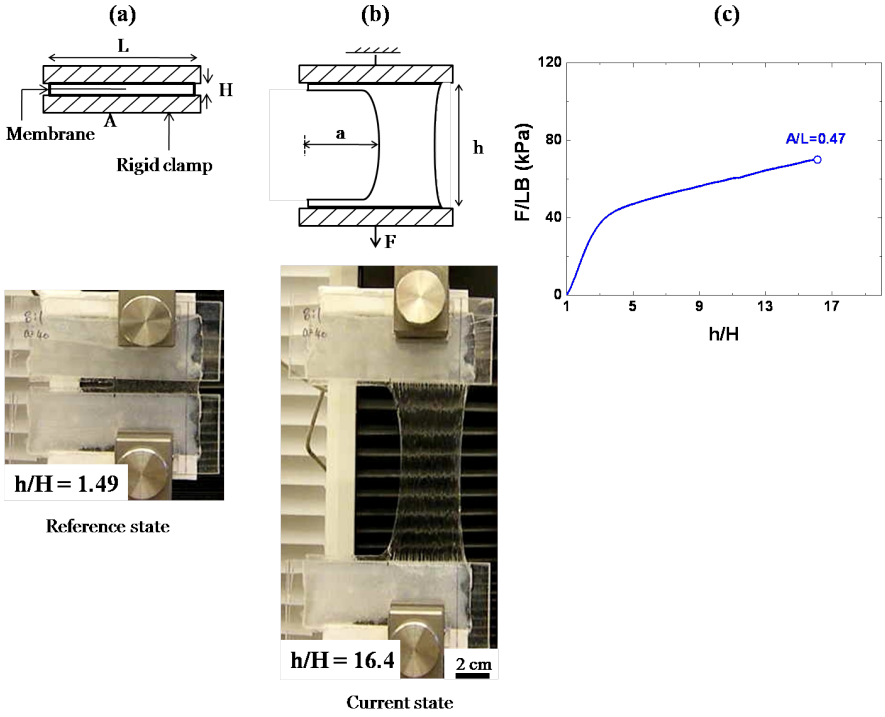

Figure 3.2 (a) Reference state of polyacrylamide-alginate hydrogel with a pre crack of length *A*. Schematic of the reference state is shown at the top and the experimental figure is shown at the bottom. For this case, *H*=5mm, *L*=75mm, *B*=3mm, *A*=35mm and stretch rate=2/min. (b) Current state with a stretch of 16.4 at the onset of crack propagation. (c) The corresponding stress-stretch curve of the fracture test, the circle denotes the onset of crack propagation.

However very stretchable materials can be brittle when there is a pre crack and the cut can significantly reduce the amount of stretchability. But it is observed that when a pre crack is made and deformed, polyacrylamide-alginate hydrogel has a much-blunted crack and the stretchability is still very high at the onset of crack propagation as shown in figure 3.2.

The fracture energy plays an important role in understanding the nature of fracture in hydrogels. However the large deformation makes it difficult to apply the techniques

developed to measure fracture energy of materials with small deformation. Therefore, classical fracture testing methods need to be re-addressed by considering large deformation to measure the fracture energies of hydrogels.

Various fracture-testing methods are available in the literature such as peeling test [22], pure shear test [22], trouser test [49], cavitation test [51], scissor cutting [53] and wedge cutting [54]. All these methods have their own advantages and disadvantages, but we chose "pure shear test" introduced by Rivlin & Thomas because of its simplicity of analysis [22]. According to Rivlin and Thomas, the pure shear test is valid only when the sample width and crack length are much larger than the sample length. However the huge blunted crack tip of polyacrylamide-alginate hydrogel can easily violate the pure shear test criteria. We have examined whether the pure shear method still works when the material is extremely stretchable and flaw insensitive. The validity of the test was confirmed with two other experimental methods (tensile test with various crack lengths and double peeling test) and finite element analysis. The geometry and size effects of the sample on fracture energy were studied by varying the crack length, sample length and sample thickness.

3.2 Pure shear test

Pure shear test is widely used because of its simplicity. When the width of the sample (L) and the crack length (A) are much larger than the specimen length (H) and when the sample is deformed parallel to H, the specimen can be divided into four regions as shown in figure 3.3.

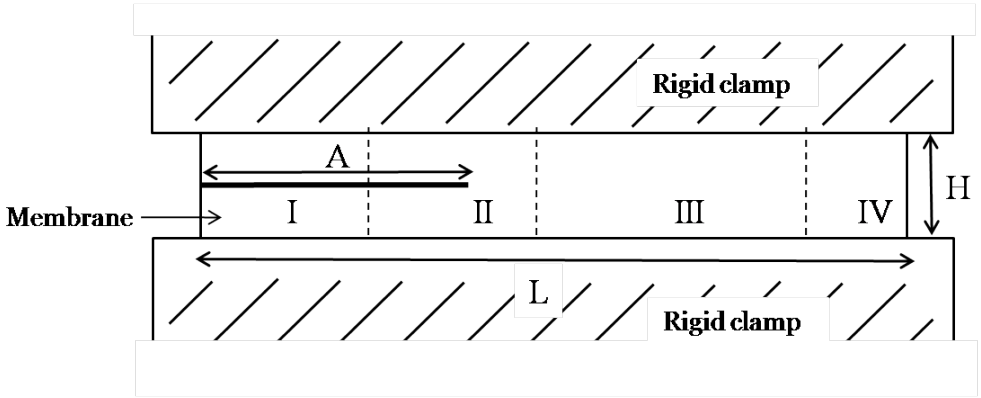

Figure 3.3 Pure shear tear test piece. Sample length is denoted as *L*, height as *H* and crack length as *A*. Test sample is clamped with two rigid clamps. Four regions of the sample are identified.

Region I is in undeformed state, region III is in the state of pure shear, and region II is in a complicated state of strain due to the crack tip. Further, a slight departure from pure shear takes place close to the force-free edge of the region IV. An increase in crack length *dA*, does not change the state of strain in region II but shifts the region along the direction of crack allowing region I to grow at the expense of region III which has a uniform strain energy density, $W(\lambda_c)$ where λ_c is the critical stretch for crack propagation. Thus an increase in crack length (dA) releases energy (dU) of $W(\lambda_c).H.B.dA$, where *H* is the sample length between the clamps and *B* is the sample thickness.

Thus,

$$\left(\frac{\partial U}{\partial A}\right)_h = W\left(\lambda_c\right).H \tag{3.1}$$

The suffix *h* denotes that the differentiation carried out at a constant displacement.

An analytical solution to find the fracture toughness of an elastomer, which is in the pure shear state, is given as follows [22].

For a sheet of elastomer of thickness *B*, work done to extend the crack by amount *dA*,

$$dU = \Gamma B dA \tag{3.2}$$

where Γ is the fracture energy of the elastomer.

When there is no work done by the external forces, change in free energy of deformation of sheet becomes,

$$\left(\frac{\partial U}{\partial A}\right)_h = \Gamma B \tag{3.3}$$

When λ_c is known, considering equations (1) and (3), the fracture toughness for crack initiation (Γ) can be given by,

$$\Gamma = W(\lambda_c).H \tag{3.4}$$

3.3 Experimental

3.3.1 Sample Preparation

Alginate (FMC Biopolymer, LF 20/40) and acrylamide (Sigma, A8887) powders were dissolved in deionized water. The weight of water over the total weight of water, alginate and acrylamide was fixed as 86 % and the weight of acrylamide to alginate was used as 8:1 ratio. N,N-methylenebisacrylamide (MBAA; Sigma, M7279), 0.0006 the weight of acrylamide, was added as the crosslinker for polyacrylamide. Ammonium persulfate (AP; Sigma, A9164), 0.0017 the weight of acrylamide, was added as a photo initiator for polyacrylamide. After degassing the solution in a vacuum chamber, N,N,N',N'-tetramethylethylenediamine (TEMED; Sigma, T7024), 0.0025 the weight of acrylamide, was added as the crosslinking accelerator for polyacrylamide. Calcium sulfate slurry ($CaSO_4 \cdot 2H_2O$; Sigma, 31221), 0.1328 the weight of alginate, was added as the ionic crosslinker for alginate. The solution was

poured into a glass mold, 75.0 x 150.0 x 3.0 mm^3, covered with a 3-mm thick glass plate. The gel was cured in one step, with ultraviolet light (Hoefer, UVC 500) for 1 hour, with 8 W power and 254 nm wavelength. The gel was then left in a humid box over night to complete the reaction.

3.3.2 Fracture test

In order to obtain the fracture toughness, two specimens, one for tensile test and the other for fracture test, were prepared with same dimensions, sample length (H) of 75mm, sample width (L) of 5mm and thickness (B) of 3mm a shown in figure 3.4.

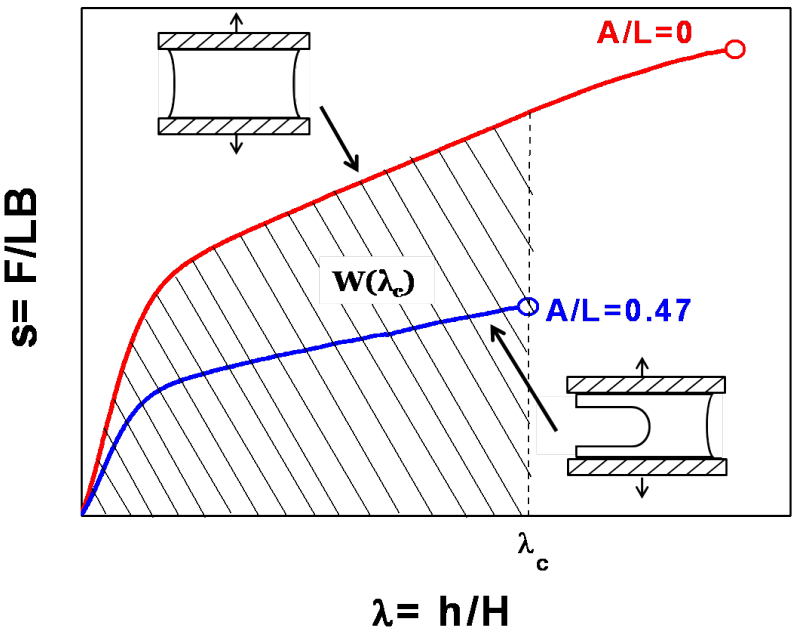

Figure 3.4 The stress-stretch curves for tensile test (red) and fracture test (blue). The fracture sample has A/L=0.47 initial notch. The circle in the blue curve represents onset crack propagation with stretch λ_c and the circle in the red curve shows the rupture of the sample. The energy release per unit volume (W) is calculated by integrating the area under the tensile test graph up to the critical stretch (λ_c).

The tests were performed on a tensile test machine (Instron model 3342) with 500 N capacity load cell with a constant stretch rate (2/min) and the nominal stress and stretch were recorded until the failure. Fracture test was performed with the notched specimen to obtain the onset critical stretch for crack propagation (λ_c). From the tensile test, which was performed with an un-notched specimen, the strain energy density $W(\lambda_c)$ was calculated by integrating the area under the stress-stretch curve, corresponding to the onset crack propagating stretch λ_c and the fracture toughness was obtained using equation (3.4).

3.4 Results and Discussion

3.4.1 Verification of pure shear test with other methods

By integrating the area under the stress-stretch curve of the tensile test in figure 3.4 with critical stretch λ_c, the critical energy density $W(\lambda_c)$ is obtained as 1470 kJ/m^3 and using equation (3.4), the obtained fracture toughness is calculated as 7350 J/m^2. Because of the large magnitude of the fracture energy and the pronounced blunting, we verified the toughness measuring method with two other methods, tensile test with various crack lengths and double peeling test [22]. Although the crack propagation was occurred at a huge stretch, the toughness obtained from our experiment matched very well with the other methods.

Verifying with tensile test with various crack lengths

This is an experimental method to obtain fracture energy with samples with different crack lengths. [22]. This method is used to verify that the pure shear test method works for extremely stretchable materials. Samples with dimensions H=5mm, L=75mm and thickness B=3mm were prepared with various crack lengths, A. The configuration of the test is similar

to figure 3.2. Force-extension curves were obtained until the onset of crack propagation for various crack lengths *A* as indicated figure 3.5(a).

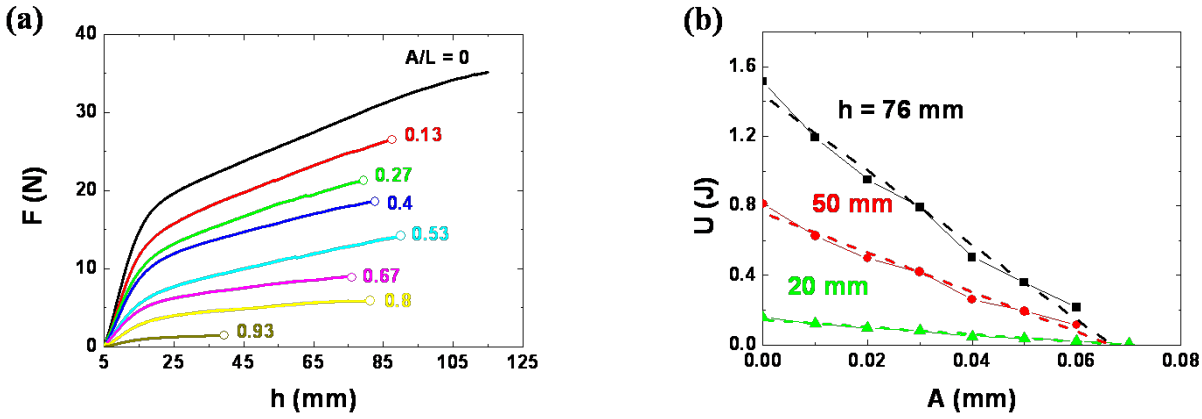

Figure 3.5 Verification of the pure shear test method for extremely stretchy materials with tensile test with various crack lengths. (a) Force-extension curves for various crack lengths (*A*) are plotted, the circles in each curve corresponds to the onset of crack propagation. (b) The work done in deforming a test piece with various crack lengths was obtained from the area under the force-extension curve with the selected *h* values.

h is the change in distance between the clamps. The total energy *U* stored in the test piece at deformation *h* is obtained by measuring the area under the force-extension curve and *U* is plotted with the crack lengths, *A* as shown in figure 3.5(b). *A* suitable *h* value is selected in a way that it corresponds to *h* of at least one fractured sample. $\left(\frac{\partial U}{\partial A}\right)_h$ is calculated from the slope of the total energy vs crack length curve. Thus the fracture energy is given by,

$$\Gamma = -\frac{1}{B}\left(\frac{\partial U}{\partial A}\right)_h \tag{3.5}$$

Using this method the obtained fracture energy was $7155 \pm 400 J/m^2$ which is comparable with the pure shear test results.

Verifying with double peeling test

In order to verify the pure shear test for extremely stretchy materials, we also used the double peeling test [22]. Samples with dimensions D=15mm, L=80mm and thickness B=3mm were prepared with various crack lengths, A as shown in the schematic view in figure 3.6(a). The experimental figures are shown in figure 3.6(b).

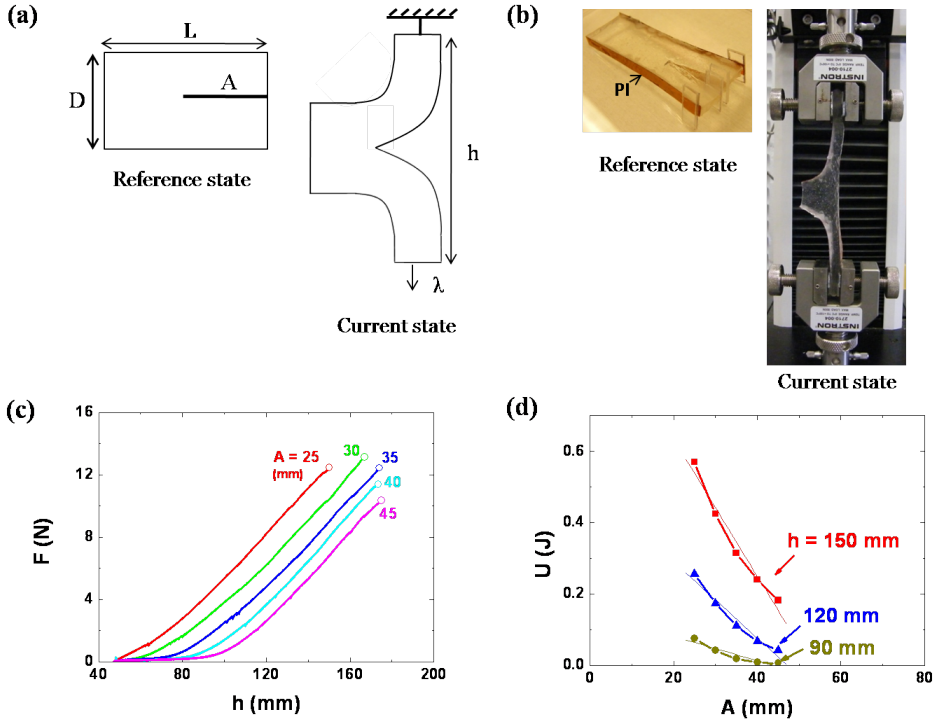

Figure 3.6 Verification of the pure shear test method for extremely stretchy materials with double peeling test method. (a) Schematic figures of the reference state with dimensions D=15mm, L=80mm, B=3mm and current state after deformation are shown. (b) Experimental figures of the double peeling test are shown. PI (Polyimide) strips are attached to the two ends of the specimen to control the deformation in the arms. (c) Force-extension curves for various crack lengths (A) are plotted. (d) The work done in deforming a test piece with various crack lengths were obtained from the area under the load-extension curve with selected h values.

Force-extension curves are obtained until the onset of crack propagation for various crack lengths A as indicated figure 3.6(c). The total energy U stored in the test piece at

deformation h is obtained by measuring the area under the force-extension curve and U is plotted with the crack lengths A as shown in figure 3.6(d). A suitable h is selected as 150mm and $\left(\frac{\partial U}{\partial A}\right)_h$ is calculated from the slope of the total energy vs crack length curve. Fracture energy obtained according to equation (3.5) is $7981 \pm 803 J/m^2$ which is comparable with the pure shear test results.

Verifying with finite element analysis

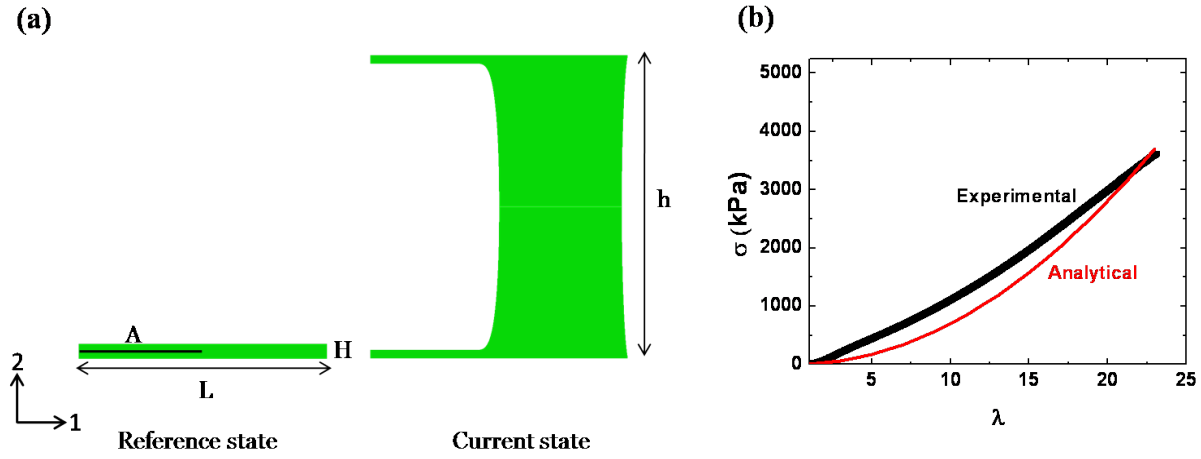

Figure 3.7 (a) Reference state and current state of the finite element model, sample is deformed along direction 2. (b) Comparison of true stress vs stretch curves using Neo-Hookean material model with the experimental results. A shear modulus of μ=7kPa is selected to fit the Neo-Hookean model with the maximum stress level obtained from experimental curve.

To verify the pure shear test for stretchable materials, we used finite element analysis with Neo-Hookean material model. Using the Neo-Hookean material model the energy density function is,

$$W = \frac{\mu}{2}(\lambda_1^2 + \lambda_2^2 + \lambda_3^2 - 3) \quad (3.6)$$

Where λ_1, λ_2 and λ_3 are the stretches in all three directions as shown in figure 3.7(a), direction 2 is the stretching direction, 1 is perpendicular to stretching direction and 3 is into the plane. μ is the small deformation shear modulus.

For the pure shear test method $\lambda_1 = 1$ and considering $\lambda_2 = \lambda$, and using the incompressibility condition,

The stress in direction 2 becomes,

$$\sigma_2 = \sigma = \mu(\lambda^2 - \frac{1}{\lambda^2}) \quad (3.7)$$

True stresses in stretching direction are compared for both analytical results using Neo-Hookean material model and experimental data in figure 3.7(b). Shear modulus of, $\mu = 7kPa$ is used to fit with the upper stress level of the experimental curve. It is observed that Neo-Hookean material model is not the best material model to fit the experimental stress-stretch curve of polyacrylamide-alginate hydrogel but what we are interested is the generic features independent of the material model.

Using the commercial finite element analysis ABAQUS, we have established a 2D model with a pre-crack A/L=0.5. Reference state of the finite element model is shown in figure 3.8(a), and only half of the geometry was considered due to its symmetry. Plane stress, 2 dimensional quadrilateral elements were used for the analysis. At the stretch of 15 the deformed configuration can be observed with a highly blunted crack as shown in figure 3.8(a) current state.

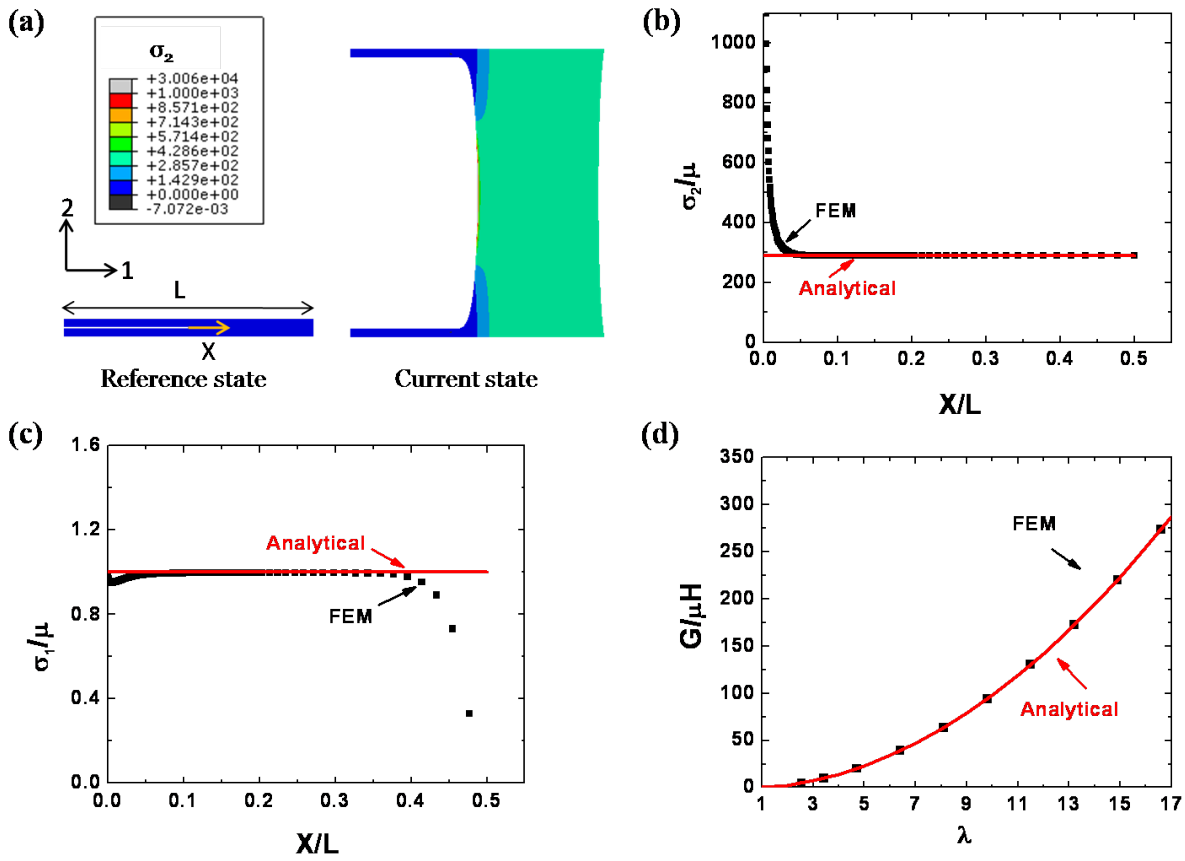

Figure 3.8 (a) Contour plot for true stress in direction 2 (σ_{22}) using FEM and this analysis corresponds to a stretch of 15 in direction 2 (b) σ_{22} is plotted with the distance from the crack tip, *X*, both FEM results and analytical results are compared. (c) σ_{11} is plotted with the distance from the crack tip, both FEM results and analytical results are compared. (d) FEM and analytical results for normalized energy release rate (with shear modulus, μ and sample length, *H*) vs stretch.

The true stresses are plotted along direction 1 from the crack tip in figure 3.8(b, c). Figure 3.8(b) shows the true stresses in direction 2 as a function of the length *X* measured from the crack tip. It is observed that only a very small region near the crack tip ($X/L < 0.05$) shows stress concentration due to the crack and the rest of the sample is under a uniform stress. The stresses obtained from finite element method is compared with analytical

solution using equation (3.7), with λ=15, so that σ_2/μ~225. Figure 3.8(c) shows true stresses in direction 1 and the result of the finite element method are compared with analytical solution by taking $\sigma_1/\mu = (1 - \frac{1}{\lambda^2})$, with λ=15, so that σ_1/μ ~1. It is observed that stresses in direction 1 are much less compared to the stresses in direction 2. That means when the sample is highly deformed, only a negligible amount of stresses are relaxed in direction 1. Both figures 3.8(b) and (c) give the regions where there is a uniform energy density and a region where the pure shear method should work. It also suggests that when length *X* is very small and very large the method cannot predict reasonable results. Figure 3.8(d) shows energy release rate (G) as a function of applied stretch (λ). In the finite element analysis, energy release rate (G) was calculated by using the J integral method considering contour integrals. Calculated energy release rate is compared with analytic solutions, for the pure shear test method, $\lambda_1 = 1$ and energy release rate becomes $G = \Gamma = W \cdot H$. By taking $\lambda_2 = \lambda$,

$$\frac{G}{\mu H} = \frac{1}{2}\left[\lambda^2 + \frac{1}{\lambda^2} - 2\right] \tag{3.8}$$

3.4.2 Geometry and size effect

In order to check whether the measured toughness of polyacrylamide-alginate hydrogel, which is very tough, is independent of the specimen size, we have varied all the sizes of the sample including crack length (A), sample length (H) and sample thickness (B) normalized with sample width (L) and compared the toughness value.

Crack length effect

To check the crack length effect, samples were prepared for both tensile and fracture test as shown in figures 3.1 and 3.2 with the same dimensions but with various crack lengths. Stress- stretch curves were obtained for both tensile test (black) and fracture tests as shown in figure 3.9(a).

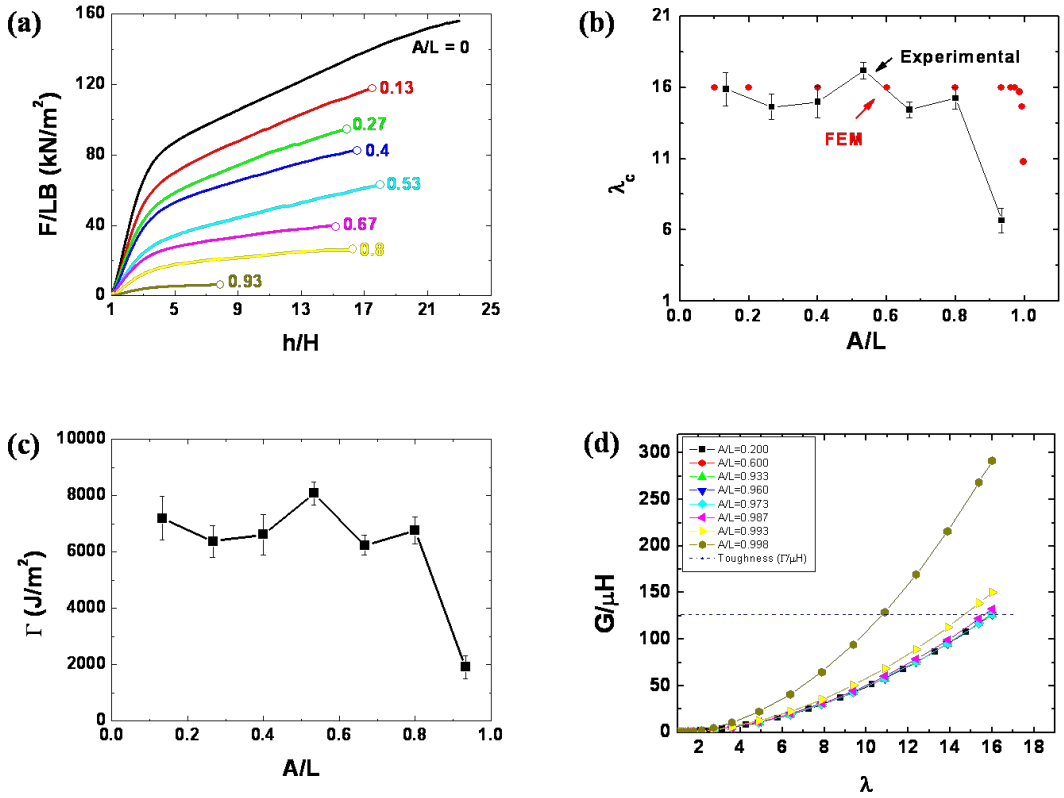

Figure 3.9 Effect of pre crack length on toughness value. (a) Stress- stretch curves for various crack lengths; the circles denote the onset of crack propagation. Stress- stretch curve for tensile test without a pre crack is shown in black color. (b) Critical stretch of the sample with various crack lengths normalized with sample width. Both experimental and the FEM results obtained from figure 9(d) are compared (c) Fracture toughness of the sample as a function of pre-crack length. (d) Normalized energy release rate as a function of stretch, pre-crack sizes are varied. Dotted line denotes average toughness measured by experiments.

From the fracture tests critical stretches were recorded when the samples fracture and shown in figure 3.9(b) with a black color curve. The critical stretches do not vary much by varying crack lengths in the range of $A/L<0.8$. However, the critical stretch decreased to less than half of its value when the ligament length reaches less than 10% of the whole sample width. By using equation (3.4), fracture toughness is calculated and plotted in figure 3.9(c) as a function of crack lengths. Because critical stretches are almost same in the region of $A/L<0.8$, we obtained a consistent fracture toughness within that range. Figure 3.9(d) shows the normalized energy release rate obtained using finite element analysis with J integral method with increasing stretch for different crack lengths. Average fracture toughness obtained from figure 3.9(c) is also plotted as a dotted line by normalizing with shear modulus μ=15.03kPa and sample length H=5mm. Critical stretch can be calculated from figure 3.9(d) by using $G=\Gamma$, and is plotted in figure 3.9(b) with red dots for comparison. From the experiments, the fracture toughness kept consistent in the range of $A/L<0.8$ and decreased when the ligament length reached less than 10% of the whole sample width. This means when the crack size is larger than 90% of the whole sample width, pure shear method may break down. By contrast, the region specified by finite element analysis where the pure shear method breaks down is much smaller than the experimental results. This is because our material model, which is Neo-Hookean is not the exact material model which can capture the behavior of this specific hydrogel.

Sample length effect

According to Rivlin and Thomas, the pure shear test is valid only when the sample width and crack length are much larger than the sample length. Thus, we also need to check the sample length effect to measure the accurate fracture toughness values. Samples were prepared for both tensile and fracture tests as shown in figures 3.1 and 3.2 with various sample lengths. Stress-stretch curves were obtained with different initial sample lengths as shown in figure 3.10(a).

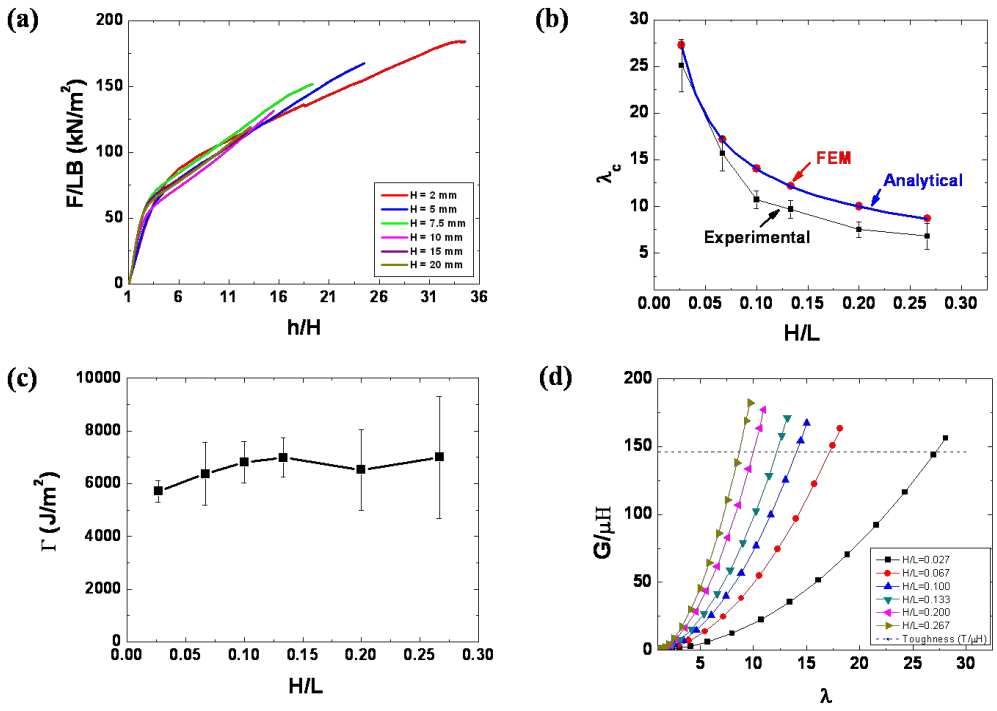

Figure 3.10 Effect of sample length on toughness value. (a) Stress- stretch curves for various sample lengths. (b) Critical stretch of the sample with sample lengths. The experimental values are compared with FEM and analytical results (c) Fracture toughness of the sample as a function of sample length measured according to pure shear test method. (d) Normalized energy release rate calculated using J integral method with various sample lengths. Dotted line denotes average toughness measured experimentally.

From the fracture tests, critical stretches were recorded and plotted in figure 3.10(b) with a black color curve. The critical stretch was decreased by increasing the sample length. This phenomenon is understood as follows. When the crack is propagating, if the sample stores same energy density, longer samples may release more energy. So the only way to release same amount of energy is by limiting the critical stretch to decrease the stored energy density. Fracture toughness is calculated with the sample lengths according to the pure shear test method and plotted as a function of sample length in figure 3.10(c). One remarkable point is that we obtained consistent fracture toughness even with decreasing critical stretches, and it agrees well with the concept of fracture toughness. Figure 3.10(d) shows the energy release rate obtained using FEM with J integral method. Average fracture toughness value obtained from figure 3.10(c) is plotted by normalizing with shear modulus μ=15.03kPa and sample length H=5mm. Critical stretch can be calculated from figure 3.10(d) by using $G=\Gamma$, and is plotted in figure 3.10(b) with red dots for comparison along with the analytical results given in a blue curve.

Sample thickness effect

The pure shear test assumes the test sample is very thin, and the membrane is treated as a plane stress 2D model. To check the sample thickness effect, samples with various thicknesses are prepared, and stress-stretch relationships are measured as shown figure 3.11(a).

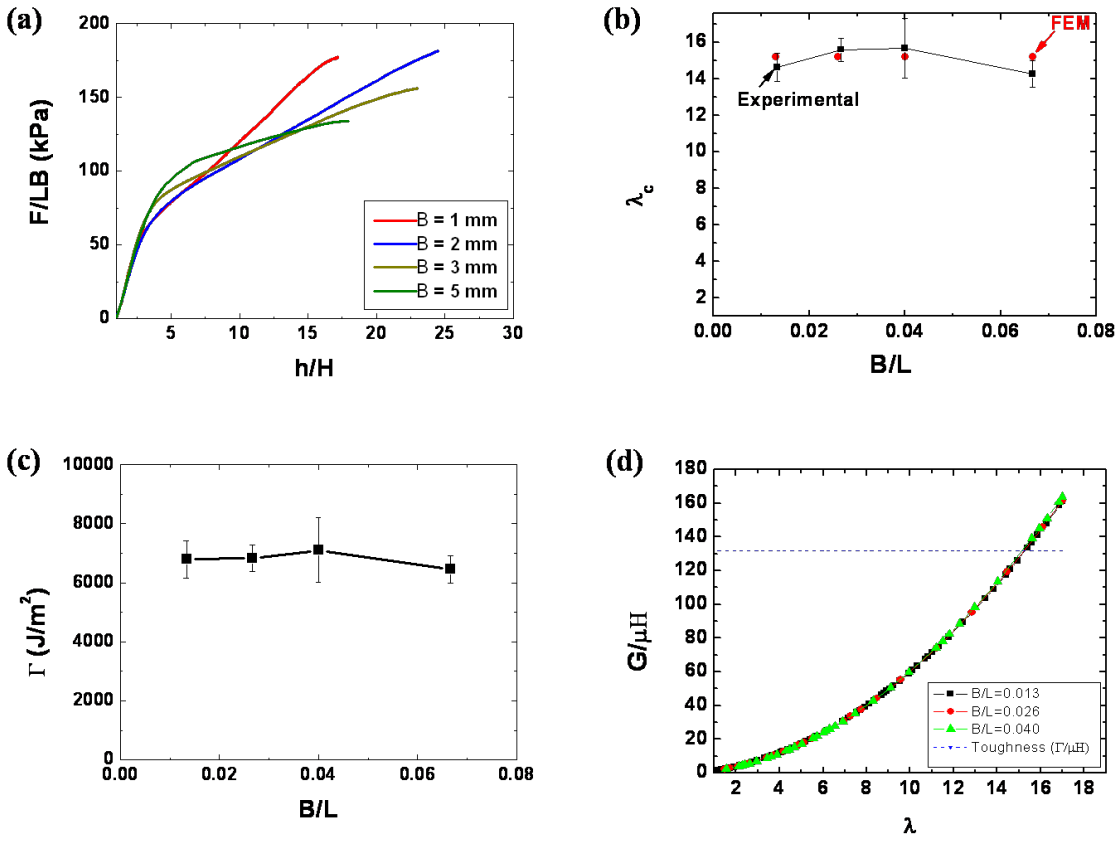

Figure 3.11 Effect of sample thickness on toughness value. (a) Stress- stretch curves for various thicknesses. (b) Critical stretch of the sample with various thicknesses. FEM results are obtained from figure 11(d) with an average toughness. (c) Fracture toughness as a function of sample thickness. (d) Normalized energy release with various sample thicknesses. Dotted line denotes average toughness measured by experiments.

From the fracture tests, critical stretches are plotted in figure 3.11(b) with a black curve, and by combining stress-stretch relationship and critical stretch, fracture toughness is calculated as a function of the sample thickness and plotted in figure 3.11(c). Both critical stretch and fracture toughness are not influenced by the sample thickness. The energy release rate obtained from FEM, shown in Figure 3.11(d), also supports the experimental results. Therefore, in the range of $B/L<0.07$, sample thickness do not influence the fracture

toughness value.

3.5 Summary

According to Rivlin and Thomas, the pure shear test to measure fracture energy is valid only when the sample width and crack length are much larger than the sample length. However, when the test materials are extremely stretchy, sample geometry can easily violate the pure shear test criteria. Under this condition we have verified that the fracture energy obtained from pure shear test is comparable with two other experimental methods along with FEM results. We conclude that the pure shear method is still valid to measure fracture energy of extremely stretchy materials. The geometry and size effects of the sample on fracture energy were studied by varying the crack length, sample length and sample thickness and available working ranges of pure shear test method were addressed.

Chapter 4

Fiber reinforced tough hydrogels

4.1 Introduction

Many applications of hydrogels rely on the combined attributes of a solid that provides strength and a liquid that transports matter. Most existing hydrogels, however, are brittle, with fracture energies on the order of 10 J/m^2 [4,15]. This limits their use in structural applications where they are subjected to mechanical loading. This problem could be circumvented by reinforcing the hydrogels with fibers to improve their mechanical behavior [3]. This effort is hampered, however, by the low toughness of hydrogels: as the composite is loaded, the fibers cut through the hydrogel matrix, destroying the synergy between fibers and matrix, and leading to rapid failure of the composite. A hydrogel-based composite is only effective if the hydrogel matrix is tough enough to resist the fibers cutting through the matrix. Cartilage is one example of such a composite taken from nature: cartilage consists of a collagen fiber-reinforced proteoglycan gel. It contains more than 70% water, but is remarkably stiff and tough [55,4]. It comes as no surprise, then, that hydrogel-based composites are being actively explored for use as synthetic tissues and in biocompatible products [16-18,57-61].

Many attempts have been made to improve the toughness of hydrogels [16-19, 60]. Double-network hydrogels were the first class of hydrogels to exhibit significant fracture toughness, with fracture energies in the range of 100-1000 Jm^{-2} [16]. Recently, we developed a new group of hybrid hydrogels synthesized from polymers that form networks with

covalent and ionic cross-links, and that have an extraordinary combination of toughness and stretchability [21]. These hybrid gels consist of a covalently cross-linked polyacrylamide (PAAm) network and an ionically cross-linked alginate network, and can attain fracture energies as large as 9000 Jm^{-2}. The need for a tough composite matrix is illustrated graphically in Figure 4.1, where we use a metal wire to cut through two different types of hydrogels, a standard technique for measuring the fracture toughness of foods and soft gels [62,63].

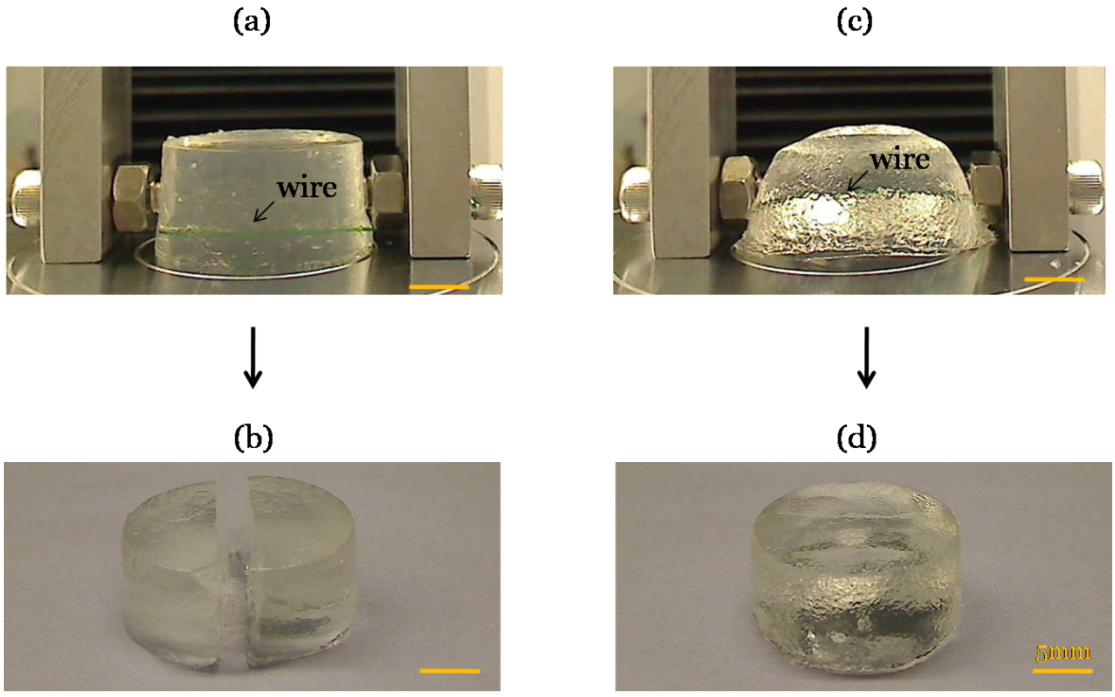

Figure 4.1 Wire cutting tests for a brittle (a, b) and a tough hydrogel (c, d). (a) Alginate hydrogel being cut by a steel wire. (b) The cut sample is turned 90° and the two pieces are separated to show the cut. (c) Alginate-Polyacrylamide hybrid hydrogel deforms, but resists cutting. (d) The sample recovers its original shape when the wire is removed.

Two examples are shown: (1) a brittle alginate gel and (2) a tough alginate-polyacrylamide hybrid hydrogel. The difference between the gels is obvious. The alginate gel

is readily cut by the wire; the hybrid gel deforms elastically, but resists being cut. Thus an alginate matrix would result in a composite with poor mechanical properties. The hybrid gel, on the other hand, would make a very good matrix in a fiber-reinforced composite. Such a composite would have significantly better stiffness and strength than the hybrid hydrogel, and could be used in structural applications. Lin et al [60] have investigated the toughening mechanism of alginate-polyacrylamide hydrogels reinforced by a stretchy fiber mesh fabricated from thermoplastic polymers. When a notched sample of such a composite is deformed, the hydrogel matrix maintains the integrity of the sample, while fracture of the fibers in the bridging zone dissipates mechanical energy.

In this study we investigate the mechanical behavior of composites that consist of a tough alginate-polyacrylamide hydrogel matrix reinforced with a random network of stiff fibers, for which we conveniently use stainless steel wool. Steel wool fibers are strong and can easily create a random continuous fiber network – they have been used for this purpose in a number of applications [64,65]. We evaluate the stress-strain curves of the fiber-reinforced gels and evaluate the mechanism by which they fail.

4.2 Experimental

4.2.1 Synthesis of fiber reinforced hydrogels

Powders of alginate (FMC Biopolymer, LF 20/40) and acrylamide (Sigma, A8887) were dissolved in deionized water. After the powders were fully dissolved, the solution was held at 35^{o}C for 1 hour. Weights of alginate and acrylamide were fixed at 1:6, and the water content was fixed at 86 wt.%. Ammonium persulfate (AP; Sigma, A9164), 0.0017 times the weight of

acrylamide, was added as a photo initiator for the acrylamide polymerization process. N,N-methylenebisacrylamide (MBAA; Sigma, M7279), 0.0006 times the weight of the acrylamide, was added as the cross-linker for the acrylamide. N,N,N',N'-tetramethylethylenediamine (TEMED; Sigma, T7024), 0.0025 times the weight of acrylamide, was added as the cross-linking accelerator for the polyacrylamide. Calcium sulfate slurry ($CaSO_4 \cdot 2H_2O$; Sigma, 31221), 0.1328 times the weight of alginate, was added as the ionic cross-linker for alginate. Stainless steel wool (Type 316, fine, McMaster-Carr 7364T74) with an average cross-sectional area of the fibers of ~ 80μm × 70μm was chosen to provide the reinforcing fibers. The fibers in this type of steel wool are arbitrarily oriented and have lengths that exceed the sample dimensions. After the wool was distributed evenly inside dumbbell-shaped molds, the gel solution was poured into the molds and covered with a glass plate. Before casting the gel solution, the steel wool was thoroughly wetted with the solution to reduce the formation of bubbles inside the samples. The composite samples were then cured at room temperature by exposing them for eight minutes to ultraviolet light with a wavelength of 350 nm (OAI LS 30 UV flood exposure system, 1.92W/cm² power density). The samples were kept in a sealed container at room temperature for one day to ensure complete reaction. The weight fraction of steel wool in the composite hybrid gels was varied from 0 to 12 wt%.

4.2.2 Wire cutting test

Hydrogel samples with a diameter of 35mm and a thickness of 17mm were fabricated from an unreinforced alginate-polyacrylamide hybrid hydrogel and an alginate hydrogel (Figure 4.1). Wire cutting tests were performed in air, at room temperature, using a tensile tester (Instron model 3342) with a 1000 N load cell. A 580 μm diameter steel wire was

pulled through the specimen at a displacement rate 10 mm/min.

4.2.3 Tensile test

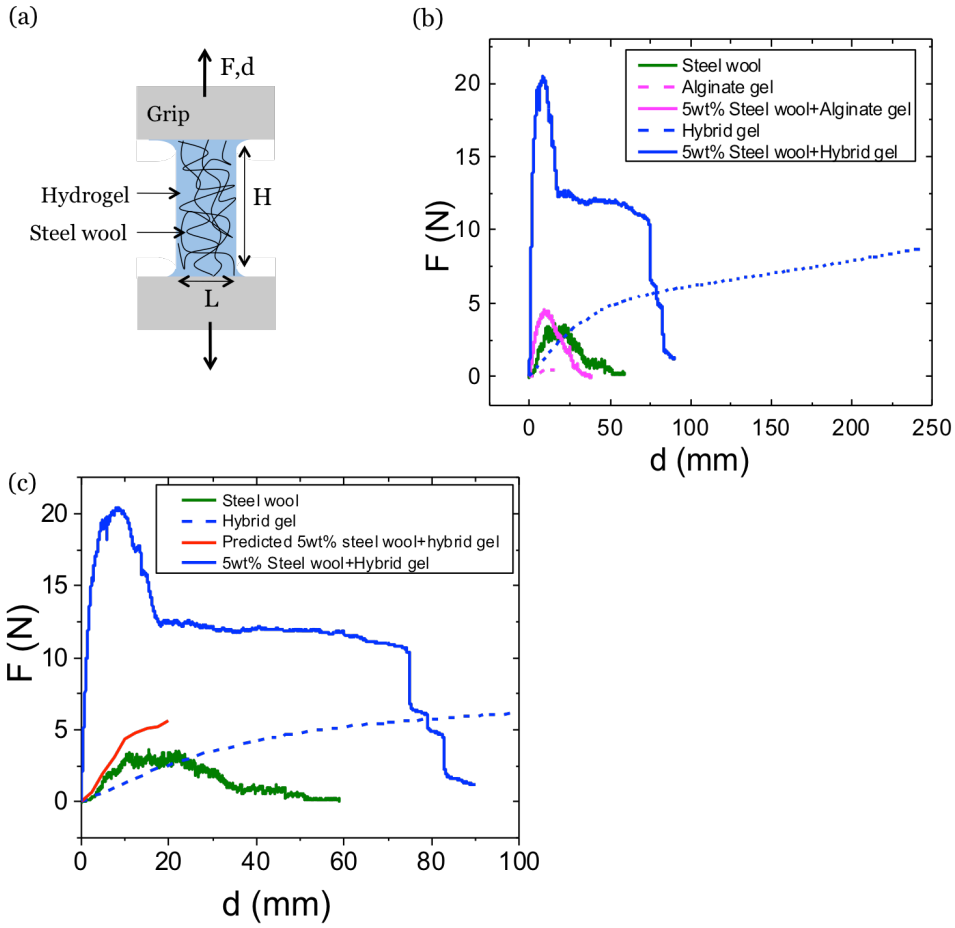

Figure 4.2 Tensile tests of hydrogel composites. (a) Schematic of the tensile test samples of the fiber-reinforced hydrogels. Steel fibers form a random network throughout the entire sample. (b) Force-displacement curves for a fiber-reinforced hybrid hydrogel and a fiber-reinforced alginate hydrogel, compared with similar curves for steel wool and unreinforced hydrogels. (c) Force-displacement curve of hybrid hydrogel composite is predicted from hydrogel and steel wool at small displacements and compared with the experimental composite curve.

Tensile experiments were performed using the dumbbell-shaped samples. The gauge sections of the samples were 35mm long, 15mm wide, and 3mm thick (figure 4.2(a)).

The wide sections of the samples were glued between two acrylic plates of dimensions

$10 \times 20 \times 3 mm^3$ using super glue (VWR, 500031-578) and the acrylic plate/gel sandwiches were inserted into the grips of the tensile tester. Measurements were performed at room temperature in air using a 1000 N load cell. The force-displacement curves were measured at a displacement rate of 10mm/min. Tests were performed until rupture of the samples. The force-extension curve for steel wool was measured by performing measurements on the same amount of steel wool, randomly distributed in the same volume as the composite samples. Five experiments were performed per condition.

4.2.4 Fiber pullout test

The friction between the hydrogel matrix and the stainless steel fibers was measured using a fiber pullout test. A long fiber was embedded inside an alginate-polyacrylamide hydrogel during synthesis of the gel, such that a significant length of the fiber extended outside the gel on both sides of the sample. The samples had a height of 75mm, width of 15mm, and thickness of 3 mm. Fiber dimensions were measured at three locations along the length of each fiber by means of optical microscopy. The samples were mounted in the tensile tester and one end of the fiber was attached to the grip of the tensile tester. Pullout tests were performed in air, at room temperature, using a 1000 N load cell. Force-displacement curves were measured at a displacement rate of 10 mm/min. Tests were performed on five different samples.

4.3 Results and discussion

4.3.1 Force-displacement curves of hydrogel composites

Figure 4.2(b) shows the force-displacement curves for two different composites, a fiber-

reinforced alginate-polyacrylamide hybrid gel and a fiber-reinforced alginate gel, along with the force-displacement curves of the various components that make up the composites. Both composites have the same weight fraction of stainless steel fibers. The pure alginate hydrogel is very weak and can sustain very small loads and displacements only. The pure hybrid hydrogel, in contrast, is very stretchable and can sustain much higher forces, but is quite compliant. The steel wool sample has poor mechanical properties and the sample essentially disintegrates during the test. The force-displacement curve of the alginate composite is not much different from that of the steel wool. Since the alginate is too weak to keep the fibers together, its behavior is almost completely controlled by the steel wool. The effect of fibers on the hybrid hydrogel, on the other hand, is substantial: it is much stronger and stiffer than the unreinforced hybrid gel, and it is significantly stronger than the reinforced alginate. Additionally, the force-displacement curve has a very different shape from both the steel wool and the hybrid gel; the force rises quickly, goes through a maximum, and then plateaus. To predict the force-displacement curve of the hydrogel composite at small displacements, the curves for steel wool and hydrogel are vertically added and plotted in figure 4.2(c). Evidently, the experimental curve does not follow the rule of mixtures based on the behavior of the constituents. This is understood as follows. The fibers in the steel wool are held together by entanglement only; they are not bonded in any way. During tensile testing, the fibers slide with respect to one another. Consequently, the tensile behavior is not representative of the mechanical behavior of the fibers; instead it is a measure for the frictional resistance encountered during fiber disentanglement. In contrast, the behavior of the fibers in the hydrogel is very different: the hydrogel matrix keeps the fibers in place and

makes disentanglement very difficult. Disentanglement only occurs during the second stage after the fibers debond from the matrix. In other words, there is a strong synergistic effect when fibers and hydrogel are combined.

4.3.2 Fibers cutting through the matrix

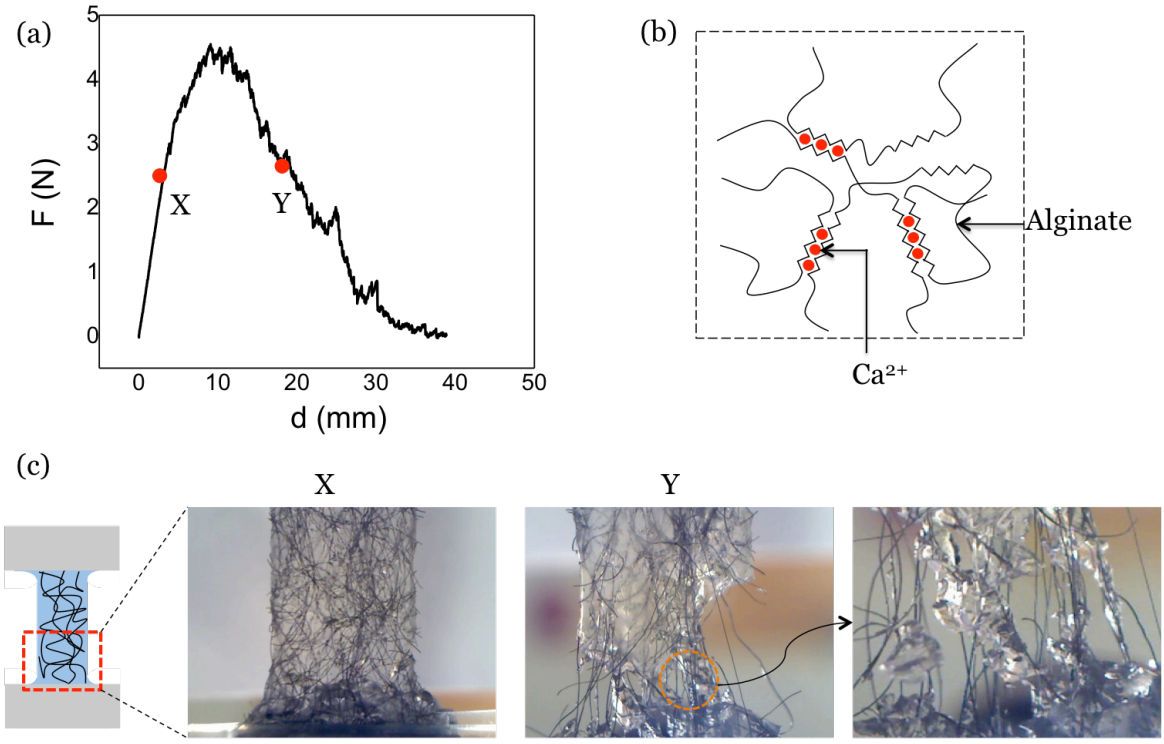

Figure 4.3 Failure mechanism of a brittle and weak alginate hydrogel composite. (a) Force-displacement curve of an alginate hydrogel composite. (b) Schematic of the molecular structure of alginate hydrogel. (c) Photos at two stages during the tensile test. At small deformations (point X), the fibers are bonded to the matrix. After reaching a maximum force, the composite starts to fail by fibers cutting through the matrix (point Y).

Figure 4.3 shows the deformation of the reinforced alginate gel during the tensile test in more detail. The figure also shows a schematic of the molecular structure of the alginate

chains with the Ca^{2+} crosslinks. As the load on the sample rises, the composite remains intact initially. When the load reaches a maximum, which is comparable to the maximum load supported by just the steel wool, the fibers start to disentangle, cutting through the alginate matrix in the process. This process continues with increased deformation until the fibers have completely shredded the matrix at the point of failure.

4.3.3 Fibers pulling out of matrix

The tensile response of the fiber-reinforced alginate-polyacrylamide hydrogel is illustrated in detail in Figure 4.4. The figure also shows a schematic of the molecular structure of the alginate-polyacrylamide hydrogel, with MBAA crosslinks in the polyacrylamide network and Ca^{2+} crosslinks in the alginate network. Initially, the fibers and matrix deform in concert. With continued deformation, the fibers rotate toward the loading direction and the load rises quickly to a value that is much larger than that predicted by the rule of mixtures applied to matrix and steel wool. At this point, the interface between fibers and matrix starts to debond and the load decreases until it reaches a plateau value characterized by continuous fiber sliding and pull out. During the fiber sliding stage, the matrix undergoes extensive deformation, but remains intact; there is no cutting by the fibers. Eventually the fiber network is ripped apart causing abrupt failure of the sample.

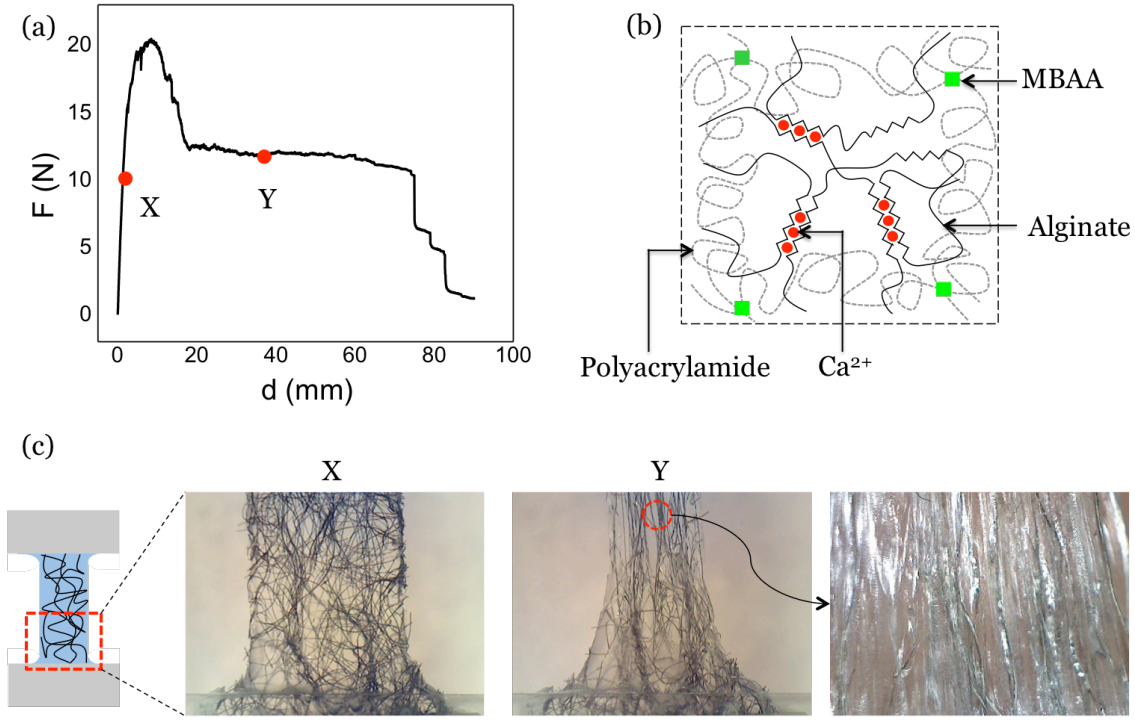

Figure 4.4 Failure mechanism of a tough hybrid hydrogel composite. (a) Force-displacement curve of an alginate-polyacrylamide hydrogel composite. (b) Schematic of the molecular structure of alginate-polyacrylamide hydrogel. (c) Photos at two stages during the tensile test. At small displacements (point X), the fibers are bonded to the matrix. Fiber debonding is observed near the peak force. At larger displacements (point Y), the fibers slide through the matrix.

4.3.4 Frictional sliding of steel fiber through tough hydrogel matrix

Because frictional sliding is an important aspect of the failure mechanism, single-fiber pullout tests were performed to investigate the interfacial properties (Figure 4.5(a)). Figure 4.5(b) shows a typical force-displacement curve for a fiber pullout experiment.

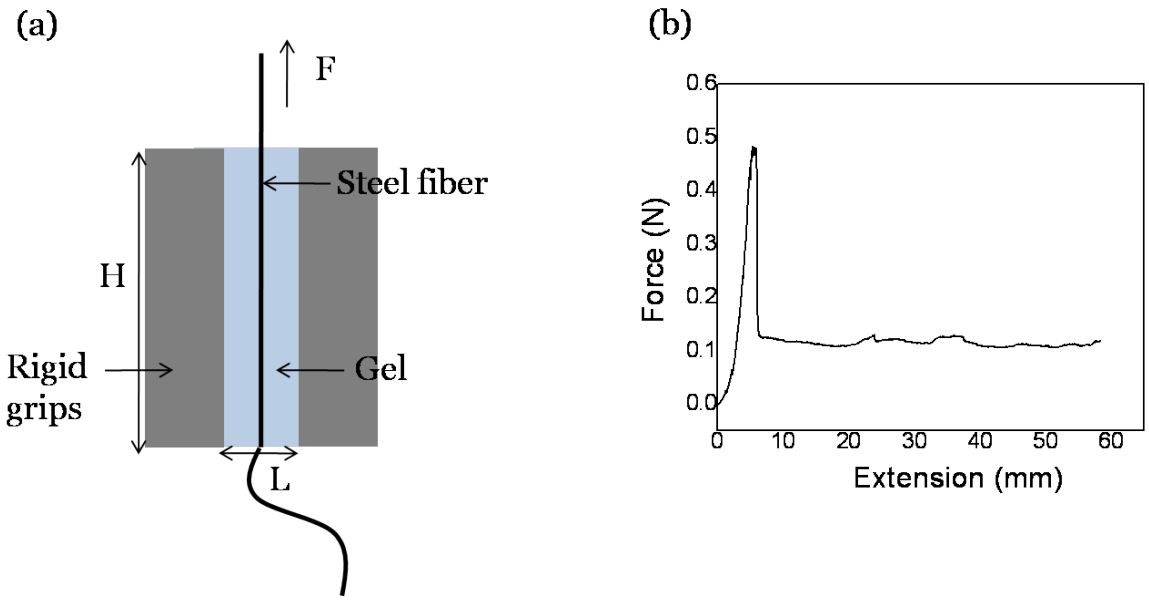

Figure 4.5 Single fiber pull out test. (a) Schematic of the single fiber pullout test sample; (b) Force required to pull the fiber is recorded as a function of fiber extension.

The curves go through a maximum, which coincides with the failure of the interface between fiber and matrix. After debonding, the fiber pulls out of the matrix at a constant frictional force of approximately 0.155 ± 0.052 N. In the experiments, the peak load was difficult to reproduce, but the magnitude of the plateau force was very consistent. The average friction stress between fiber and matrix was calculated by dividing the frictional force by the total interfacial area between fiber and matrix, yielding a value of approximately 5kPa. This result was used to estimate the energy dissipated by frictional sliding of the fibers. The total fiber length (6.78 m) was calculated from the mass of the fibers embedded in a typical sample (0.3 g), the density of steel (7.8 g/cm^3), and the average cross-sectional area (80 μmx 70 μm) of the fibers. An upper bound for the energy dissipated in friction during the tensile test, can be found by multiplying the frictional force with the total fiber length, yielding a value of approximately 1.06 ±0.35 J. The total energy dissipated during the tensile

test can be calculated from the force-displacement curve in figure 4.2(b), resulting in a value of 1.02 J. Part of this energy is dissipated in the deformation of the hydrogel matrix and this part can be estimated from the force-displacement curve of the hydrogel to yield 0.30 J. Thus the energy dissipated by fiber sliding is approximately 0.72 J, which compares favorably with the upper bound – approximately 70% of the total energy dissipation during the tensile test is associated with frictional losses.

4.3.5 Effect of fiber concentration on modulus and tensile strength

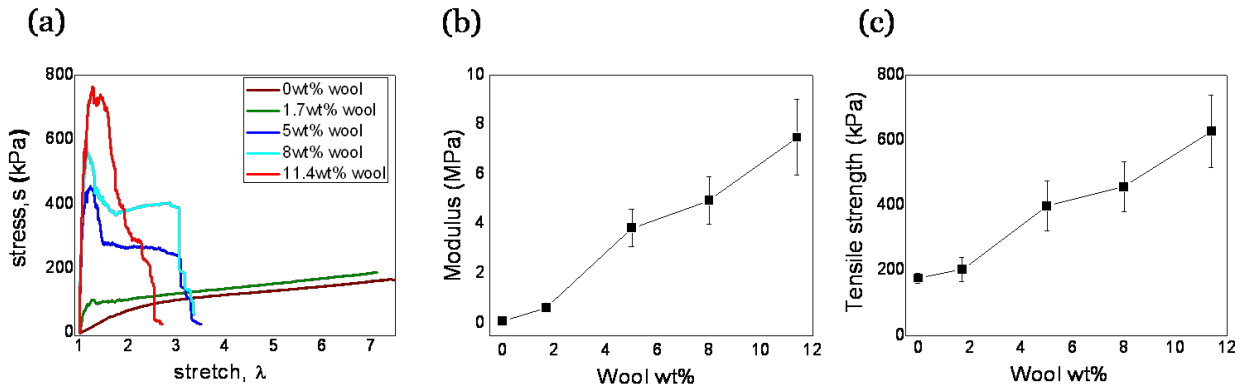

Figure 4.6 Effect of fiber concentration. (a) Stress-stretch curves of hybrid gels with various fiber concentrations; (b) Modulus of hybrid gels with various fiber concentrations; (c) Tensile strength of hybrid gels with various fiber concentrations.

Figures 4.6(a) through (c) illustrate the effect of the volume fraction of the steel wool on the mechanical response of the composites. The nominal stress was obtained by dividing the force by the initial cross-sectional area of the sample; stretch was calculated by dividing the length of the deformed sample by its initial value. The tensile strength was defined as the

maximum nominal stress supported by the composites. The elastic modulus was calculated from the slope of the stress-strain curves up to 5% strain. The fiber concentration was varied from 0 to 11.4 wt%. Without fiber reinforcement, the hybrid gel has a very large stretch to failure, but low stiffness and strength. Introducing the fibers reduces the stretchability of the gel, but increases the modulus and strength significantly. Evidently the weight fraction of the steel wool has a large effect on the stress-stretch curves: At low weight fraction, the response of the composite is dominated by the hydrogel and the stress-stretch curve is similar to that of a pure hydrogel. As the weight fraction is increased, the shape of the curve is altered and it develops a distinct peak followed by a plateau, associated with fiber debonding and sliding, respectively. At even higher weight fractions, the steel wool completely dominates the response, the plateau disappears, and the stress-stretch curve becomes similar to that of steel wool.

Synthesis of fiber-reinforced composites involves a large number of variables, including the type of fibers, the arrangement of the fibers, and the behavior of the fiber/matrix interface. As a result of this diversity, composites with very distinct attributes can be fabricated using the same matrix material. For example, recently Lin et al [60] reinforced the same hydrogel with highly aligned fibers of a stretchy thermoplastic polymer. A comparison between their composites and ours is interesting. Our composites have a stress-strain behavior where the stress first peaks and then drops to a plateau of constant stress. The plateau makes it possible to tailor the stress at which energy dissipation occurs. This behavior is distinctly different from the behavior reported by Lin et al, where no plateau was observed. In our composites, fiber sliding is an important aspect of the failure mechanism

and frictional losses represent a significant fraction of the energy dissipated during failure. In the composites described by Lin et al., energy is dissipated mainly as a result of fiber fracture. Our composites can sustain much higher stresses than predicted based on the rule of mixtures for the individual components: there is a strong synergistic effect between the steel wool and the matrix material. The stress-strain curves of the composites reported by Lin et al, in contrast, follow the rule of mixtures.

4.4 Discussion

Our results suggest that fiber-reinforced tough hydrogels may be useful in applications that require toughness, strength and stiffness – examples include materials for energy absorption, materials for tendon repair surgery, flexible electronics and sensors. The distinct stress-stretch behavior of our composites are ideal to use as energy absorbing materials, for instance, to soften the effect of an impact on a helmet [66]. Although the total energy dissipated by the composite is similar to the energy absorbed by the tough hydrogel when stretched to rupture, the level of stress during the deformation can be tailored by changing the fiber concentration, a distinct advantage over the unreinforced hydrogel. When designing an energy absorbing material for helmets, the material should absorb as much energy as possible, while limiting the maximum stress to the head to approximately 0.9 MPa to prevent injury [66, 67]. The hydrogel composites have high energy absorption and a plateau stress that can be tailored to not exceed the maximum allowable value. For example, a 5 wt% composite has an energy absorption of approximately 0.6 MJ/m^3 and a plateau stress of 0.3 MPa; an 8 wt% composite has an energy absorption of 0.9 MJ/m^3 and a plateau stress of

0.4 MPa. These values compare favorably with commonly used energy absorbing materials such as expanded polystyrene, which has an energy absorption of 0.8 MJ/m^3 and a maximum stress in the range of 0.7-0.9 MPa [67].

Another possible application of hydrogel composites would be in tendon repair surgery, where reinforcing patches are used to help torn tendons heal. Current reinforcing patches are made from materials including porcine dermis, porcine intestine submucosa, or porous polyurethaneurea (Artelon®). Current tendon repair patches have an initial stiffness comparable to our composites and a higher stiffness at large strains. Despite advances in surgical techniques, the structural failure rate of these patches can be very high. Failure has been attributed mainly to sutures cutting through the reinforcing patches [68], which should not be an issue for the tough hydrogel. A fiber-reinforced tough hydrogel may serve as a potential reinforcement patch for suturing, although different biocompatible reinforcing fibers would need to be used.

Finally, one can also envision applications where electronics and living tissue are coupled using flexible and stretchable devices [69-72], an area that has gained much interest recently. These devices are used to probe the electrical activity near the surfaces of the heart, brain, or skin. Recent work includes embedding a 3D network of silicon nanowires with electronic circuitry into a soft gel matrix [73]. By integrating electrical sensors within the 3D scaffolds, cellular activities and physicochemical changes can be monitored. One can envision a similar approach to probe cells in a beating heart or to instill a sense of touch in a soft robotic hand. When electronics and biological tissues are coupled with flexible and stretchable devices, these devices need to be matched to the mechanical properties of the

biological tissues. The hydrogel composites have stiffness values up to 10 MPa. By comparison, cartilage has a stiffness in the range of 6-15 MPa, while skin has a stiffness of 1-3 MPa [74]. The properties of the hydrogel composite can be optimized to the specific application by selecting the appropriate fiber material, orientation distribution, and volume fraction.

4.5 Summary

We have used brittle and tough hydrogel matrices to prepare random fiber-reinforced composites. Composites that have a brittle matrix such as an alginate hydrogel fail by fibers cutting through the matrix. Composites based on tough alginate-polyacrylamide hybrid hydrogels, on the other hand, fail by debonding and sliding of the fibers, dissipating a significant amount of energy in the process. They can carry significantly more load than either matrix or the random fiber network. The combination of high strength, stiffness, and toughness, and the ability of sustaining large strains, along with easy method of synthesis, makes fiber-reinforced tough hydrogel composites good candidates for a range of applications.

Chapter 5

Fire-retarding tough hydrogel-fabric laminates

5.1 Introduction

Millions of people suffer burn injuries all over the world, including many children. The American Burn Association reports that approximately 3400 individuals die and around 450,000 people receive medical treatment for burn injuries each year in the United States alone [75]. Among these incidents around 72% of burn injuries occur at home [75]. Tight spaces such as high-rise buildings, boats, or airplanes pose particularly significant fire risk [76]. Firefighters wearing the best fire-retarding materials have only a few seconds to evacuate from a flashover fire, which can reach temperatures as high as 600^{o}C [77]. The availability of affordable and effective fire-retarding apparel or protective gears such as fire blankets have the potential to save many lives.

Significant advances have been made in recent decades in developing fire-retarding fabrics [78]. Fire-retarding fabrics are made with intrinsically fire-retarding polymers or by combining with fire-retarding additives. They function with different fire-retarding mechanisms such as high decomposition temperature, low thermal conductivity and char formation [79, 80]. Several drawbacks have been noted in existing fire-retarding fabrics. These highly engineered fabrics are expensive and not widely available. Some fabrics have relatively low decomposition temperature (e.g., 400^{o}C for aramids) [80], and do not retard hot flames. One example of a commercially available aramid fabric is poly-meta-phenyleneisophthalamide (Nomex, DuPont Company) that is widely used in fire retarding

applications [81]. Even for fabrics of high decomposition temperatures (e.g., 1500°C for oxidized polyacrylonitrile) [82], the temperature near the skin becomes high unless the fabric is very thick. Fabrics made from oxidized polyacrylonitrile (O-PAN) fibers are also used in preparing fire-retarding apparel (CarbonX, Chapmen Innovations Company) [83]. The drawbacks of existing fire-retarding polymer fabrics have highlighted a challenge: there is a need for affordable fire-retarding fabrics that can avoid burn injuries at high temperature flames.

Here we break away from the existing approaches, and introduce a new family of fire-retarding materials: hydrogel-fabric laminates (Figure 5.1).

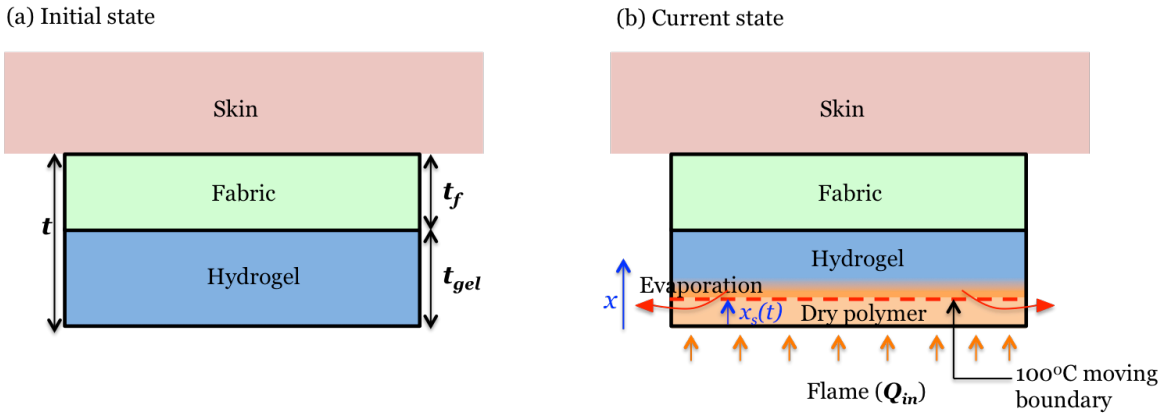

Figure 5.1 Design of hydrogel-fabric laminates to protect skin. (a) Initial state of laminate before the exposure of the flame. (b) At current state the hydrogel layer carries the flame heat away due to water evaporation. This creates a dry polymer layer. The 100°C boundary at the hydrogel-dry polymer interface moves through the hydrogel until all the water is evaporated. During this process, fabric with low thermal conductivity protects the skin.

Instead of searing for materials that sustain high temperature, our design uses the evaporation of water in the hydrogel to take heat away, and the low thermal conductivity of the fabric to reduce the temperature near the human skin. Hydrogels contain mostly water, which has a large specific heat (4187 J/kgK), and evaporates at 100°C with a large heat of evaporation (2.26×10^6J/kg). We show that the hydrogel-fabric laminate provides superior fire protection compared to existing fire-retarding polymers. The National Fire Protection Association (NFPA) standards require that corresponding to a flashover fire with a heat flux of 2cal/cm^{2}s, firefighters' coat should have at least 17.5 seconds to survive without causing second-degree burns [84]. Most of the coats have similar/slightly better survival time under flashover fire. We show that hydrogel-fabric laminates can achieve much higher survival time both experimentally (with a reduced heat flux) and with a model (with standard heat flux). Results from the heat transfer model shows that, under flashover fire with a heat flux of 2cal/cm^{2}s, a 9mm thick hydrogel-wool fabric can achieve more than 200 seconds survival time. This number is significantly higher than what is reported in the literature and can make a huge impact on designing fire-retarding apparel.

As the hydrogel contains 90% water, the laminates can be made with low cost. Hydrogel-fabric laminates retard fire via a different mechanism. When the hydrogel is exposed to fire, much of the heat is consumed by heating up water proceeded by evaporation of water from the hydrogel. As water evaporates, it creates two layers: a layer of dry polymer that starts to char and a layer of hydrated hydrogel. These regions are separated by a moving boundary at the boiling point of water, a fixed temperature of 100°C. Consequently, even though the thermal conductivity of water is high (~0.58W/mK), the remainder of the hydrogel heats up

to at most 100°C. To further reduce the temperature near the human skin, we laminate the hydrogel with a fabric of a low thermal conductivity, such as wool of thermal conductivity of 0.04W/mK [85, 86].

Water has been an important tool in the fire-fighting industry. When water is sprayed on a fire, it coats the fuel and creates a barrier, which prevents oxygen from reaching the fire. The large latent heat of evaporation is very effective at cooling down fuel and thus slowing the fire. Unfortunately, only a small fraction of water sprayed on a fire is effective, because most of the water simply runs off. A recent development in the fire-fighting industry is the use of thixotropic hydrogel slurries [87]. These hydrogel slurries consist of hydrophilic polymers dispersed in water. They flow readily under pressure, but stick to the surface they are sprayed upon. Since these slurries consist mainly of water, they have a similar heat capacity and latent heat of evaporation, and have a similar effect on fire. There are many successful commercial applications of these hydrogel slurries. For instance, hydrogel slurries are sprayed on structures to protect them from wildfires [87-89]. Thick layers of hydrogel slurries are sometimes applied to protect a stunt performer from extreme heat for a short period of time [90]. Hydrogel slurries are also impregnated into different fabrics to make heat-resisting blankets [91, 92], although they do not provide good protection for the skin for a long period of time because of the high thermal conductivity of water.

Here we compare fire-retarding properties of the hydrogel-fabric laminates compared to the individual components. Conventional hydrogels are too weak and brittle to be formed into robust laminates, but recently developed tough hydrogels are ideal for the application [3, 16, 21]. Hydrogel-fabric laminates have several advantages compared to

hydrogel-infused fabrics: 1) the thermal conductivity of the laminate is determined by the insulating fabric, not the hydrogel; and 2) the amount of hydrogel used in the laminate is not limited by the amount of slurry absorbed by the fabric. Tough hydrogels are self-supporting and flexible, and the hydrogel thickness can be selected depending on fire resistance requirements.

We test the fire-retarding properties of laminates containing polyacrylamide-alginate hydrogels and compare them to a number of commercially available fire-retarding fabrics. We develop a simple heat transfer model to quantify the heat absorbed by the skin when protected with a hydrogel-fabric laminate and calibrate the model using a standard test known as the thermal protective performance (TPP) test. We introduce a new method for measuring the performance of fire-retarding fabrics and use the heat transfer model to optimize the design of the laminates for maximum survival time under flashover fire conditions.

5.2 Experimental

5.2.1 Hydrogel synthesis

Polyacrylamide-alginate hybrid hydrogels were prepared using the following procedure: Powders of alginate (FMC Biopolymer, LF 20/40) and acrylamide (Sigma, A8887) were dissolved in deionized water. Ammonium persulfate (AP; Sigma, A9164), 0.0017 the weight of acrylamide, was added as the photo initiator for polyacrylamide. N,N-methylenebisacrylamide (MBAA; Sigma, M7279), 0.0006 the weight of acrylamide, was added as the cross-linker for polyacrylamide. N,N,N',N'-tetramethylethylenediamine

(TEMED; Sigma, T7024), 0.0025 the weight of acrylamide, was added as the crosslinking accelerator for polyacrylamide. Calcium sulfate ($CaSO_4 \cdot 2H_2O$; Sigma, 31221), 0.1328 the weight of alginate, was added as the ionic cross-linker for alginate. The solution was poured into a glass mold, 75.0 x 55.0 x 6.0 mm^3, covered with a glass plate. The gel solution was then cured at room temperature by exposing it for eight minutes to ultraviolet light (OAI LS 30 UV flood exposure system, 350 W power with a wavelength of 350 nm). Gel samples were kept at room temperature for one day to ensure complete reaction. Hydrogel-fabric laminates were prepared by threading hydrogels with aramid fabric (Nomex Aramid strips, McMaster, 8796K56), fire-retarding wool (Keane Fire and Safety Equipment Company, Inc.), and O-PAN fabric (CarbonX fabric, CX-6080, Concord Companies, Inc.).

5.2.2 Heat resistance test

The heat resistance was tested qualitatively using a hot plate (Dataplate Digital Hotplate 720 Series) at two temperatures; T_h=350°C and 500°C. Samples with dimensions of 55mm × 37.5mm × 3mm were placed on the hot plate for 30 seconds and the top surfaces were observed. Wool, aramid, O-PAN and hydrogels were compared for heat resistivity.

5.2.3 Fire resistance test

A blowtorch (Bernzomatic TS3000KC Self Igniting Torch Kit) with a high-temperature flame of approximately ~1000°C was used to test fire resistance. The distance between the tip of the blowtorch and the samples was kept at 6cm. All wool, aramid, O-PAN and hydrogel samples had a length of 75mm, a width of 55mm, and a thickness of 6 mm unless otherwise

noted. Tests were conducted until the flame burned through the samples.

5.2.4 Thermal protective performance (TPP) test

The performance of several fire-retarding materials was measured using a hot plate (Thermolyne Cimarec 2) with a constant heat flux. The heat flux of the hot plate was measured using a power meter (P3 International Kill A Watt EZ Electricity Usage Monitor, P4460). The TPP test was performed with a reduced heat flux of 0.8 cal/cm^{2}s compared to 2.0 cal/cm^{2}s in the standard test procedure developed by the National Fire Protection Association (NFPA) [93] because of limitations of the hot plate. Samples of wool, aramid, O-PAN and hydrogel, each 3 mm thick, as well as laminates of 3 mm hydrogel with 3 mm of wool, aramid, O-PAN were tested. The hydrogel-fabric laminates were prepared by sowing hydrogel and fabric together. All the samples had an area of 180 mm × 180 mm, similar to the area of the hot plate. Samples were placed on top of the hot plate, which was immediately covered by 18cm × 18cm × 2cm insulating board with a copper calorimeter attached to the surface facing the fire-retarding material. The copper calorimeter was a disc with a 40 mm diameter and a 1.5 mm thickness. Two thermocouples (Fluke Thermocouple Thermometer Model 52-2 with a K type thermocouple) were attached to the side of the calorimeter facing the insulating board. The temperature rise of the calorimeter was recorded as a function of time during the experiments. The total heat absorbed by the calorimeter was obtained by multiplying the temperature change of the copper calorimeter with the heat capacity of the calorimeter.

5.3 Results and discussion

5.3.1 Heat resistance

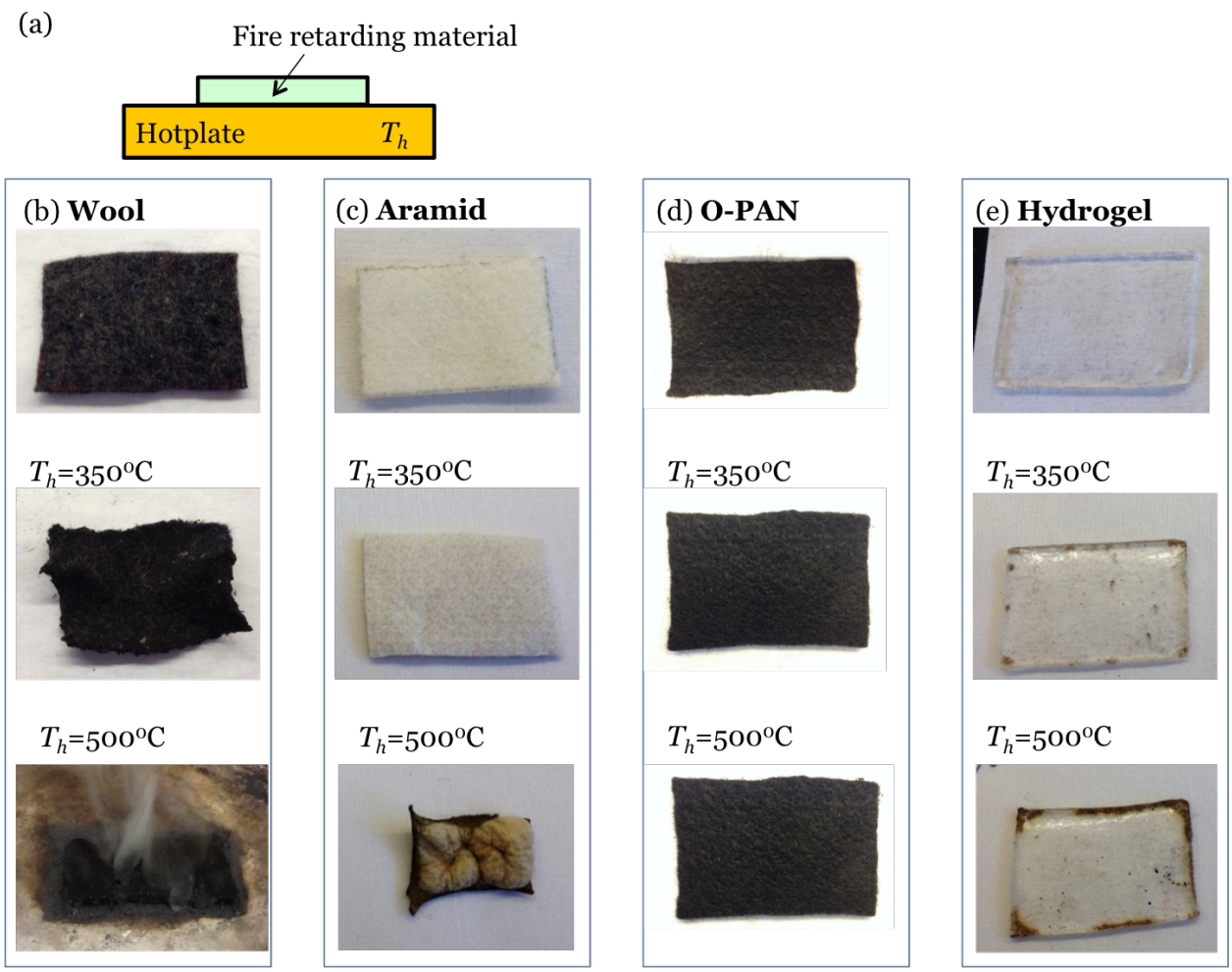

Figure 5.2 Heat resistance of different fire-retarding materials (a) Samples were placed on a hotplate at temperatures T_h=350°C and 500°C and the top surfaces were observed after 30 seconds. (b) Wool carbonized at 350°C and became brittle and stiff compared to initial state. At 500°C it melted on top of the hotplate and cannot be recovered. (c) Aramid fabric resisted heat efficiently at 350°C. But at 500°C it shrank rapidly, it carbonized and turned into a stiff piece of fabric. (d) O-PAN fabric resisted heat efficiently at both temperatures and did not shrink. (e) Hydrogel did not shrink at high temperature and only few parts of the bottom of the hydrogel carbonized but most parts remained undamaged and flexible.

We test the heat resistance of several fire-retarding materials by placing them on a hotplate at 350°C and at 500°C for a period of 30 seconds. Figure 5.2 shows the results for three commercially available fire-retarding fabrics, fire-retarding wool, aramid, O-PAN, as

well as a polyacrylamide-alginate hydrogel.

At 350°C, the wool starts to carbonize and becomes brittle. At 500°C, it disintegrates on top of the hot plate and cannot be recovered. The aramid fabric resists a temperature of 350°C nearly unchanged, but starts to carbonize at 500°C and also becomes stiff and brittle. Aramid fibers are known to start charring around 400°C [79]. On exposure to heat, both wool and aramid form a protective coating or char that insulates the rest of the fabric from the heat source [78]. The fabric, in turn, protects the skin due to its low thermal conductivity. But at high temperatures that are much higher than the decomposition temperature, the fabric decomposed rapidly and provided little or no protection.

The O-PAN fabric (Figure 5.2(d)) resists temperatures up to 500°C with only a slight change in color observed at the side of the fabric in contact with the hot plate. The results for the hydrogel are shown in figure 5.2(e): the hydrogel resists temperatures up to 500°C, except for some slight charring at the edges of the sample. This simple test suggests that both O-PAN fabric and hydrogel can survive temperatures up to 500°C without significant damage. The temperatures of the top surfaces of samples were measured using infrared imaging (FLIR thermal camera) as shown in figure 5.3.

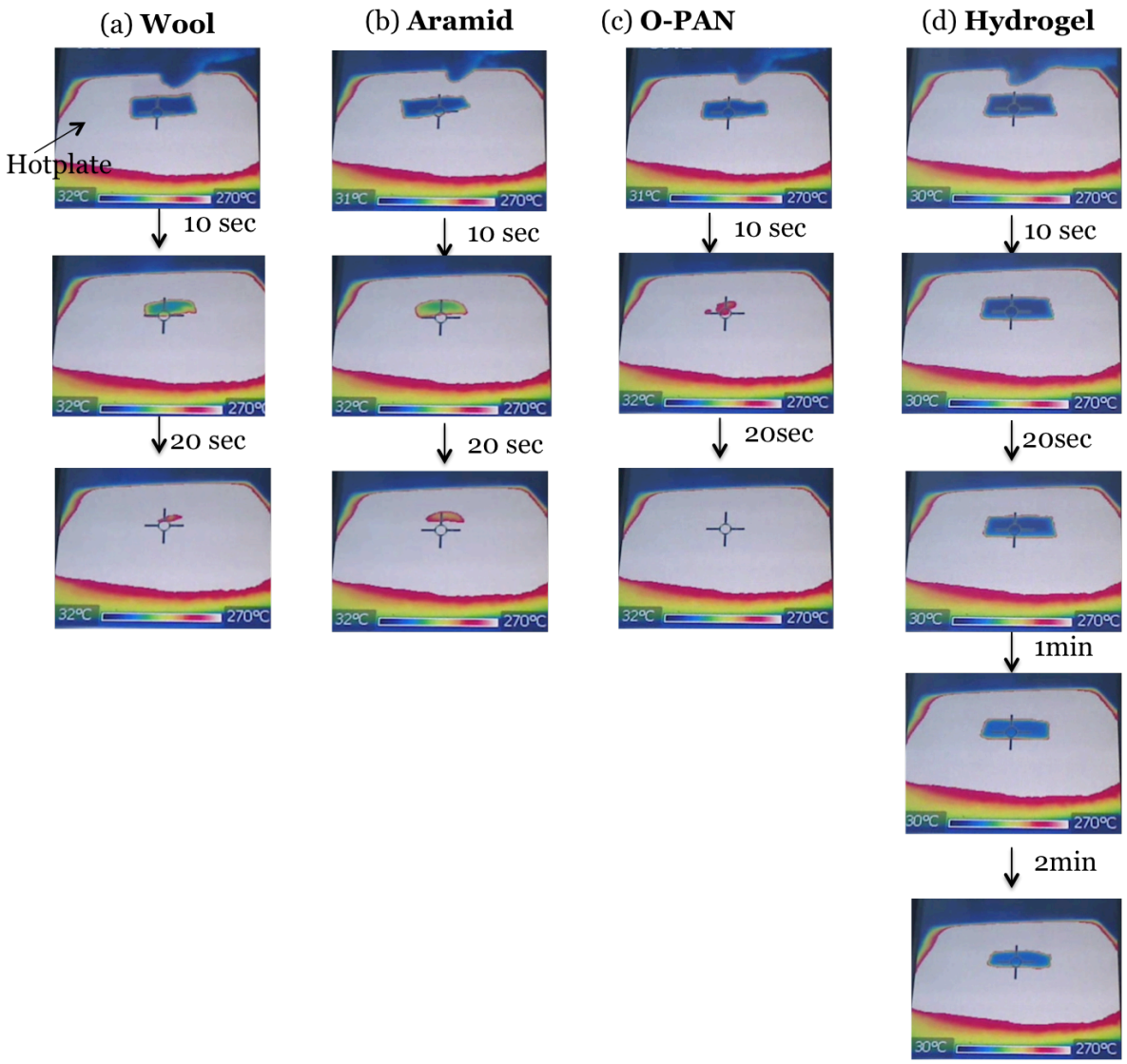

Figure 5.3 Thermal imaging of fire retarding materials**.** Time-lapse infrared thermal images of (a) Wool, (b) Aramid, (c) O-PAN and (d) hydrogel on top of a hotplate at 500°C. All the samples are 3mm thick, 55mm length and 37.5mm width.

It is observed that wool, aramid, O-PAN heat up very rapidly, while the temperature of the hydrogel remains low for a long period of time. Even though O-PAN fabric resists high temperatures very well (figure 5.2(d)), it does not provide good thermal protection. This is understood as follows. Even though the decomposition temperature of this material is much higher than for aramid or wool, the surface facing the heat source can reach very high

temperature. Even with the low thermal conductivity of the O-PAN (~0.04W/mK [94]), the very large temperature gradient across the fabric results in a sufficiently large heat flux to cause skin trauma. When compared with existing fire-retarding fabrics, hydrogels are likely to provide better protection because of their large heat capacity and the large enthalpy of evaporation of the water inside the hydrogel. As the water evaporates, it creates a dry polymer layer that starts to char and a fully hydrated hydrogel layer. These regions are separated by a moving boundary at a fixed temperature of 100°C. This behavior is indeed observed experimentally as shown in figure 5.4. Consequently the remainder of the hydrogel heats up to at most 100°C.

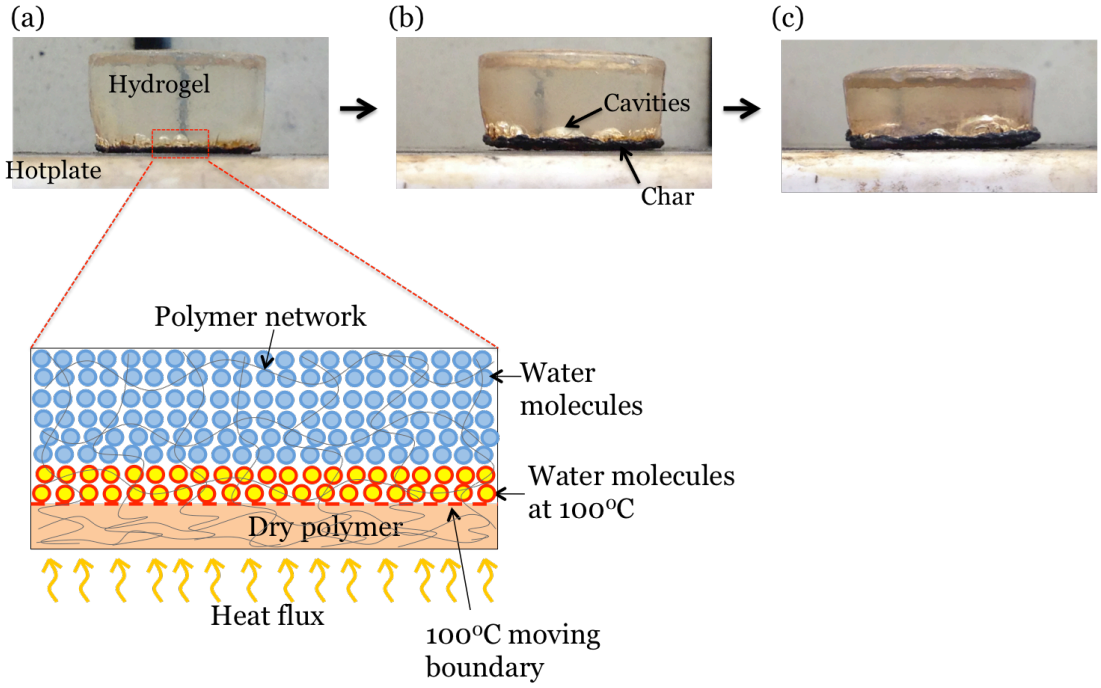

Figure 5.4 Burning process of a hydrogel. (a) 15mm thick and 30mm diameter hydrogel sample is placed on a hotplate with 500°C temperature. Tiny cavities are formed inside the hydrogel near the bottom surface. A schematic is drawn to understand what is happening inside the hydrogel. It seems polymer network suppresses water coming out but due to phase transition at 100°C steam comes out by forming small cavities. Tiny bubbles form inside the

(continued) hydrogel, which collapse eventually. When water is evaporated a dry polymer region form at the bottom and this creates a moving boundary between dry polymer and un-burnt hydrogel. The dry polymer tends to char eventually. (b) The tiny cavities are combined together to form bigger cavities and when they collapse, dry polymer region grows at the expense of un-burnt hydrogel layer. Eventually dry polymer starts to carbonize. (c) With time the hydrogel becomes thinner as the water evaporates and charring layer grows.

5. 3.2 Fire resistance

The fire resistances of wool, aramid, O-PAN fabrics are compared with that of hydrogels in figure 5.5. Wool and Aramid fabrics burn through within a few seconds when exposed to the flame as shown in figures 5.5(a) and 5.5(b). Both O-PAN and the hydrogel, however, withstand the high-temperature flame for a much longer period of time (figures 5.5(c) and 5.5(d)). The O-PAN fabric remains relatively unchanged even after one minute of exposure. Front and rear views of the hydrogel while exposed to the flame are shown in figure S2. As water evaporates from the side exposed to the flame, the hydrogel on that side starts to char. This process is very slow and the remainder of the hydrogel stays flexible (figure 5.5(d)). Figure 5.5(e) shows the burn-through time as a function of sample thickness for several fire-resistant materials. It is evident that both O-PAN and hydrogel are much superior to aramid and fire-retarding wool, and that the fire resistance increases linearly with sample thickness. Even though O-PAN has excellent fire resistance, it heats up rapidly (Figure 5.3) and does not provide much protection to the wearer. The hydrogel, on the other hand, stays much cooler, opening up the possibility of using it as protection in flashover fires.

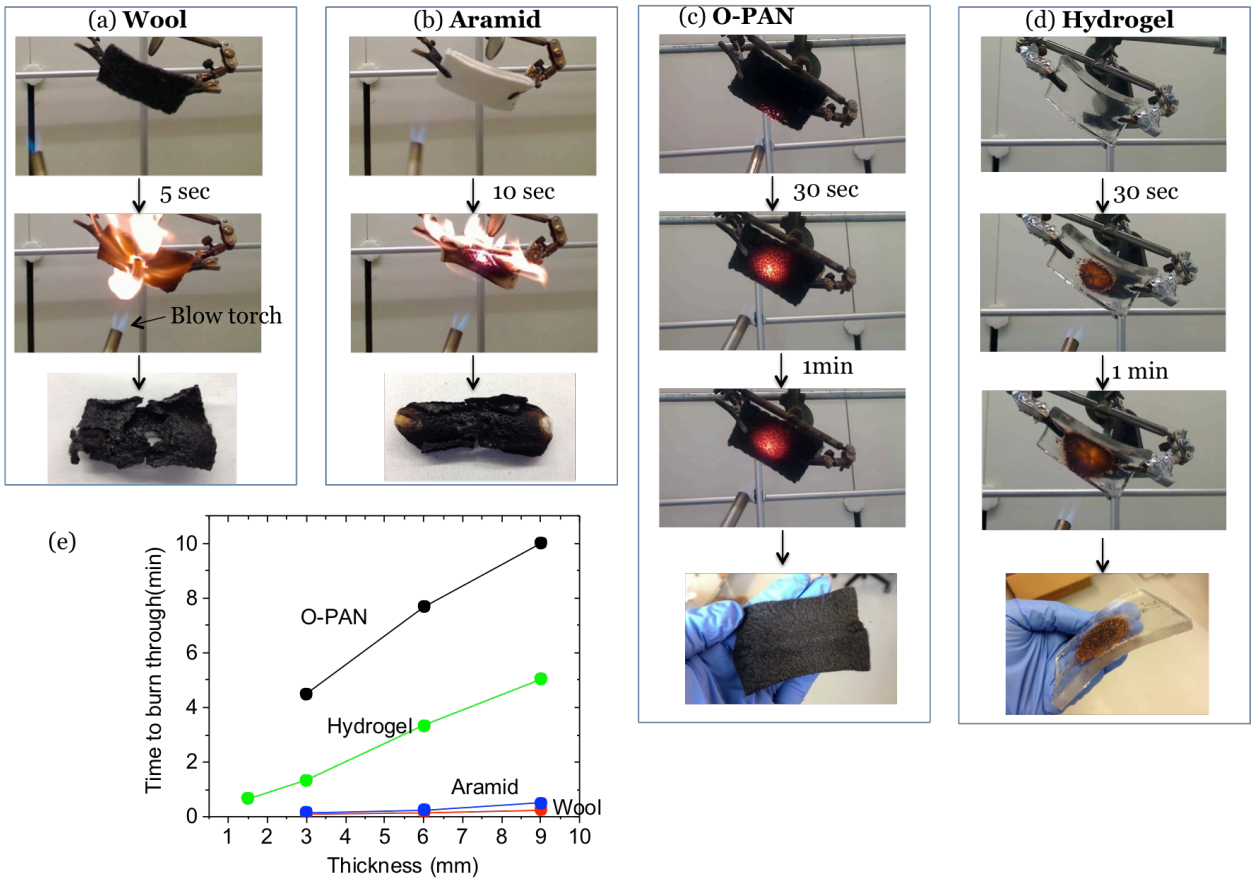

Figure 5.5 Fire resistance of different fire-retarding materials. A blowtorch with a flame temperature of approximately 1000°C is used to perform the tests; all samples had a thickness of 6 mm unless otherwise noted. (a) Wool burned through within a few seconds when exposed to the flame and turned brittle after the test. (b) Aramid fabric burned and shrank rapidly when exposed to flame and became brittle. (c) O-PAN fabric did not burn through until 8 minutes. It remained similar to initial fabric when observed after 1 minute. (d) Hydrogel survived for 4minutes before burning through. It remained flexible even after 1 minute of high-flame exposure. (e) Time to burn through is reported as a function of sample thickness.

5.3.3 Heat transfer model

The goal of this section is to develop a simple model for heat transfer through hydrogels and hydrogel-fabric laminates. We approximate the evaporation of water in the

hydrogel as a one-dimensional heat transfer problem with a moving phase boundary, which we then solve with an enthalpy method [95]. Similar enthalpy models are used for other materials with a moving boundary such as cement mortar mixed with polymer gels [96, 97]. We neglect any flow of water or steam inside of the material. Figure 1 shows a hydrogel-fabric laminate with total thickness t. It contains a hydrogel layer of thickness t_{gel} and a fabric layer of thickness t_f. The hydrogel consists of a polymer network with density ρ_p and heat capacitance c_p, and of water with density ρ_w and heat capacitance c_w. The heat of evaporation of water at its boiling temperature T_b is h_f. The concentration of polymer in the hydrogel is w_p by weight. The insulating fabric has a density ρ_f and a heat capacitance c_f. When a heat flux is applied to the bottom of the hydrogel, the hydrogel heats up until water starts to evaporate. We model the zone in which the phase transition takes place as an infinitely thin boundary at the boiling temperature of water that travels through the hydrogel as shown in Figure 1. The boundary at $x=x_s(t)$ divides the hydrogel in two regions. The material in region I ($x>x_s(t)$) consists of the original hydrogel at temperatures below the boiling temperature. In region II ($x<x_s(t)$), the water is evaporated and the remaining polymer network is at a temperature above the boiling temperature – we neglect the effect of possible charring in the model. While the boundary moves through the hydrogel, the entire sample becomes thinner because the hydrogel dries out. We assume that the layer of insulating fabric constrains the deformation of the hydrogel in the plane of the laminate.

The stretch λ is the ratio of the thicknesses of the dry gel and the swollen gel, and is given by

$$\lambda = \frac{1}{\frac{\rho_p}{\rho_w}\frac{1-w_p}{w_p}+1}. \tag{5.1}$$

In both regions of the hydrogel, Fourier's law [95],

$$q = -k_i \frac{\partial T}{\partial x}, \tag{5.2}$$

is valid, where q is the heat flux per area, T is the temperature, and k_i has to be replaced by the heat conductivities k_I and k_{II} depending on the region. The energy balance requires that in both regions

$$\frac{\partial h}{\partial t} + v\frac{\partial h}{\partial x} = k_i \frac{\partial^2 T}{\partial^2 x}, \tag{5.3}$$

where h is the enthalpy of the material per unit volume in the current state (i.e., either swollen or dehydrated depending on the region) and v the speed at which the material moves due to drying of the hydrogel. The enthalpy of the hydrogel can be described as

$$\begin{aligned} T < T_b: &\quad h = \frac{\frac{c_w}{c_p}\frac{1-w_p}{w_p}+1}{\frac{\rho_p}{\rho_w}\frac{1-w_p}{w_p}+1} c_p \rho_p (T - T_b), \\ T = T_b: &\quad 0 < h < \frac{(1-w_p)}{w_p}\rho_p h_f, \\ T > T_b: &\quad h = \frac{(1-w_p)}{w_p}\rho_p h_f + \rho_p c_p (T - T_b). \end{aligned} \tag{5.4}$$

We take T_b as reference temperature to simplify the equations. If we define the heat capacitance of the hydrated gel referred to the volume of the dry polymer,

$$\tilde{c} = \left(\frac{c_w}{c_p}\frac{1-w_p}{w_p} + 1\right)\rho_p c_p, \tag{5.5}$$

and define the enthalpy of evaporation per unit volume of dry polymer,

$$\tilde{h}_f = \frac{m_w}{V_p} h_f = \frac{(1-w_p)}{w_p}\rho_p h_f, \tag{5.6}$$

then the expression for h can be written as

$$\begin{aligned} T < T_b: &\quad h = \lambda \tilde{c}(T - T_b), \\ T = T_b: &\quad 0 < h < \tilde{h}_f, \\ T > T_b: &\quad h = \tilde{h}_f + c_p \rho_p (T - T_b). \end{aligned} \tag{5.7}$$

To simplify the mathematical analysis we express all quantities in material coordinates; X describes the location of a material point with respect to the original swollen hydrogel. In this coordinate system the phase boundary is at location

$$X_s(t) = \frac{x_s(t)}{\lambda}. \tag{5.8}$$

The energy balance then becomes

$$\begin{aligned} X > X_s(t): &\quad \frac{\partial H}{\partial t} = k_I \frac{\partial^2 T}{\partial^2 X}, \\ X < X_s(t): &\quad \frac{\partial H}{\partial t} = \frac{k_{II}}{\lambda} \frac{\partial^2 T}{\partial^2 X}, \end{aligned} \tag{5.9}$$

where H=λh is the enthalpy of the material in the material coordinate system. In the swollen hydrogel λ=1 and H = h. In the dehydrated region, λ is smaller than one. By introducing the transformation $\hat{T} = T - T_b$ in region I and $\hat{T} = (T - T_b)k_{II}/(k_I\lambda)$ in region II, we reduce both equations in (9) to

$$\frac{\partial H}{\partial t} = k_I \frac{\partial^2 \hat{T}}{\partial^2 X}. \tag{5.10}$$

We also rewrite equation (7) as

$$\begin{aligned} \hat{T} < 0: &\quad H = \lambda \tilde{c} \hat{T}, \\ \hat{T} = 0: &\quad 0 < H < \lambda \tilde{h}_f, \\ \hat{T} > 0: &\quad H = \lambda \tilde{h}_f + \lambda^2 c_p \rho_p k_I / k_{II} \hat{T}. \end{aligned} \tag{5.11}$$

Heat transfer in the insulating fabric is described by the standard heat equation,

$$\rho_f c_f \frac{\partial T}{\partial t} = k_f \frac{\partial^2 T}{\partial^2 X} \tag{5.12}$$

where k_f is the thermal conductivity of the fabric. We integrate equations (5.10) and (5.12) over time with an explicit Euler algorithm and use a central difference scheme to approximate the special derivatives [95]. After each integration step, we use equation (5.11) to update the temperature at each node [95]. In the following, the heat transfer model is validated using a standard test for fire-retarding materials and is then used to optimize the performance of hydrogel and hydrogel-fabric laminates.

We should point out that the thermal model does not consider heat transfer through the hydrogel by radiation. Direct heat transfer by radiation could conceivably raise the temperature of the fabric above 100°C, even if the hydrogel is still fully hydrated. However, water absorbs strongly in the infrared range of the electromagnetic spectrum [98], thus

severely limiting this mode of heat transfer. At temperatures that are sufficiently high for objects to start emitting in the visible range, it may be possible to reduce radiative heat transfer by adding an absorbent dye to the hydrogel.

5.3.4 Thermal protective performance (TPP) test

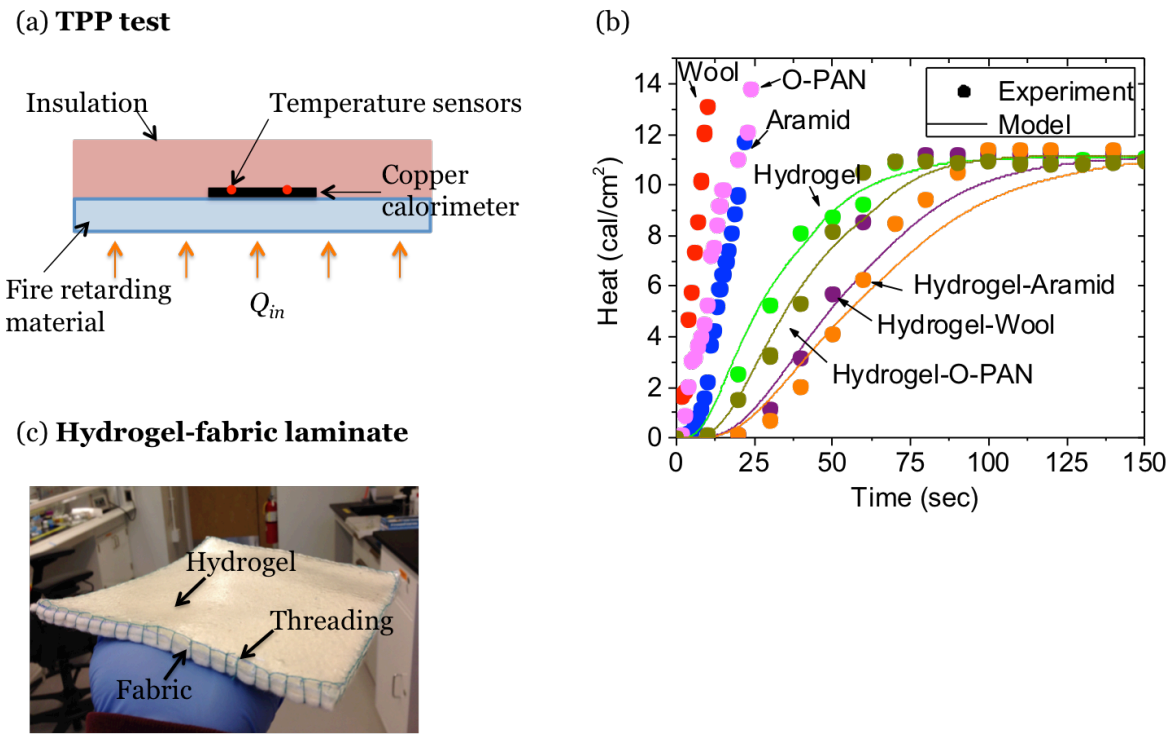

Figure 5.6 Thermal Protective Performance (TPP) test. (a) TPP test set up. (b) Experimental data of heat absorbed by the Copper calorimeter for different fire-retarding materials, along with model predictions. The model curves were calculated using the following materials properties. The specific heats of Aramid, O-PAN, and Wool were taken to be 1748, 740, and 1200 J/kgK, respectively [85,86,94]. The thermal conductivities for Aramid, O-PAN, and Wool were 0.15, 0.031, and 0.04 W/mK [85,86,94,100]. Densities of Aramid, O-PAN, and Wool were respectively 446, 75, and 162 kg/m^3 [measured]. (c) Photo of a hydrogel-fabric laminate. A sheet of hydrogel is threaded with fabric to prepare laminates.

The thermal protective performance test is a standard test developed by the National Fire Protection Association to quantify the performance of fire-retarding materials [93, 99]. The TPP test measures the ability of a fabric to block a heat flux. The test involves exposing the fabric to a combination of radiant and convective heat flux and uses a copper calorimeter placed above the fabric to record the heat transferred through the specimen. The heat/time curve obtained in this test is then compared with the tolerance of human tissue to heat to get a TPP rating [99]. Here we used a modified version of the test using a hot plate (figure 5.6(a)) as described in the experimental section.

The total heat absorbed by the copper calorimeter is plotted in figure 5.6(b) for various fire-retarding materials, both single layers and hydrogel laminates (figure 5.6(c)). The heat transmitted through the Aramid, wool, and O-PAN fabrics increases quickly with time – these materials clearly do not provide adequate protection as the temperature of the hot plate (~500^{o}C) is higher than the fabric decomposition temperature. Heat transmission through the hydrogel sample, on the other hand, is much slower and the total heat absorbed by the calorimeter approaches a steady state as the top surface of the sample reaches 100°C. The laminates show even better performance than the hydrogel sample, with a rate of heat transmission through the hydrogel-aramid sample of half that of the hydrogel sample.

The solid curves in the figure are predictions of the total heat transmitted through the laminates based on the thermal model and data for material properties obtained from the literature. The predictions are in good agreement with the experimental data with only a small discrepancy at higher heat levels, presumably because of charring of the dehydrated

hydrogel. This discrepancy is of little interest since human tissue cannot absorb more than 4-5 cal/cm²s heat during this time period without suffering second-degree burns.

5.3.5 Optimization of hydrogel-fabric laminates

It is evident from figure 5.6(b) that hydrogel-fabric laminates perform better than the individual components of the laminate. We use the thermal model to optimize the laminate design using more realistic boundary conditions and an experimental criterion for second-degree burns, i.e., burns that cause blisters in the epidermis. We only consider hydrogel laminates with wool and aramid, but the optimization is readily extended to other materials.

In the TPP test, the insulating layer on top of the sample imposes a zero-heat flux condition on the top surface of the fire-retarding material. In a more realistic scenario, this flux is not zero. In fact, in a worst-case scenario, the fire-retarding material is in direct contact with the skin. Since even a small increases in temperature can cause a second-degree burn, it seems reasonable to impose a fixed temperature of 37°C, the normal skin temperature of a human, as a boundary condition. To mimic a flashover fire, a heat flux of Q_{in} = 2cal/cm²s is used as a boundary condition for the bottom surface, which faces the heat source (figure 5.7(a)). Figures 5.7(b) and (c) show the heat output from the laminate, i.e., the heat absorbed by the skin, for hydrogel-aramid and hydrogel-wool laminates, respectively. Curves are shown for different ratios of hydrogel to laminate thickness.

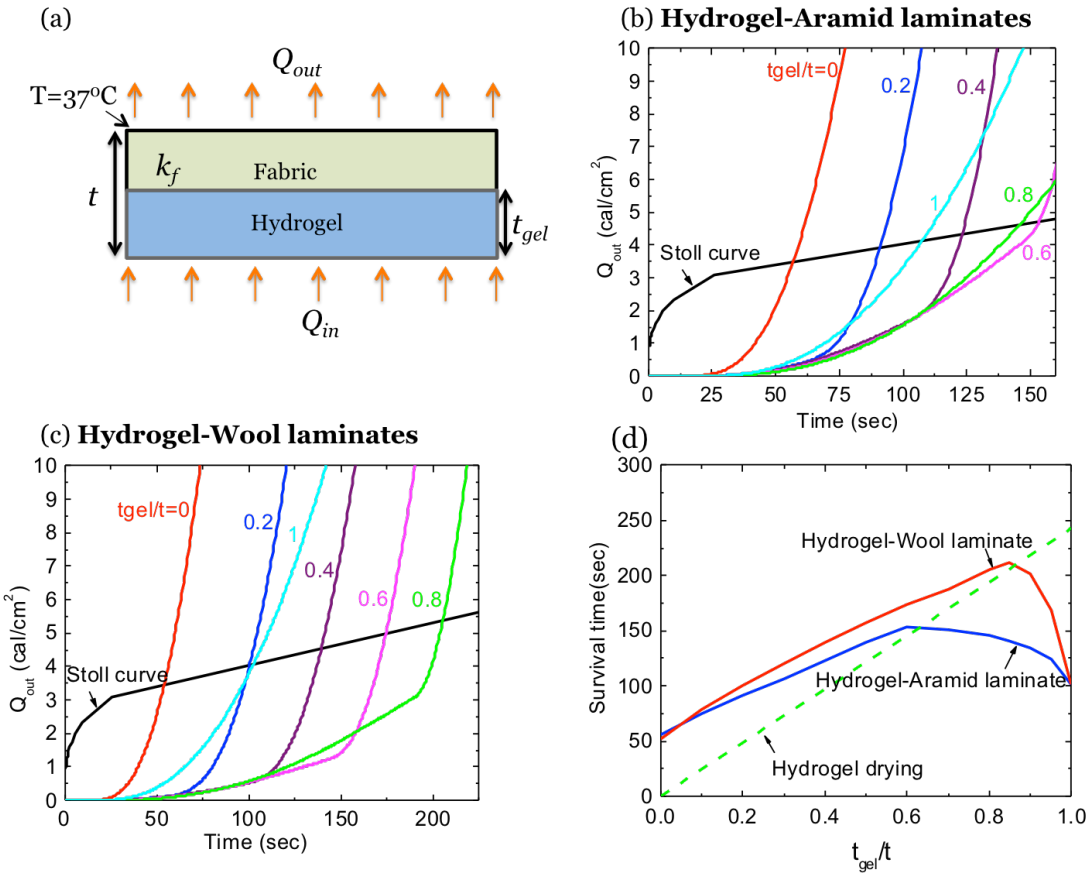

Figure 5.7 Optimizing the parameters with heat transfer model. (a) Proposed set up to measure the performance of hydrogel-fabric laminates. (b) Heat output from hydrogel-Aramid laminates for different t_{gel}/t values are compared with the Stoll curve. Total thickness used is t=9mm. (c) Heat output from hydrogel-wool laminates for different t_{gel}/t values are compared with Stoll curve. Total thickness used is t=9mm. (d) The survival times are obtained from the intersection points of Stoll curve and heat out put of laminates. Dash line denotes the time to evaporate all the water in hydrogels for different thicknesses.

Along with the results from the thermal model, we also show the Stoll curve, an experimental criterion for second-degree burns. Stoll et al used heat exposures on human skin to determine the level of total heat that caused a second-degree burn in a given amount of time [101]. They varied the heat flux and measured the time to cause a second-degree burn. The Stoll curve is then a graph of the total heat, obtained by integrating the heat flux over

time, versus the time it takes to cause a burn. As long as the heat transmission curve for a laminate lies below the Stoll curve, the laminate provides sufficient protection. The intersection points with the Stoll curve provide the onset of second-degree burns and thus the maximum time the laminate is effective. These survival times are plotted in figure 5.7(d) as a function of the ratio of hydrogel to laminate thickness. The dashed line in the figure represents the time to completely dry out the hydrogel. As soon as the hydrogel is dehydrated, its temperature can rise beyond 100°C, leading to possible decomposition of the insulating fabric. Since the thermal model does not take into account thermal decomposition, care must be exercised interpreting the survival curves to the left of the dashed curve – the dashed curve is effectively a lower bound for the survival time. It is evident from the figure that the hydrogel laminates perform much better than the individual components used to fabricate the laminate and that there is an optimum thickness ratio that maximizes survival time. Furthermore, the laminates with wool perform better than those with aramid because wool has a lower thermal conductivity. In fact, the thermal conductivity of the fabric is more important to the performance of the laminate than its heat resistivity or decomposition temperature.

Given the thermal properties of hydrogel-fabric laminates, use of these laminates in fire-retarding products such as fire blankets and apparel seems attractive. The laminates are inexpensive compared to most of the highly engineered fire-retarding polymer fabrics and are fabricated from materials that are widely available. One can easily imagine use of these laminates as fire blankets in house fires, a leading cause of burn injuries. Similarly one can envision protective suits for use by fire fighters.

5.4 Summary

Widely used fire-retarding polymer fabrics protect skin from burn injuries mainly due to their high decomposition temperature and low thermal conductivity. Above the decomposition temperatures, they do not provide good protection. Hydrogels can be used in fire-retarding applications, but cannot be used for a long period of time since they quickly reach 100°C because of the high thermal conductivity of water. By combining hydrogels and fabrics into laminates, it is possible to design fire-retarding materials that perform better than either fabric or hydrogel: the hydrogel protects the fabric from high temperatures, while the fabric keeps the skin at a safe temperature because of its low thermal conductivity.

Chapter 6

Force and stroke of a hydrogel actuator

6.1 Introduction

A hydrogel consists of a network of cross-linked hydrophilic polymer chains dispersed in water. The water concentration in the gel, and hence its degree of swelling, can vary markedly with temperature [102, 103, 104], pH [105, 106] or even electric field [107]. This ability to respond to an external stimulus can be used in a range of applications, including sensors [108, 109], actuators in microfluidic devices [110, 111, 112] and drug delivery [113, 114]. Here we are interested in exploring the performance of hydrogels in actuator applications. Actuators are usually characterized by their force-stroke curves [115, 116]. The stroke of an actuator is defined as the displacement achieved by the actuator under a given force, critical information when designing an actuator. In general, stroke and force are inversely related [115, 117, 118]. Even though the concept of a force-stroke curve is widely used in the field of actuators, it is not in the field of hydrogels. Free swelling of hydrogels has of course been studied extensively, but constrained swelling where the hydrogel exerts a force, is much less explored [104, 119]; complete force-stroke curves for hydrogels are not currently available in the literature.

We derive expressions for the force-stroke curve of a hydrogel and explore the use of force-stroke curves to characterize the actuating properties of hydrogels, using poly (N-isopropylacrylamide) as a model material. Poly (N-isopropylacrylamide), commonly abbreviated as PNIPAm, is a widely studied temperature-sensitive hydrogel. PNIPAm

hydrogels exhibit a reversible, continuous volume phase transition, when the temperature is increased above a critical temperature T_c [102, 120]. The volume phase transition is attributed to a coil-globule transition of the polymer chains that occurs at this temperature [121]. As illustrated in figure 6.1, the hydrogel can absorb a large amount of water at temperatures below T_c, but not at higher temperatures. This ability to swell and shrink in response to a temperature change makes PNIPAm a candidate for use in actuators.

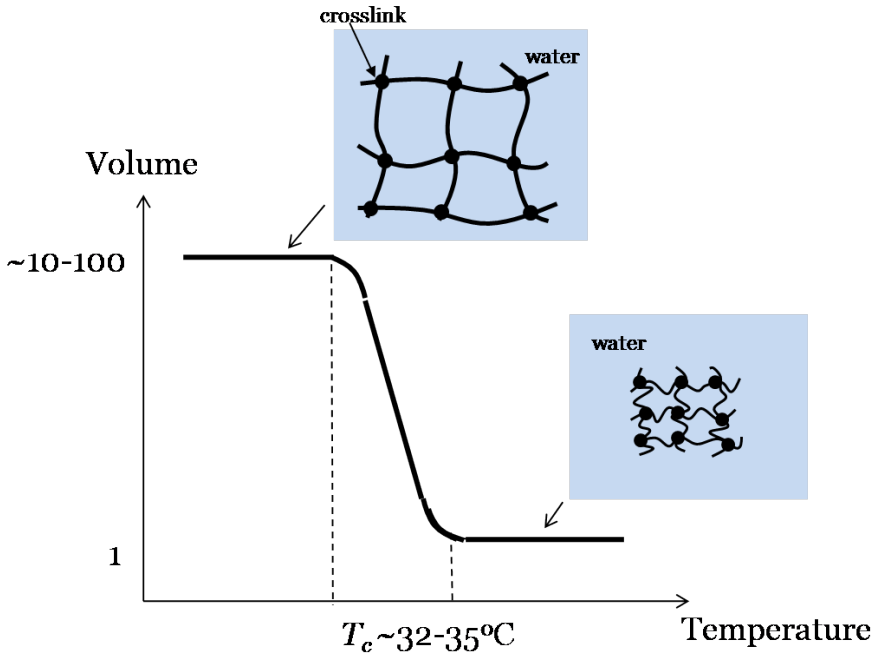

Figure 6.1 Volume phase transition of PNIPAm hydrogels. In the figure, the y-axis is the volume of the hydrogel relative to the volume of the dry polymer network. A swollen PNIPAm hydrogel is ~ 10-100 times the volume of the dry polymer network. Upon heating the PNIPAm hydrogel, the volume drastically reduces in the range of T_c~32-35°C. At high temperature, the volume of the hydrogel approaches the volume of the dry polymer network.

In this paper, we first use the model of the ideal elastomeric gel [122, 123] to predict the

force-stroke curves of a temperature-sensitive hydrogel. We then describe an experimental method for measuring the force-stroke curves and evaluate the effect of cross-link density. We demonstrate very good agreement between the theoretical curves and the experiments measurements for a broad range of cross-link densities.

6.2 The ideal elastomeric hydrogel

According to the classical theory of Flory and Rehner [124], the elasticity of a polymer network can be described by the Gaussian chain model, while the mixing of polymer and solvent can be described by the Flory-Huggins model [125, 126].These original models have often been modified to fit experimental data [103, 127]. Here we use the model of the ideal elastomeric gel [122], which does not invoke the Flory-Huggins model, but instead relies on the following two basic assumptions. First, the volume of the gel is equal to the sum of the volume of dry polymer network and the absorbed solvent. Second, the Helmholtz free energy of the gel is separable into a contribution due to stretching of the network and one due to mixing of polymer and solvent. The latter is conveniently represented by the osmotic pressure as a function of the swelling ratio, $\Pi_{mix}(J)$. Li et al [123] verified the model of the ideal elastomeric gel for polyacrylamide gels and demonstrated that the $\Pi_{mix}(J)$ obtained through different experimental methods is consistent.

We use the model of the ideal elastomeric gel to describe the chemo-mechanical behavior of a temperature-sensitive hydrogel. Consider a stress-free cube of dry gel with unit dimensions as shown in figure 6.2.

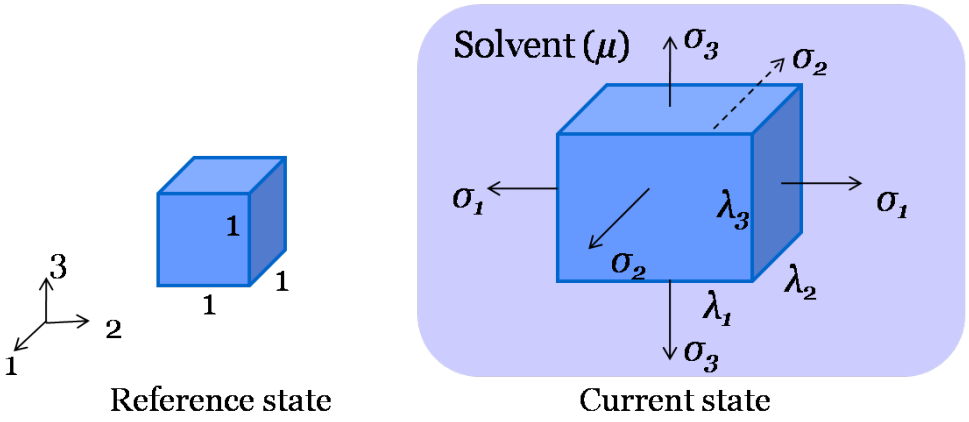

Figure 6.2 The reference state is a dry polymer network of unit dimensions, subjected to no applied stresses. The current state is a swollen gel stretched into a rectangular block. The gel is submerged in an aqueous environment in which the chemical potential of water is μ, and is subjected to stressess$_1$,s$_2$, and s$_3$.

We take this state as the reference state. In the current state, the gel is submerged in an aqueous environment in which the chemical potential of water isμ, and the gel is subjected to Cauchy stresses s$_1$, s$_2$, and s$_3$. By convention, the chemical potential of pure liquid water is set to zero. The gel absorbs C water molecules and turns into a block of dimensions $\lambda_1 \times \lambda_2 \times \lambda_3$. The swelling ratio J is then given by $J = \lambda_1\lambda_2\lambda_3$.If we take the Gaussian chain model to describe the mechanical behavior of the polymer network, the equations of state of a swelling hydrogel can be written as [21, 22, 27],

$$\sigma_1 = \frac{NkT}{J}(\lambda_1^2 - 1) - \Pi_{\text{mix}}(J,T) - \frac{\mu}{\Omega}, \tag{6.1a}$$

$$\sigma_2 = \frac{NkT}{J}(\lambda_2^2 - 1) - \Pi_{\text{mix}}(J,T) - \frac{\mu}{\Omega}, \tag{6.1b}$$

$$\sigma_3 = \frac{NkT}{J}(\lambda_3^2 - 1) - \Pi_{\text{mix}}(J,T) - \frac{\mu}{\Omega}. \tag{6.1c}$$

$$J = 1 + WC \tag{6.1d}$$

where N is the crosslink density of the gel, kT the temperature in units of energy, and W the

volume per water molecule. The osmotic pressure has two contributions: $\Pi_{mix}(J, T)$ is the osmotic pressure inside the hydrogel in equilibrium with pure water, and μ / W is the additional contribution if the hydrogel is in equilibrium with an aqueous environment in which the chemical potential of water is different from zero. P_{mix} is a function of the swelling ratio J and the temperature T, but not of the crosslink density of the gel [123]. The quantity NkT is the shear modulus of the dry polymer network. The Gaussian chain model is not an essential part of the ideal elastomeric gel model. Any model that accurately describes the mechanical behavior of the polymer network can be used.

According to equation (6.1), the applied stresses are balanced by the stresses that arise because of the elastic deformation of the polymer network and the total osmotic pressure inside the gel. To fully characterize the response of a temperature-sensitive gel that follows the Gaussian chain model, it is sufficient to know the scalar NkT and the function Π_{mix} (J, T). If we fix the temperature, then $\Pi_{mix}(J)$ is a single variable function that does not depend on crosslink density and that is a unique function for each type of hydrogel.

6.3 Derivation of the force-stroke curves

Consider a hydrogel immersed in pure liquid water ($\mu = 0$). Subject to a change in temperature, the hydrogel goes through a volume phase transition. As the volume changes, the hydrogel is free to expand or contract in the x_1 and x_2-directions, but exerts a force in the x_3-direction. Figure 6.3 illustrates schematically how to generate the force-stroke curve for the hydrogel.

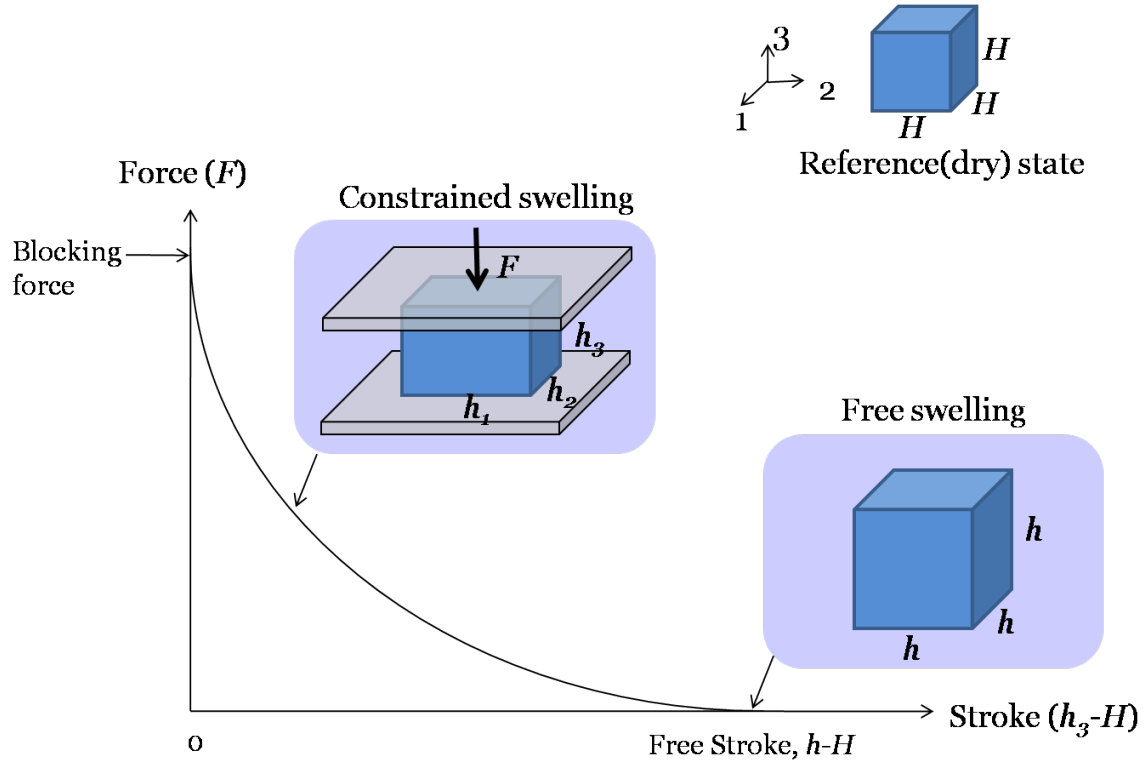

Figure 6.3 Force-stroke curve of a hydrogel actuator. In the reference state, the gel is dry and forms a cube with side H. F is the actuation force and h_3–H is the stroke. When the hydrogel swells freely without applying any force, it generates the maximum stroke, h-H, called the free stroke. If the hydrogel swells under constraint, it generates a force that increases with decreasing stroke. The hydrogel generates the maximum, or blocking, force, at zero stroke.

The reference state of the hydrogel is a cube of the hydrogel in the dry state, at a temperature above the critical temperature, T_c. The length of the cube edge is designated by H. If the gel is allowed to swell under zero external force at a temperature below T_c, it forms a cube with edge length h. The corresponding actuator displacement, h-H is defined as the "free stroke". If the height of the gel is limited to $h_3 < h$, then swelling is constrained and the gel generates a force F. The force that completely blocks swelling in the x_3-direction, i.e., $h_3 = H$, is referred to as the blocking force. Define the stretches by $l_1 = h_1/H$, $l_2 = h_2/H$, $l_3 = h_3/H$, the true stress by $s_3 = F/(h_1h_2)$, and the nominal stress by $s_3 = F/H^2$.

We derive the force-stroke curves based on the model of the ideal elastomeric gel. In the current state, $\sigma_1 = \sigma_2 = 0$ and $\lambda_1 = \lambda_2$. Thus the swelling ratio can be written as, $J = \lambda_1^2\lambda_3$. From equation (6.1a), it follows that

$$\frac{NkT}{\lambda_1^2\lambda_3}(\lambda_1^2 - 1) - \Pi_{\text{mix}}(J,T) = 0, \tag{6.2}$$

Whereμ/W was set to zero because the hydrogel is in equilibrium with pure water. If the function $\Pi_{\text{mix}}(J)$ is known for the hydrogel, equation (6.2) can be used to calculateλ_1 as a function of λ_3. Equation (1c) then yields

$$\sigma_3 = NkT\left(\lambda_3 - \frac{1}{\lambda_3}\right) - \Pi_{\text{mix}}(J,T)\lambda_3^2 \tag{6.3}$$

And the nominal stress becomes,

$$s_3 = NkT\lambda_1^2\left(\lambda_3 - \frac{1}{\lambda_3}\right) - \Pi_{\text{mix}}(J,T)\lambda_1^2\lambda_3^2. \tag{6.4}$$

This is the expression for the force-stroke curve of a hydrogel. The derived force-stroke relation is the steady-state relation; solvent migration makes the actual performance of a gel actuator highly time-dependent. It is evident from equation (6.4) that the force-stroke curve can be calculated if the function $\Pi_{\text{mix}}(J,T)$ is known. Figure 6.4 shows this relationship for PNIPAm hydrogels using the $\Pi_{\text{mix}}(J,T)$curve measured using the procedure described in the next section. It is observed that the blocking force ($\lambda_3 = 1$) increases with increasing cross-link density, while the free stroke ($s_3 = 0$) decreases.

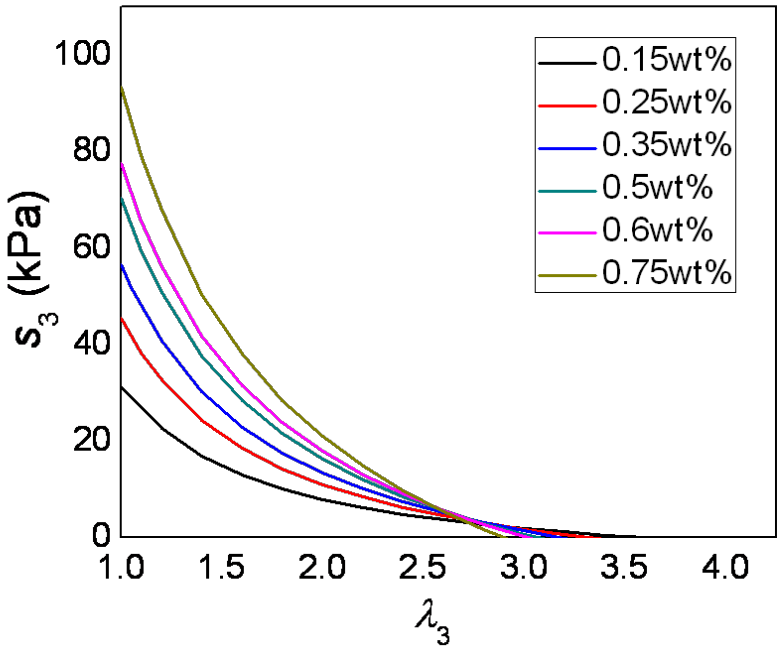

Figure 6.4 Force-stroke curves for PNIPAm hydrogels with different cross-link densities, derived using the ideal elastomeric gel theory and the experimentally measured $\Pi_{mix}(J,T)$ function. Force is converted to nominal stress s_3 and stroke is converted to stretch λ_3. The blocking force (λ_3=1) increases and the free stroke (s_3=0) decreases with increasing cross-link density.

6.4 A procedure for measuring $\Pi_{mix}(J)$

The force-stroke curve of a hydrogel requires knowledge of the $\Pi_{\text{mix}}(J,T)$ function. Here we describe a simple procedure for measuring this function experimentally based on free swelling of gels in environments with controlled chemical potentials. Under conditions of free swelling, no stresses are applied to the gel and swelling is isotropic. If $\lambda_1 = \lambda_2 = \lambda_3 = \lambda_f$, then equation (6.1) implies that

$$\sigma_1 = \frac{NkT}{\lambda_f^3}\left(\lambda_f^2 - 1\right) - \Pi_{\text{mix}}(J,T) - \frac{\mu}{\Omega} = 0. \tag{6.5}$$

Solving for the osmotic pressure yields

$$\Pi_{\text{mix}}(J,T) = G\left(1 - \frac{1}{\lambda_f^2}\right) - \frac{\mu}{\Omega}, \tag{6.6}$$

where G = NkT/λ_f is the shear modulus of the gel in the swollen state. It is clear from equation (6.6) that the osmotic pressure can be determined by measuring the free-swelling stretches as a function of the chemical potential of water in the environment. These measurements can be implemented using the following approach, suggested in references [129, 130]. Enclose a hydrogel in a flexible water-permeable membrane and submerge it in a mixture of water and a second compound. This second compound needs to satisfy two conditions: 1) the compound cannot migrate through the membrane and 2) the chemical potential of water in the mixture must be well known, e.g., through a series of osmotic pressure experiments such as those described in references [131, 132]. If the chemical potential of water in the hydrogel is different from that in the mixture, water will migrate through the membrane to equalize the potentials and the gel will expand or shrink, as may be the case. The flexible membrane serves to prevent the second compound from diffusing into the gel and thus change the chemical environment, but should not impede the volume change in any way. Once equilibrium is established, the function $\Pi_{\text{mix}}(J,T) = \Pi_{\text{mix}}(\lambda_f^3, T)$ can be calculated from the chemical potential of water in the mixture and the stretch λ_f using equation (6.6). Repeating this procedure for different water mixtures and temperatures, establishes $\Pi_{\text{mix}}(J,T)$ as a function of J and T.

6.5 Experimental

6.5.1 Sample fabrication

PNIPAm hydrogels were prepared using the following procedure: 1.1111 g of N-Isopropylacrylamide (NIPA, Sigma-Aldrich, 415324) and different amounts of N-N-

methylenebisacrylamide(MBAA, Sigma-Aldrich, M7279) were dissolved in distilled water as shown in table 1.To these mixtures, 9.889 mg of ammonium persulfate (AP, Sigma-Aldrich, A9164) was added as photo initiator and 25.56 mg ofN,N,N¹,N¹-tetramethylethylenediamene (TEMED, Sigma-Aldrich, T1024) was added as cross-link accelerator. The solutions were poured into glass molds with dimensions 70 × 30 × 3mm³and covered with glass slides. The gels were cured at room temperature by exposing them to ultraviolet light with a wavelength of 254 nm and a power of 8 W for a period of 4 hours inside a UVC 500 system (Hoefer). This procedure resulted in PNIPAm hydrogels with various levels of cross-linking as listed in Table 6.1.

Sample	Amount of MBAA (mg)	$\frac{W_{MBAA}}{W_{MBAA}+W_{NIPAm}}\times 100\%$
1	1.7	0.15
2	2.8	0.25
3	3.9	0.35
4	5.6	0.5
5	6.7	0.6
6	8.4	0.75

Table 6.1 Synthesis data for PNIPAm hydrogels.

6.5.2 Characterization of $\Pi_{mix}(J,T)$

The P_{mix} (J, T) function was measured for the PNIPAm samples using the procedure outlined earlier in this paper. Immediately after synthesis, PNIPAm samples with different

cross-link densities were submerged in mixtures of water and polyethylene glycol (PEG, BioUltra, MW20000, Sigma-Aldrich 95172), which is a convenient method of controlling the chemical potential of water in the environment. PEG was selected because it is a water-soluble polymer that is readily available in different molecular weights. Mixtures of PEG and water have been extensively characterized and the chemical potential of water in these mixtures is well known (Fig. 6.5(a)) [131, 132].

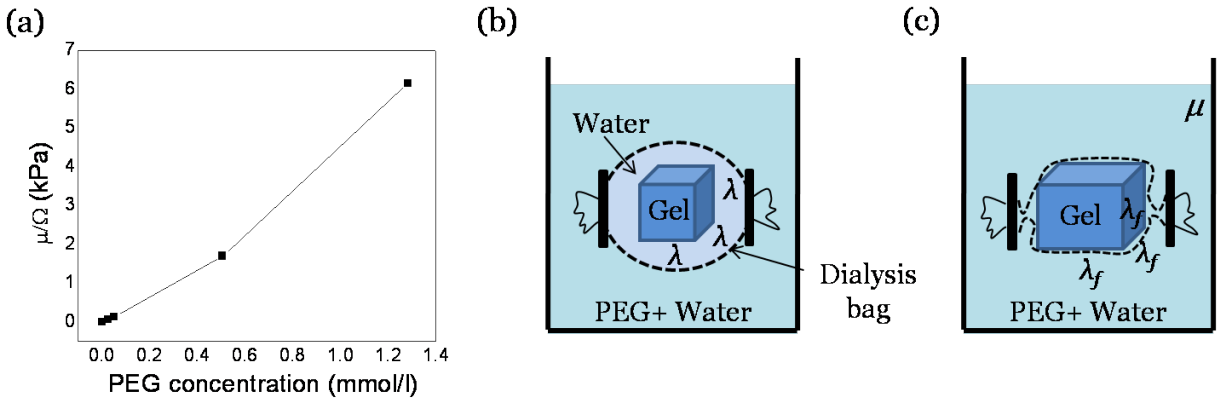

Figure 6.5 Free swelling of hydrogels in equilibrium with an aqueous solution of PEG. (a) Chemical potential of water in aqueous solutions of PEG [131, 132]. (b) Freshly prepared PNIPAm hydrogels are enclosed inside dialysis bags containing deionized water and are immersed invarious concentrations of water/PEG solutions. The stretch l represents the stretch of the freshly prepared sample with respect to its dry reference state. (c) When the hydrogel equilibrates with the water/PEG solution, all water in the dialysis bag disappears. The free stretch l_f represents the stretch of the equilibrated sample with respect to its dry reference state.

To prevent the PEG from diffusing into the PNIPAm, the samples were enclosed inside dialysis bags (cellulose membrane, Sigma Aldrich D9527) along with a small amount of deionized water (figure 6.5(b)). Dialysis bags were selected as water-permeable membranes

because the pores in dialysis membranes allow water to pass through, but not PEG. The dialysis bags were much larger than the samples, so that they did not exert any mechanical constraint on the samples. This experiment was performed right after synthesizing the PNIPAm samples so that their water content was fixed at approximately 90% for all samples. Six different water/PEG solutions were prepared with PEG concentrations of 0, 0.025, 0.05, 0.505 and 1.282 mmol/l. All experiments were performed at 20°C. The samples, $10 \times 10 \times 3\text{mm}^3$ in size, were submerged for a period of one week, which was sufficient to establish equilibrium between the sample and the PEG solution. The samples were then removed from the dialysis bags, any surface water was removed by blotting with a tissue paper, and the free swelling ratio, l_f, was measured for each sample using the gravimetric method. Specifically, the samples were weighed using an analytical scale to obtain weight, W_{gel},of the samples in equilibrium with the PEG solution. The weight of the dry samples, W_{dry}, was determined after freeze-drying the samples. This was accomplished by freezing the samples at -80°C and then transferring them to a freeze-dry system (Labconco Corporation) at a temperature of -50°C.The samples were removed from the freeze-dry system after 3 days when they were fully dehydrated. The free swelling ratio, l_f, was calculated from

$$\lambda_f = \left(\frac{W_{\text{gel}}}{W_{\text{dry}}}\right)^{1/3}. \tag{6.7}$$

The osmotic pressure was calculated from l_f and μ using equation (6.6). Because all measurements were performed at 20°C, we denote P_{mix} (J, T) henceforth as $\Pi_{mix}(J)$.

6.5.3 Mechanical characterization and Measurement of force-stroke curves

Uniaxial compression tests were performed using an AR-G2 rheometer (TA

instruments) as shown in figure 6.6(a).

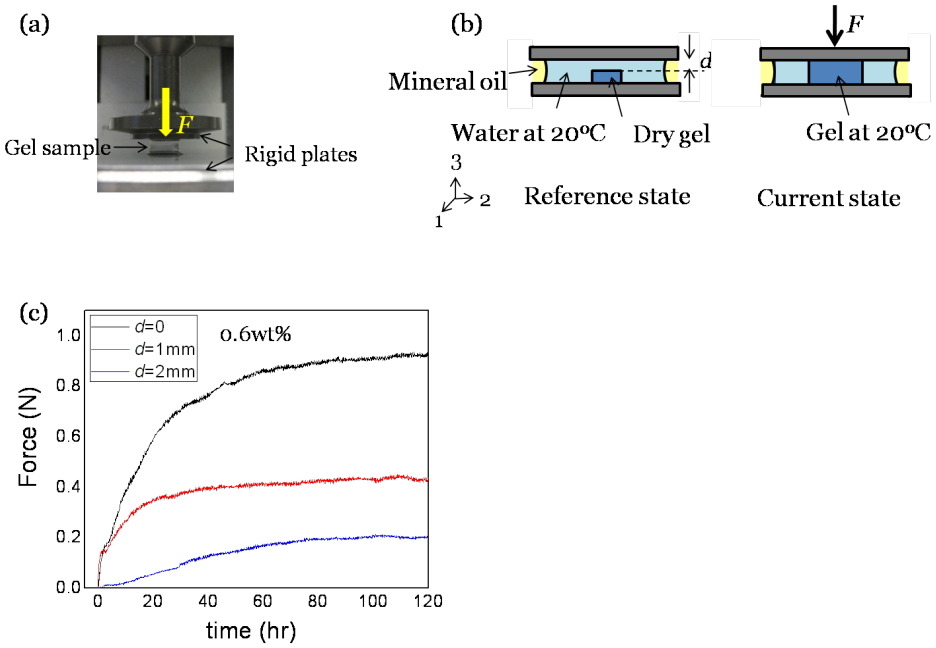

Figure 6.6 Mechanical characterization and measurement of the force-stroke curves. (a) Uniaxial compression test for measuring the shear modulus. Hydrogels were compressed under two rigid plates and the force-displacement data were recorded to obtain the shear modulus. (b) Setup for the constrained swelling experiment. The reference state shows a dry PNIPAm gel submerged in water at 20°C; this gel is placed between two rigid plates with a gap, d between the sample and the upper plate. Mineral oil is used to prevent water evaporation during the experiment. The current state shows the swollen gel in the equilibrium state. The force F generated by the hydrogel is recorded as a function of time until it saturates. (c) Force-time curve for a 0.6wt% PNIPAm hydrogel and for different values of d.

Rectangular samples with dimensions of 4× 4× 3 mm^3were compressed at a rate of 100μm/min until a strain of 5% strain was reached. Young's modulus was calculated from the slope of the stress-strain curves and the shear modulus, G, was obtained as one third of the Young's modulus on the assumption that hydrogels are incompressible at small strains and on the time scale of the experiment. A total of three PNIPAm samples were tested for each cross-link density.

The force-stoke curves were measured following the approach described earlier. Specifically, after synthesis the PNIPAm gels were allowed to fully swell in DI water at room temperature. Cylindrical samples with a diameter of 10 mm were cut from the swollen gels using a hole punch. The thickness of the samples was approximately 5 mm, but varied somewhat with cross-link density. These samples were heated to 50°C and kept at this temperature for three days to allow them to reach their dry equilibrium state. The dried samples were then allowed to cool to room temperature before performing constrained swelling experiments inside the AR-G2 rheometer. The initial state is shown schematically in figure 6.6(b), where a dry PNIPAm sample is placed between two rigid plates and submerged in water at 20°C. The sample swells by absorbing water and generates a force when it touches the upper plate. This force was recorded as a function of time until the sample was fully saturated and the force reached a steady-state value as shown in figure 6.6(c). Force-time curves were measured as a function of the initial gap d between sample and plate (figure 6.6(b)). The saturation force was converted to a nominal stress by normalizing the force with the initial cross-sectional area of the sample; the stroke was converted to stretch, l, by normalizing with the initial sample height. Force stroke curves were measured for all PNIPAm samples listed in Table 6.1. The subscript 3 in the remainder of the text refers to the loading direction.

6.6 Results and discussion

Figure 6.7(a) shows the free swelling ratio, λ_f as a function of PEG concentration for PNIPAm samples with different levels of cross-linking; figure 6.7(b) shows the corresponding shear moduli.

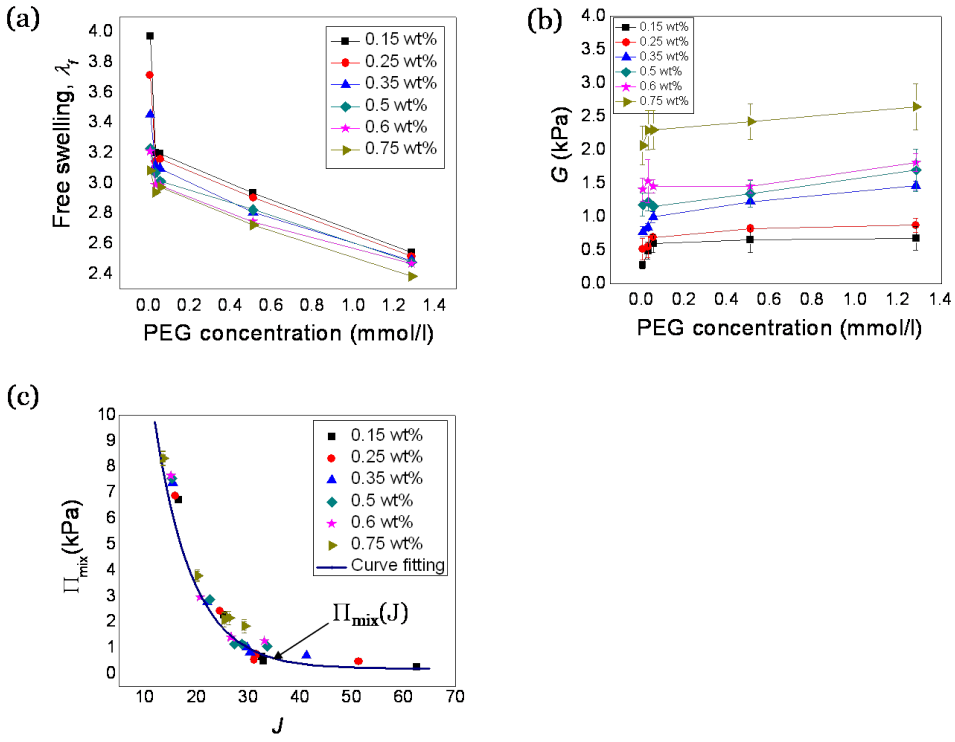

Figure 6.7 Determination of the osmotic pressure function $\Pi_{mix}(J)$. (a) Free swelling ratio λ_f of PNIPAm hydrogels as a function of PEG concentrations. Curves with different symbols represent the free swelling ratios for hydrogels with different cross-link densities.(b) Shear modulus of PNIPAm hydrogels with different cross-link densities as a function of PEG concentration. (c) Experimental values of the osmotic pressure for PNIPAm hydrogels with different cross-link densities. Data for different cross-link densities collapse into a single $\Pi_{mix}(J)$curve.

Together with the chemical potential of water in aqueous PEG solutions, figure 6.5(a), these experimental results can be used to calculate $P_{mix}(J)$ from equation (6.6). The result is plotted in figure 6.7(c). Even though samples with different cross-link densities have different shear moduli and different swelling ratios, their osmotic pressure functions collapse into a single master curve. This master curve is independent of cross-link density and can be regarded as a material property of PNIPAm hydrogels. Evidently, the cross-link density of the hydrogels is low enough that the cross-links do not substantially alter the

chemical interactions between the PNIPAm polymer chains and the surrounding water. This observation is not unique to PNIPAm, but has also been established for other gels such as polyacrylamide gels [123].Even though the osmotic function was derived from free-swelling data, it can be used to predict the behavior of PNIPAm hydrogels under complex conditions of loading and in various chemical environments. It is convenient to represent the data in figure 6.7(c) by a curve fit

$$\Pi_{\text{mix}}(J) = 0.2 + 50 \times \exp(-0.138J)\text{kPa}, \tag{6.8}$$

which is valid at 20°C in the range 12 < J < 65.

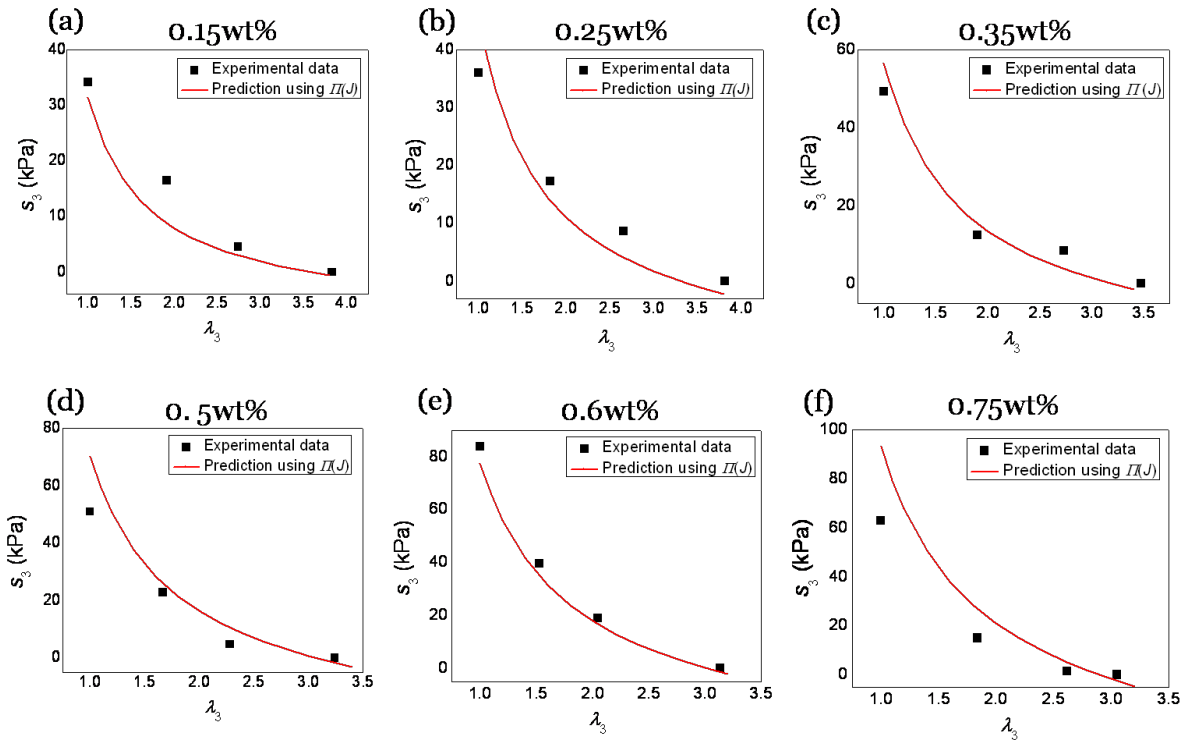

Figure 6.8 Force- stroke curves. Force is converted to nominal stress s_3 and stroke is converted to stretch λ_3. Curves (a)-(f) show s_3- λ_3 curves for PNIPAm hydrogels with different cross-link densities. Cross-link weight percentages are denoted for each curve. Black squares correspond to experimental results and curves are predictions from the ideal elastomeric model.

Figure 6.8 shows normalized force-stroke or stress-stretch curves for samples with different cross-link densities. Black squares correspond to experimental data and the red lines are predictions based on the ideal elastomeric model, equation (6.4), and the curve fit to the osmotic pressure function, equation (6.8). The shape of the curves in figure 6.8 is typical for force-stroke curves: The force is greatest when the actuator is blocked and decreases with increasing stroke. The blocking force increases with increasing crosslink density, while the free stroke decreases. The effect of cross-link density on the free swelling of PNIPAm hydrogels is well documented in the literature [133, 134]: Increasing the cross-link decreases the free swelling without changing the transition temperature. This observation is consistent with our results that the free stroke decreases with cross-link density. The effect on the blocking force is, however, subtler: As the cross-link density increases, the hydrogel becomes stiffer and swells less. The blocking force depends on both of these factors. Even though our experimental results show that blocking force increases with increasing cross-link density, it is clear that the gel cannot generate a large blocking force when the cross-link density is too high. This can be understood as follows. In the limit of no cross-links at all, the stiffness of the hydrogel vanishes and the blocking force approaches zero. If, on the other hand, the cross-link density is very high, the stiffness of the hydrogel is very large and the free-swelling ratio approaches one. The hydrogel cannot swell and generates no blocking force. Consequently the blocking force must peak at an intermediate level of cross-linking. This prediction is illustrated in figure 6.9, where the blocking stress derived from equation (6.6) is plotted as a function of NkT. Phase separation [135] in the PNIPAm hydrogels prevented us from confirming this behavior at large cross-

link densities, but it may be possible to access this regime in other hydrogels.

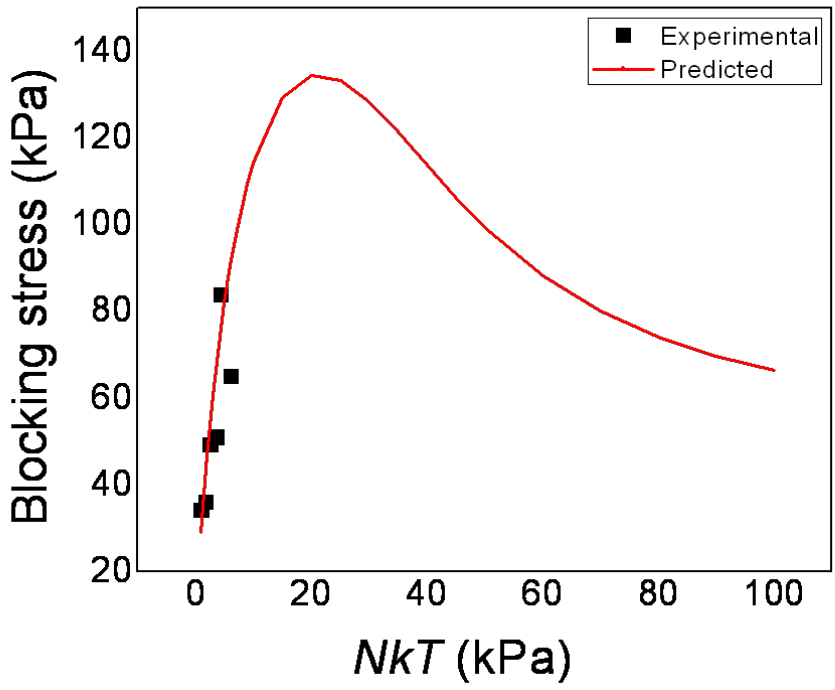

Figure 6.9 Blocking force as a function of cross-link density. The solid curve is a prediction based on the $\Pi_{mix}(J,T)$ relation.

In many applications, a quick and uniform actuator response is required. The speed with which a hydrogel actuator responds to a stimulus is governed by the diffusion of water into or out of the hydrogel and depends sensitively on the size of the actuator. The response time of a micrometer-sized gel particle, for instance, is on the order of 10^{-2}-10^{-4} s, making it a viable actuator for a range of micro-fluidic applications. Even though the experiments presented in this paper were performed on millimeter-size samples, the results and analysis are directly applicable to gels on the micrometer scale.

6.7 Summary

We have used the ideal elastomeric gel model to derive the force-stroke curves of hydrogel actuators. The force-stroke curves depend on the shear modulus and on the osmotic pressure function of the hydrogel. We have described simple methods for measuring the osmotic pressure function and the force stroke curves. Measurement of the osmotic pressure curves for PNIPAm samples with different cross-link densities show that the osmotic pressure function is independent of cross-link density. The experimental force-stroke curves are in very good agreement with the model predictions, demonstrating that the ideal elastomeric gel model provides a very general description of the behavior of a hydrogel for a broad range of loading conditions, chemical environments, and cross-link densities.

Chapter 7

Strong and flexible hydrogels below water freezing temperature

7.1 Introduction

Hydrogels are cross-linked networks of hydrophilic polymer chains dispersed in water. The polymer network enables elasticity making the hydrogels solid-like and the water enables mass transport, making the hydrogels liquid-like. These attributes can make the hydrogels stretchable, flexible, soft and the ability to change volume. However these desirable properties of hydrogels disappear when the environment temperature goes below water freezing temperature. The water inside the polymer network freezes and disables the liquid-like behavior. The polymer network is frozen in place disabling the elastic behavior. Thus at low temperatures, hydrogels become similar to stiff pieces of ice. In this study we develop hydrogels that do not freeze even at -50^{o}C, still maintaining room temperature mechanical properties and partially frozen hydrogels that are still flexible and stretchable.

Hydrogels are traditionally studied for biomedical applications such as scaffolds in tissue engineering [6], carriers for drug delivery [7] and valves in microfluidic devices [9]. Most conventional hydrogels are brittle and weak limiting the scope of above applications [4]. Recently developed tough hydrogels improve the scope of current applications [16, 17, 19]. Among them polyacrylamide-alginate tough hydrogel demonstrate extremely high toughness, stiffness and recoverability [3, 21]. The exceptional mechanical behavior of these hydrogels are comparable to elastomers [136] and they still contain ~90% water. Due to the recent

development in the field of hydrogels, they are studied for non-traditional applications such as stretchable and transparent ionic conductors [137, 138], vibration isolation [139] and as impact energy absorbing materials [23]. These non-traditional applications need hydrogels that can function even at low temperatures.

(a) Polyacrylamide-alginate hydrogel

(b) $CaCl_2$-Polyacrylamide-alginate hydrogel

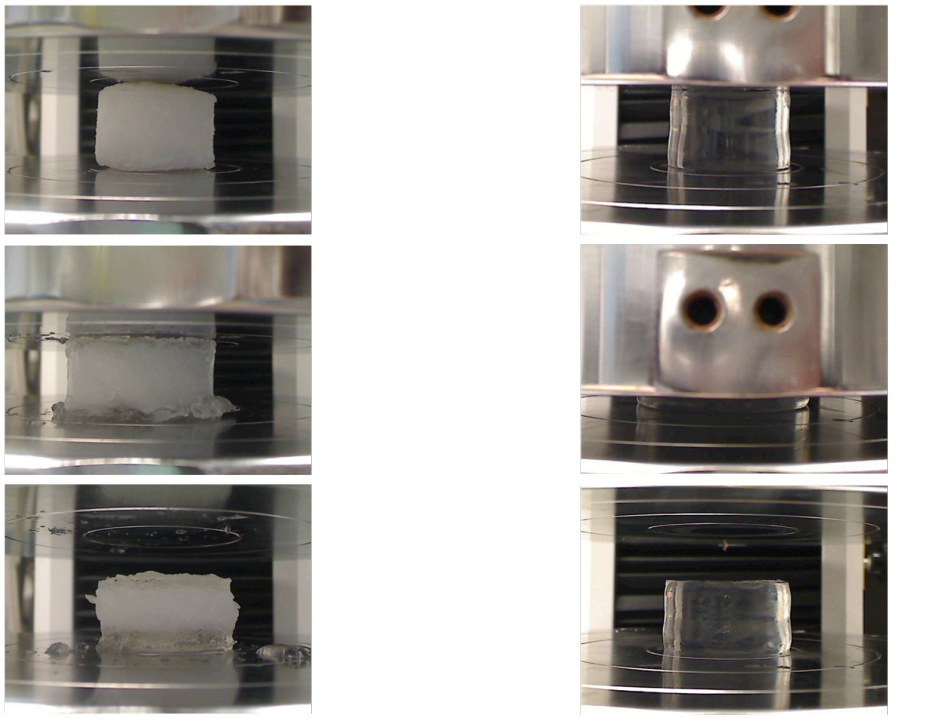

Figure 7.1 Compression tests for hydrogels that were stored in -20°C and tested at room temperature (a) Regular hydrogels become very stiff, very similar to ice and hard to compress. It slips when compressed and part of the hydrogel is broken. It does not recover the original shape. (b) 30wt% $CaCl_2$ hydrogels do not freeze at -20°C and most of the deformation is recoverable during a compression test.

Hydrogels that have good mechanical properties below water freezing temperature

have never been demonstrated before. When a Polyacrylamide-alginate hydrogel is stored at a freezer with a temperature -20°C, it becomes similar to ice and hard to compress (figure 7.1(a)).

In this study we plan to prepare hydrogels that do not freeze solid below 0°C. Freeze point depression, a process that adds a solute to a solvent to decrease freezing point is a widely studied approach. For example salt is added to roads during winter to avoid any ice formation on roads. Antifreeze liquids are mixed with water to be used in radiators that do not freeze in winter. This method is also used by organisms that live in extreme cold weather where they produce antifreeze agents to decrease the freeze point of water inside them [140, 141]. They do not freeze solid even the water freezes outside. When salt is added to pure water the freezing point of water can greatly be reduced. By adding Calcium Chloride we make hydrogels that are partially frozen or that do not freeze below 0°C. Whether the hydrogels fully freeze, partially freeze or non-freeze is determined by the amount of Calcium Chloride we add and the environment temperature, provided that we maintain constant relative humidity. Polyacrylamide-alginate hydrogels that contain 30wt% Calcium Chloride stored at -20°C do not freeze and the deformation is recoverable when compressed (figure 7.1(b)).

This new class of hydrogels can be useful in many applications. Recently developed stretchable and transparent ionic devices are made of hydrogels and dielectric elastomers [137, 138]. These ionic devices would be functionless when water inside the hydrogel freezes. Hydrogels are also studied as soft actuators [25]. Soft robots that are made of hydrogel actuators would benefit if they do not freeze at low temperatures. If the hydrogels can be

made partially frozen we can take advantage of high heat of fusion of water to absorb heat. They can be used in cooling applications that are similar to gel packs used currently. Gel packs are used to keep things cold for extended periods of time. Commonly used gel packs are made with a mixture of water, propylene glycol and hydroxypropyl methylcellulose [142]. They are soft and squishy at room temperature and remain malleable or hard when frozen. These packs can absorb considerable amount of heat before warming above 0^{o}C due to high latent heat of fusion of water. These packs are used to keep food cool in portable coolers, relieving muscle pain, insulating shipping containers to keep products cool during transportation [143-145]. As current gel packs contain the gels in the form of viscous liquid they need many compartments to avoid flowing. A partially frozen tough hydrogel can enhance the performance of gel packs. They will provide more protection when subjected to loading and the toughness can prevent any flowing or moving of the content inside the pack.

In this study we develop partially frozen and non-frozen hydrogels based on the phase diagram of Calcium Chloride-water system. Mechanical properties of these hydrogels are measured in a wide range of temperatures. Based on the phase diagram and heat capacity of Calcium Chloride-water system, we calculate the reduction of heat absorption by adding Calcium Chloride to hydrogels. We also demonstrate a touch sensing ionic device that can function at low temperature.

7.2 Experimental

7.2.1 Hydrogel synthesis

Polyacrylamide-alginate hybrid hydrogels were prepared using the following procedure: Powders of alginate (FMC Biopolymer, LF 20/40) and acrylamide (Sigma, A8887) were

dissolved in deionized water. Ammonium persulfate (AP; Sigma, A9164), 0.0017 the weight of acrylamide, was added as the photo initiator for polyacrylamide. N,N-methylenebisacrylamide (MBAA; Sigma, M7279), 0.0006 the weight of acrylamide, was added as the cross-linker for polyacrylamide. N,N,N',N'-tetramethylethylenediamine (TEMED; Sigma, T7024), 0.0025 the weight of acrylamide, was added as the crosslinking accelerator for polyacrylamide. Calcium sulfate ($CaSO_4 \cdot 2H_2O$; Sigma, 31221), 0.1328 the weight of alginate, was added as the ionic cross-linker for alginate. The solution was poured into a glass mold, 75.0 x 55.0 x 6.0 mm^3, covered with a glass plate. The gel solution was then cured at room temperature by exposing it for eight minutes to ultraviolet light (OAI LS 30 UV flood exposure system, 1.92 W/cm^2 power density). Hydrogel samples were kept at room temperature for one day to ensure complete reaction. Hydrogels were immersed in 10wt% and 30wt% Calcium Chloride ($CaCl_2$, McMaster-Carr., 3190K36) solutions for five days to obtain 10wt% and 30wt% $CaCl_2$-Polyacrylamide-alginate hydrogels.

7.2.2 Compression test

Compression experiments were performed using cylindrical-shaped samples of average dimensions 8mm diameter and 2mm height. Before obtaining the measurements the samples were equilibrated at the particular temperature for 15 minutes. For measurements below 0^oC we attached an aluminum container of ice and salt mixture to keep a constant low temperature during the test. The force-displacement curves were measured at a displacement rate of 50μm/min.

7.2.3 Measuring capacitance

We fabricated a sensor that can detect the pressure of finger touch consisting of a 2cm*2cm*0.5mm dielectric elastomer (VHB 4905, 3M) covered with two 30wt% $CaCl_2$-hydrogel layers of 2cm*2cm*0.2mm dimensions. Top and bottom hydrogels were connected to electrodes, which then connected to a capacitance meter (LCR/ESR meter, Model 885, BK Precision), set to a sinusoidal measurement signal of 1V and 100Hz. The design is similar to reference [138]. The sheet was attached to a glass plate and capacitance was measured with finger touch at 20^{o}C and inside a freezer at -11^{o}C.

7.3 Results and discussion

We have synthesized Polyacrylamide-alginate hydrogels with 0wt%, 10wt% and 30wt% $CaCl_2$ concentrations. Even though the 0wt% sample is not immersed in a $CaCl_2$ solution, it contains a very low concentration (0.3wt%) of $CaSO_4$ in the sample. All the Ca^{2+} are occupied by the G blocks in the sample as shown in figure 7.2(a).

For 10wt% $CaCl_2$-hydrogel sample all the G blocks of the alginate chains are fully saturated with Ca^{2+} [136] and the remaining Ca^{2+} are mixed with water (figure 7.2(b)). For 30wt% $CaCl_2$-hydrogel sample all the G blocks are saturated and excessive Ca^{2+} are mixed with water as shown in figure 7.2(c). Compression stress-strain curves are obtained for these hydrogels as figure 7.2(d). It is observed that 0wt% $CaCl_2$-hydrogel samples show the lowest strength and stiffness due to low crosslink density. 10wt% sample shows high strength and stiffness due to high crosslink density. But when we add more Ca^{2+}, decrease in strength and stiffness is observed in 30wt% sample. This is due to the swelling of the hydrogel when more

$CaCl_2$ is presented.

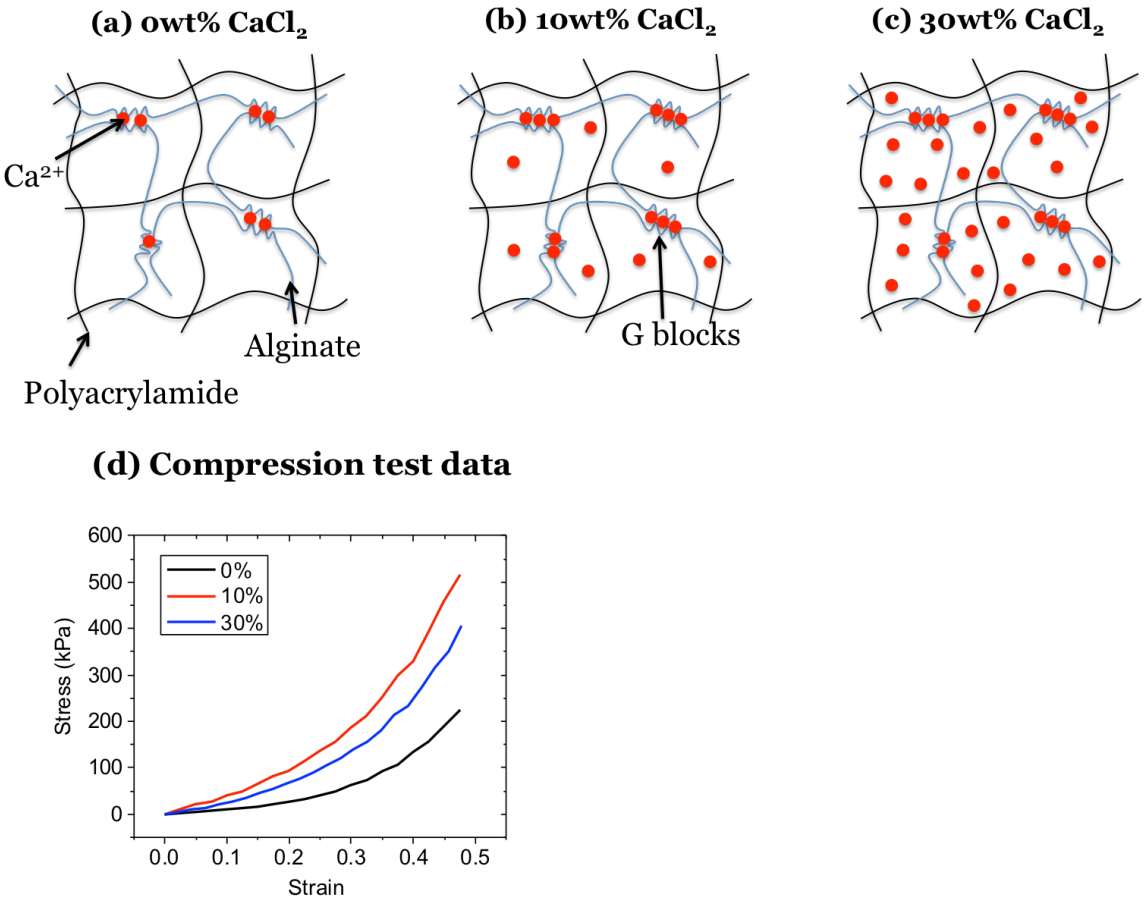

Figure 7.2 Polyacrylamide-alginate hydrogels of different $CaCl_2$ concentrations at 20°C (a) Regular tough hydrogels with 0wt% of $CaCl_2$ added. (b) When 10wt% $CaCl_2$ is added all the G blocks in alginate chains saturate. (c) When 30wt% $CaCl_2$ is added more $CaCl_2$ enter the hydrogel. (d) Compressive stress-strain curves of three hydrogels.

Even though the difference between these hydrogels at room temperature is just the Ca^{2+} concentration, the behavior of the hydrogels becomes completely different when the temperature goes below 0°C. The phase diagram of $CaCl_2$-water system in figure 7.3(a) explains this behavior [146].

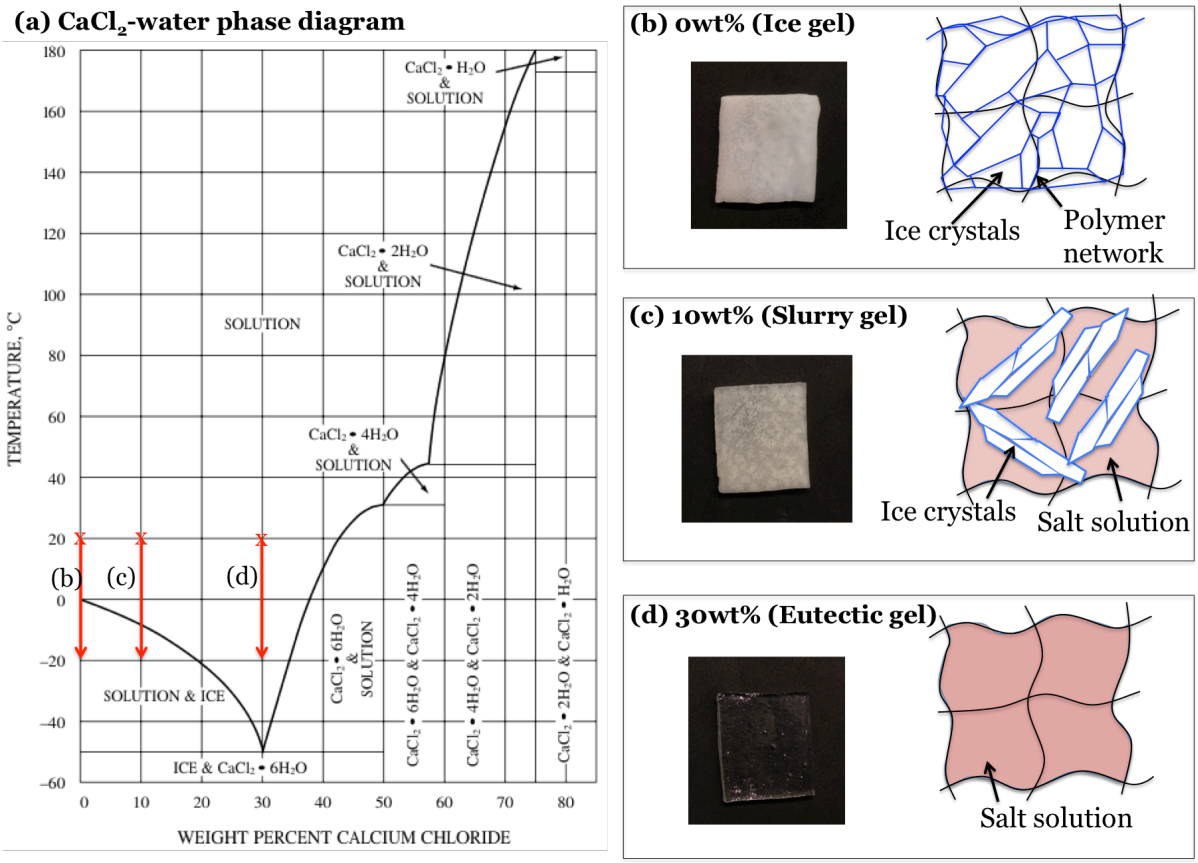

Figure 7.3: Three types of gels below 0°C (a) Phase diagram of $CaCl_2$-water system [22]. Red arrows correspond to three types of gels obtained with 0wt%, 10wt% and 30wt% $CaCl_2$ concentrations when cooled from room temperature. (b) Regular hydrogel freezes at -20°C and becomes a stiff piece of ice. The schematic shows ice crystals formed in the polymer network. (c) A 10wt% $CaCl_2$ gel creates a partially frozen slurry gel. The schematic shows ice and salt solution inside polymer network. (d) When 30wt% $CaCl_2$ is added it does not freeze at -20°C and remains transparent. Schematic of the gel shows salt solution inside polymer network.

When 0wt% $CaCl_2$ is presented it becomes pure water and below 0°C turns to ice. In the phase diagram this is represented as a straight line (b). Similar behavior is observed for 0wt% $CaCl_2$-hydrogels. When the temperature is decreased from 20°C to -20°C, ice crystals

are formed in the polymer network as shown in figure 7.3(b). Ice crystals dominate over the polymer network and the hydrogel becomes a stiff piece of ice. Thus we name this gel as ice gel. For a 10wt% $CaCl_2$ solution when the temperature is decreased from 20°C to -20°C the solution phase changes in to a slurry mixture of solution and ice crystals (line (c) in figure 7.3(a)). Similar behavior is observed for 10wt% $CaCl_2$-hydrogels when decreased from 20°C to -20°C, two phases present: ice crystals and salt solution (figure 7.3(c)) inside the polymer network. As the 10wt% hydrogel contains a slurry mixture, we name the gel as slurry gel. When goes down along line (c) more ice crystals form. It remains flexible but hardens gradually. According to the phase diagram 10wt% slurry gel stays in the flexible slurry phase until the temperature is -50°C. When the temperature of 30wt% $CaCl_2$ solution is decreased from 20°C to -20°C, it does not change the phase and stays in solution phase even until -50°C (line (d) in figure 7.3(a)). Similarly 30wt% $CaCl_2$-hydrogel remains in solution phase when cooled down as in figure 7.3(d). As this concentration corresponds to eutectic concentration, we name the gels as eutectic gels.

We have measured the apparent contact modulus of all three hydrogels for a temperature ranging from -8°C to 20°C. The test set up is shown in figure 7.4(a).

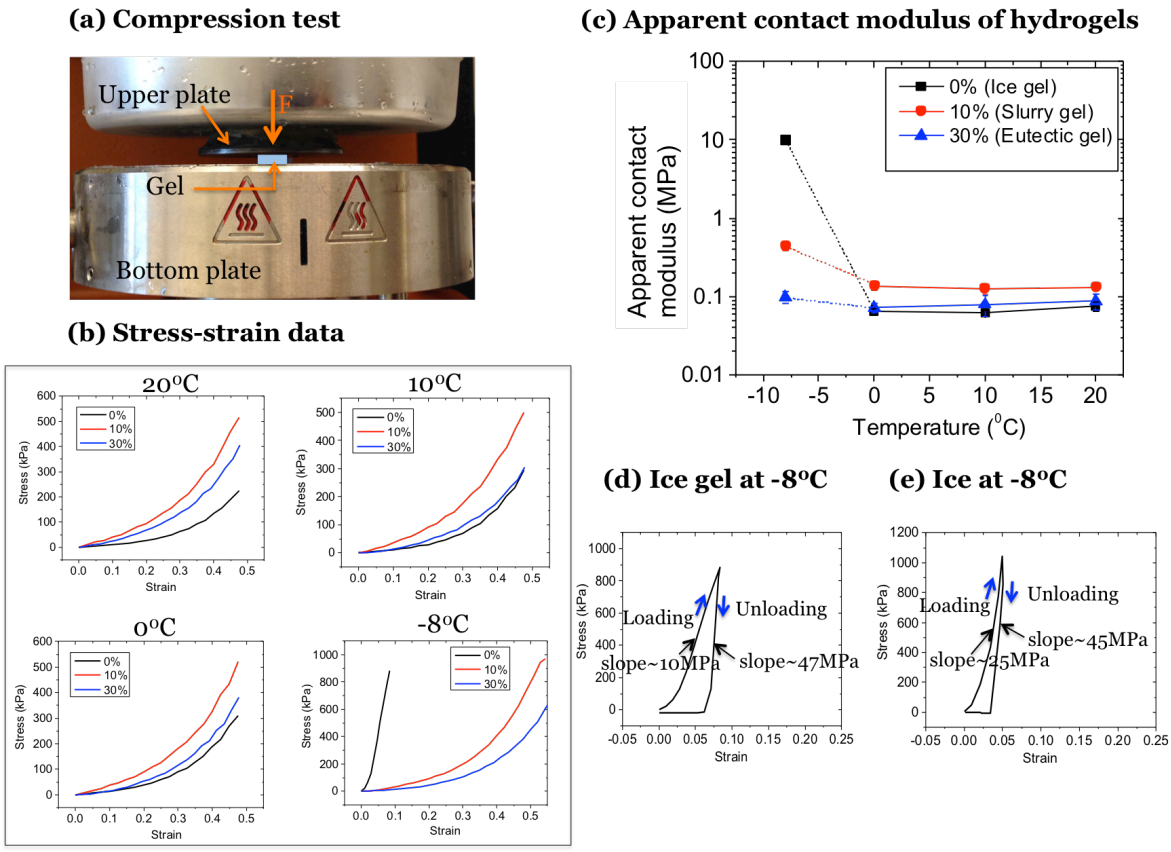

Figure 7.4 Mechanical properties of hydrogels at different temperatures. (a) Photo of the compression test set up. Upper plate is attached to an aluminum container of ice and salt mixture for the tests below 0°C. (b) Stress-strain curves of hydrogels at different temperatures. (c) Apparent contact modulus of hydrogels at different temperatures. Comparison of loading-unloading compression test of (d) ice gel and (e) ice at -8°C.

Compressive force-displacement curves are converted to stress-strain curves as in figure 7.4(b). The nominal stress was obtained by dividing the force by the initial cross-sectional area of the sample. Strain was calculated by dividing the deformation of the sample by its initial height. Figure 7.4(c) shows the apparent contact modulus data with temperature for all three hydrogels. For eutectic gels the apparent contact moduli remain constant through out the entire temperature range. For slurry gels the apparent contact moduli remains

constant from 20°C to 0°C but a slight increase is observed below 0°C due to the ice crystal formation. Due to the slurry behavior it still remains flexible. Apparent contact moduli of ice gel remains constant from 20°C to 0°C but a drastic increase in modulus is observed below 0°C as the hydrogel turns similar to ice. It is reported that modulus of ice at -10°C is ~10GPa [147]. From our experiments the contact modulus of ice gel around -8°C was observed ~10MPa which is much lower than the reported modulus of ice. We expected ice gels to behave similar to ice and this observation is contrary to what we expected. We tested the loading-unloading curves of ice gels to confirm whether this is an effect due to the misalignment of the plates and the sample. The results in figure 7.4(d) shows this is not the case. The slope obtained from loading and unloading is comparable, suggesting this effect is not due to any misalignment. We then measured the stress-strain curves of an ice sample with similar dimensions to ice gels and observed that the mechanical behavior of both ice and ice gel are very similar (figure 7.4(d), (e)). Even for pure ice samples, we do not observe the expected modulus as in literature. We believe the difference is due to increase in temperature during the test. Even though we control the temperature of the upper and lower plates, the test is performed in open air due to lack of equipment available to precisely control the temperature. Thus the temperature of the sample can be very closer to melting temperature and creep behavior can be occurred. Creep behavior is widely studied for ice near melting temperatures [148]. We also performed a stress relaxation test as in figure 7.5 and it is observed the stress is relaxed fast when the load is held constant.

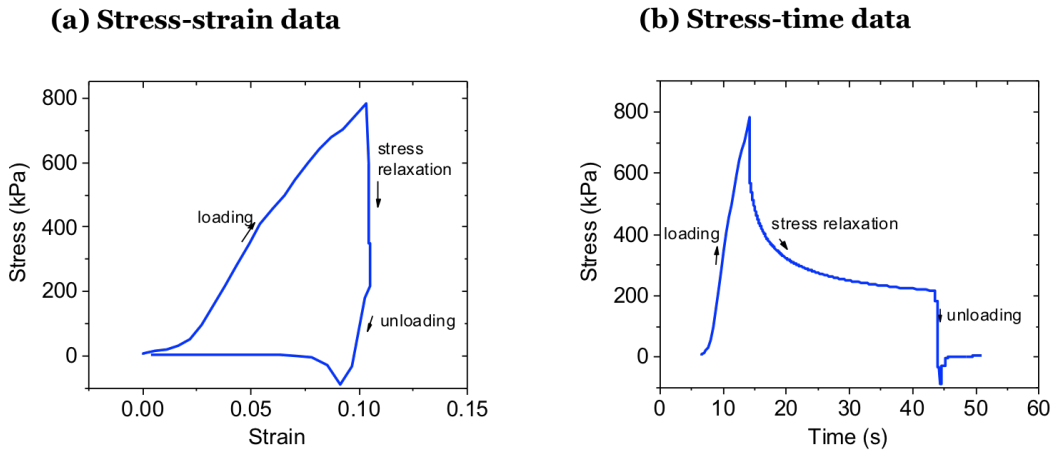

Figure 7.5 Stress relaxation test (a) Stress-strain data. (b) Stress-time data.

These tests suggest that the difference of moduli in the measurements and literature data is due to the creep of ice. Even though we were unable to obtain precise modulus measurement of ice gels, we have showed that ice gels behave similar to ice at low temperatures.

For cooling applications with slurry gels it is important to know the reduction in heat absorption by adding $CaCl_2$ in to the gels. To calculate this we use the thermodynamic properties of $CaCl_2$-water system: the phase diagram (figure 7.6(a)) and specific heat diagram (figure 7.6(b)).

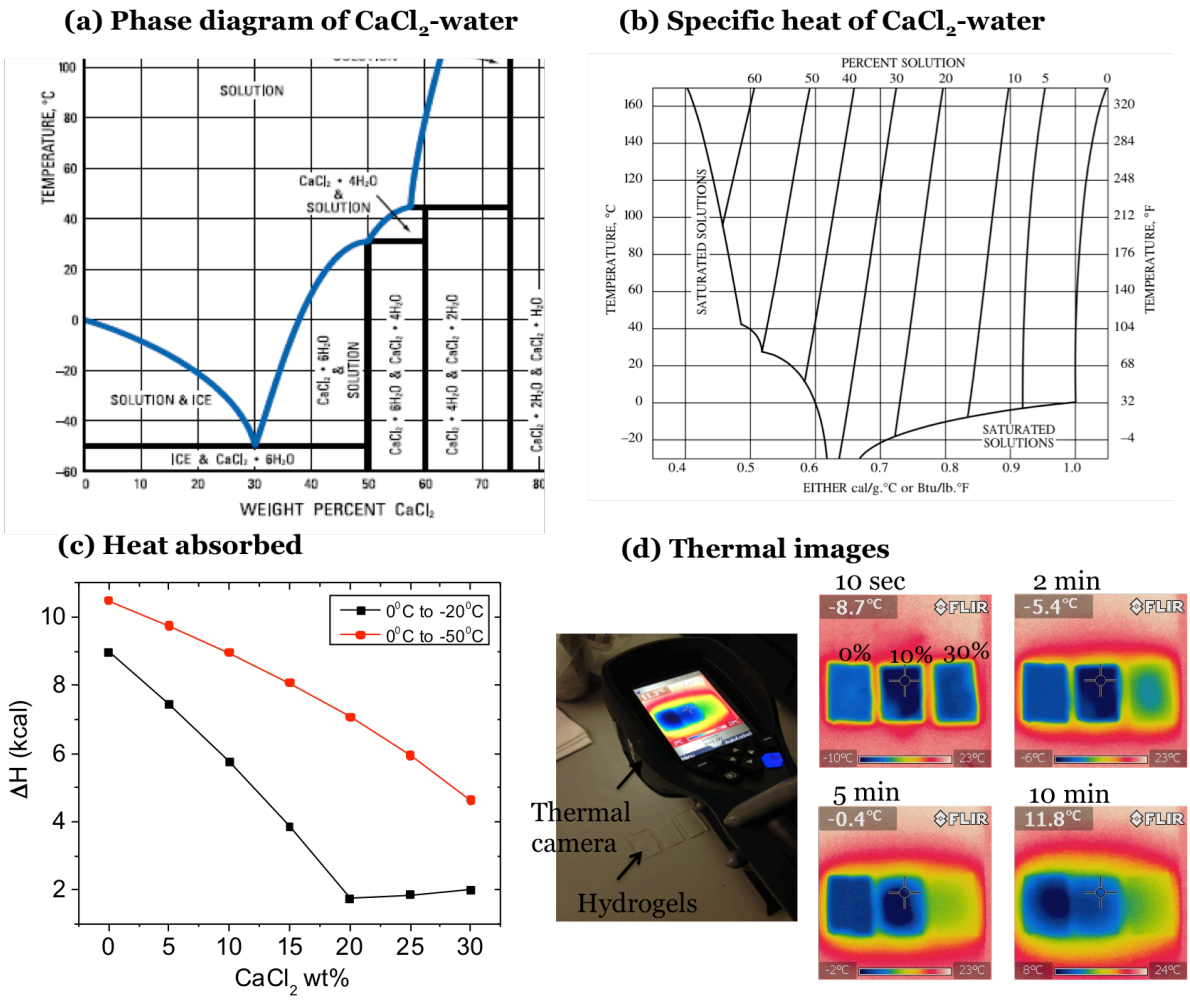

Figure 7.6 Thermodynamic properties of $CaCl_2$-water system (a) Phase diagram [22]. (b) Specific heat of $CaCl_2$-water system [22]. (c) Heat absorbed by 100g of water with different $CaCl_2$ wt% when cooled from 0°C to -20°C and from 0°C to -50°C. (d) Time lapse thermal images of three types of gels immediately after removing from a -11°C freezer.

Heat absorbed by 100g of water with different concentrations of $CaCl_2$ is calculated for two situations: when cooled from 0°C to -20°C and from 0°C to -50°C. This is calculated as follows.

$$\Delta H_{\text{Total}} = \Delta H_{\text{Heat of fusion of ice}} + \Delta H_{\text{ice}} + \Delta H_{\text{salt solution}} \quad (7.1)$$

where ΔH is change in heat and ΔT is change in temperature.

$$\Delta H_{\text{Heat of fusion of ice}} = \text{Heat of fusion of ice } \left(\frac{\text{cal}}{\text{g}}\right) \times \text{Mass of ice (g)} \quad (7.2)$$

$$\Delta H_{\text{ice}} = \text{Mass of ice (g)} \times \text{Heat capacitance of ice } \left(\frac{\text{cal}}{\text{g}^0 C}\right) \times \Delta T(^\circ\text{C}) \quad (7.3)$$

$$\Delta H_{\text{salt solution}} = \text{Mass of salt solution(g)} \times \text{Avg. heat capacitance of salt solution} \left(\frac{\text{cal}}{\text{g}^\circ\text{C}}\right) \times \Delta T(^\circ\text{C}) \quad (7.4)$$

For example let us take a 5wt% $CaCl_2$ solution that contains 100g of water and 5.26g of $CaCl_2$ with a total solution mass of 105.26g. According to the phase diagram a 5wt% solution at -20°C has 20wt% $CaCl_2$ in solution phase. This is obtained by drawing a tie line at -20°C in the phase diagram. Thus at -20°C it contains a 26.32g of $CaCl_2$ solution. This makes the mass of ice in the mixture as 78.94g.

From equation (2), $\Delta H_{\text{Heat of fusion of ice}} = 79.7 \left(\frac{\text{cal}}{\text{g}}\right) \times 78.94 \text{ (g)} = 6.295 \text{ kcal}$

From equation (3), $\Delta H_{\text{ice}} = 78.94 \text{ (g)} \times 0.5 \left(\frac{\text{cal}}{\text{g}^0\text{C}}\right) \times 20^0\text{C} = 0.789 \text{ kcal}$

From equation (4), $\Delta H_{\text{salt solution}} = 26.32 \text{ (g)} \times 0.7 \left(\frac{\text{cal}}{\text{g}^0\text{C}}\right) \times 20^0\text{C} = 0.369 \text{ kcal}$

Thus from equation (1), $\Delta H_{\text{Total}} = 7.453 \text{ kcal}$

According to figure 7.6(c), maximum heat absorption is obtained for 0wt% $CaCl_2$ samples but they limit the performance at low temperature because they freeze solid. When 30wt% $CaCl_2$ is added, the samples do not freeze at all but the heat absorption is much lower and cannot be useful in cooling applications. Samples with $CaCl_2$ concentrations between 0wt% and 30wt% are useful in cooling applications. Figure 7.6(c) provides useful information in developing gel packs for cooling applications. To show that $CaCl_2$-hydrogels behave in a similar manner to $CaCl_2$-water system we also performed infrared thermal images of three types of hydrogels. They were stored in a -11°C freezer and time lapse

thermal images were taken after immediate removal from the freezer. Thermal images show that a 0wt% ice gel remains cold for a longer period. 30wt% eutectic gel heats up rapidly. 10wt% slurry gel keeps colder than 0wt% sample until 0°C but heats faster than 0wt% ice gel above 0°C.

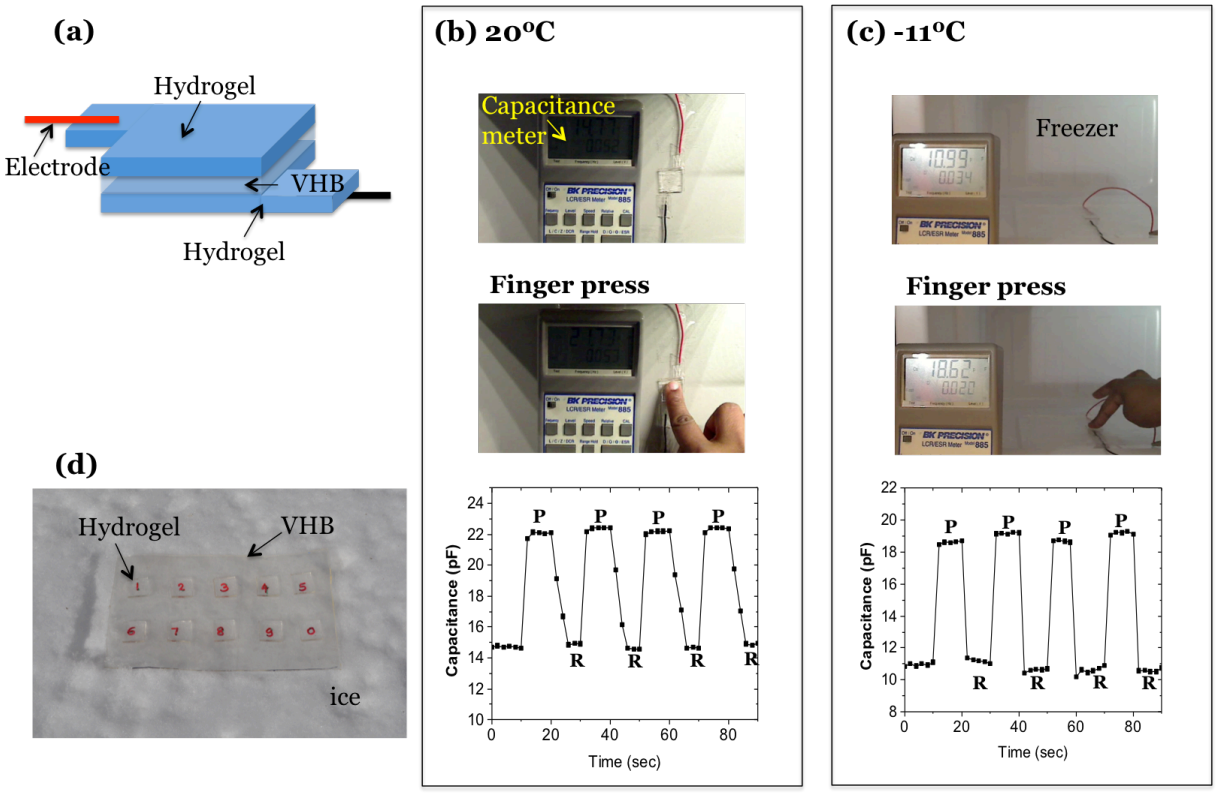

Figure 7.7 Ionic skin sensor at different temperatures (a) A pressure sensor was fabricated by sandwiching a layer of dielectric (VHB) between two layers of 30wt% $CaCl_2$ hydrogel, which were connected to two electrodes. (b) Capacitance was measured at 20°C with a finger press. 'P' denotes finger press and 'R' denotes release. (c) Capacitance was measured inside a freezer at -11°C with a finger press. (d) Hydrogel keypad on a VHB substrate was placed on ice as a demonstration of a touch sensor at low temperature.

Non-freezing hydrogels are useful in flexible ionic conductors below water freezing temperature. We have fabricated a touch sensor as in figure 7.7(a) with a simple architecture

of hydrogel-elastomer-hydrogel layers. This set up is based on reference [138] except we do not need to put additional elastomer layers on top and bottom because our hydrogels are strong and tough. Eutectic hydrogels are used for the design, as they do not freeze even at -50°C. This set up measures the capacitance with a finger touch both at 20°C (figure 7.7(b)) and at -11°C (figure 7.7(c)). This test shows the potential of eutectic hydrogel based ionic devices that can work as sensors in very low temperature environments (figure 7.7(d)).

Our results suggest that slurry gels and eutectic gels are useful in applications that require strong and flexible hydrogels below water freezing temperature. Slurry gels can overcome some of the problems associated with current gel packs. Current gel packs contain viscous liquid like gel and in order to avoid flowing, many gel packs contain number of compartments. Partially frozen strong hydrogels do not need any compartments and the flexibility allows easy wrap around. Not only can they be used to relieve muscle pain, they can also be used in keeping food or drinks cold for a long time and be useful in transporting medicine or food that need to be kept cold. There are some incidents reported with broken and leaked gel packs that have mixed with food and have become poisonous [149]. With strong gel packs any leaking problem can be avoided. Gel packs are also used in military applications such as cooling helmets and gel vests for soldiers in extreme hot weather [150]. Strength and toughness of the gels are important in rough use in military applications. Because slurry gels contain mostly water and salt, they can be made with very low cost and can also be useful as cooling jackets for workers near furnaces, gel hats or jackets to be used in extreme hot weather. Eutectic gels can be used as pressure sensors at low temperatures to sense pressure of a finger touch such as touch screen keypad or a pressure sensor that a

person can step on it. Eutectic gels might also be useful in soft robotic applications at low temperatures.

These hydrogels can absorb water from the environment when the relative humidity is high and can lose water when the relative humidity is low. Thus for applications we might need to keep them sealed. By selecting different salts, we can broaden or shorten the range of the phase. For example instead of $CaCl_2$ if we select LiCl, corresponding to a 25wt% LiCl the hydrogels can go down to -75°C without any freezing [151]. LiCl might not be suitable for Polyacrylamide-alginate hydrogels because Li^+ can exchange Ca^{2+} and reduce the toughness. But with suitable hydrogels, we can prepare non-freezing hydrogels that are strong and flexible even at environments of -75°C.

7.4 Summary

We have demonstrated hydrogels that are partially frozen and hydrogels that do not freeze below water freezing temperature. By adding suitable amount of salt we can determine the phase of hydrogels at a given temperature using the phase diagram of salt-water system. These hydrogels are strong and flexible at low temperatures compared to regular hydrogels that freeze solid. These new class of hydrogels can be used in range of applications including cooling gel packs, ionic devices and soft robotics at low temperatures.

Chapter 8

Conclusions

8.1 Summary and concluding remarks

Hard and dry materials are used for structural applications and the use of soft and wet hydrogels for structural applications might not sound feasible. But the emerging field of soft materials suggests that we can make them tough, strong and non-freezing. This thesis has explored a novel hydrogel with exceptional mechanical properties and their non-traditional structural applications.

The major accomplishments and findings of the thesis are summarized as follows.

- We developed an extremely stretchable and tough hydrogel with polymers containing ionic and covalent crosslinks. The extremely high fracture energy is attributed to the synergy of crack bridging by the polyacrylamide network and energy dissipation by unzipping the network of ionic crosslinks of alginate network over a large region of the hydrogel. Polyacrylamide network preserves the memory of the initial state, so that the large deformation is reversible when the load is removed. The unzipped ionic crosslinks cause internal damage, which heals as ionic crosslinks reform.
- We re-examined the validity of “pure shear test method” for measuring the fracture energy of extremely stretchable materials. Pure shear test method is traditionally used when the sample width and crack length are much larger than the sample length. With both experimental and finite element method we showed that pure shear test method can be used to measure fracture energy of extremely stretchable materials.

- Even though polyacrylamide-alginate hydrogel has exceptional toughness, the stiffness and strength are modest. We improved the stiffness and strength by embedding stiff fibers. Brittle hydrogels such as alginate cannot be improved by embedding fibers, instead they fail by fibers cutting through the matrix. Toughness of polyacrylamide-alginate hydrogel resists fibers cutting through the matrix and it dissipates a significant amount of energy by fibers sliding through the matrix.
- We developed inexpensive fire-retarding materials using hydrogels that provide superior protection from burn injuries. When hydrogel is exposed to a fire a significant amount of heat is carried away due to water evaporation. The temperature of hydrogel rises rapidly to 100^{o}C due to high thermal conductivity of water but it cannot exceed this temperature until the hydrogel is fully dehydrated. By combining hydrogels and fabrics of low thermal conductivity into laminates, we designed fire-retarding materials that can protect people from burn injuries.
- We characterized the force-stroke curves of hydrogel actuators using ideal elastomeric gel model and with experiments. Hydrogels that undergo a volume phase transition in response to an external stimulus can be used as actuator materials in small-scale devices. Because of the poor mechanical behavior, conventional hydrogels have limited use as actuators. Tough active hydrogels that can generate large blocking forces without sacrificing stroke would be ideal materials for soft actuators.
- Hydrogels are consisted of mostly water and they freeze when the temperature drops below 0^{o}C. All the above-mentioned applications would be functionless at low temperature. We demonstrated a new class of hydrogels that do not freeze and

hydrogels that partially freeze below water freezing temperature. Partially frozen hydrogels are ideal for cooling applications such as gel packs and non-freezing hydrogels are useful in ionic devices, soft robotics and any structural applications of hydrogels at low temperatures.

8.2 Outlook for future work

Hydrogels with enhanced mechanical properties have the potential to open up many novel applications. They can be considered as tough water and exhibit many of the amazing properties of water. Following are some applications of interest.

- A class of devices using stretchable, transparent ionic conductors have developed capable of operating at frequencies beyond 10 kHz and voltages beyond 10 kV [137]. The emergence of the field of stretchable electronics, along with its biomedical applications has highlighted the mismatch between electronic devices made of hard materials compared to tissues and cells that are soft. Stretchable conductors are needed to enable electronics to meet skin, heart and brain. Many ionic conductors, such as hydrogels take a solid form and are highly stretchable and transparent and are ideal as stretchable conductors. Keplinger et al developed transparent, large strain actuator and a transparent loudspeaker [137]. Potential applications of ionic devices include neuromuscular and neurosensory systems for soft robots, biomedical devices, and tunable optical devices. In these applications, the ionic conductors will likely be subjected to large deformations, as well as fast and cyclic loading. Hydrogels with high stretchability, toughness and fatigue resistance are critical to these

applications.

- In oil industry, equipment manufacturers have traditionally striven to develop elastomers that swell very little when exposed to oil or water. However, with the introduction of non-cemented completion system to make oil or gas wells ready for production, came the necessity of open-hole packers. These systems use a variety of packers for sealing purposes, providing an opportunity for novel swellable packers. Hydrogels can be used as packer materials that swell in the presence of water or water-based fluids. Their increasing volume can seal a well and thus prevent the outflow of fluids from the ground [12]. The extreme conditions that the packers are exposed to during operation- conditions of high pressure and temperature- impose stringent requirements on the mechanical performance of the hydrogels.

Bibliography

[1] M. A. Zwieniecki, P. J. Melcher and N. M. Holbrook, Science, 2001, 291, 1059–1062

[2] V. C. Mow, S. C. Kuei, W. M. Lai and C. G. Armstrong, J. Biomech. Eng., Biphase creep and stress relaxation of articular cartilage in compression: theory and experiments, 1980, 102, 73–84

[3] X. Zhao, Multi-scale multi-mechanism design of tough hydrogels: building dissipation into stretchy networks, Soft Matter, 10, 2014, 672-687

[4] P. Calvert, Hydrogels for soft machines, Adv. Mater. 21, 2009, 43-756

[5] C. Maldonado-Codina, C. & N. Efron, Impact of manufacturing technology and material composition on the mechanical properties of hydrogel contact lenses. Ophthal Physl Opt 24, 2004, 551-561

[6] K.Y. Lee, K. Y. & D.J. Mooney, Hydrogels for tissue engineering, Chem Rev 101, 2001, 1869-1879

[7] R. Langer, Drug delivery and targeting. Nature 392, 1998, 5-10

[8] D. Seliktar, Designing cell-compatible hydrogels for biomedical applications, Science, 336, 2012, 1124–1128

[9] D.J. Beebe, J.S. Moore, J.M. Bauer, Q. Yu, R.H. Liu, C. Devadoss & B. Jo, Functional hydrogel structures for autonomous flow control inside microfluidic channels. Nature 404, 2000, 588-590

[10] L. Dong, A. K. Agarwal, D. J. Beebe and H. Jiang, Adaptive liquid micro lenses activated by stimuli-responsive hydrogels, Nature 442, 2006, 551–554

[11] T. Murosaki, T. Noguchi, K. Hashimoto, A. Kakugo, T. Kurokawa, J. Saito, Y. M. Chen, H. Furukawa and J. P. Gong, Antifouling properties of tough gels against barnacles in a long-term marine environment experiment, Biofouling, 25, 2009, 657–666

[12] S. Cai, Y. Lou, P. Ganguly, A. Robisson and Z. Suo, Force generated by a swelling elastomer subject to constraint, J. Appl. Phys., 107, 2010, 103535

[13] K. Draget, G. Phillips & P.Williams, Alginates. Handbook of hydrocolloids, 2009, 807-828

[14] S.A.Dubrovskii, M.V.Afanaseva, M.A.Lagutina & K.S.Kazanskii, Comprehensive Characterization of Superabsorbent Polymer Hydrogels, Polym Bull 24, 1990, 107-113

[15] J.P. Gong, Why are double network hydrogels so tough, Soft Matter, 6, 2012, 2583-2590

[16] J.P.Gong, Y.Katsuyama, T.Kurokawa & Y.Osada, Double-network hydrogels with extremely high mechanical strength, Adv Mater 15, 2003, 1155-1158

[17] K.Haraguchi & T.Takehisa, Nanocomposite hydrogels: A unique organic-inorganic network structure with extraordinary mechanical, optical, and swelling/de-swelling properties. Adv Mater 14, 2002, 1120-1124

[18] T.Huang, H.Xu, K.Jiao, L.Zhu, H.R.Brown & H.Wang, A novel hydrogel with high mechanical strength: A macromolecular microsphere composite hydrogel. Adv Mater 19, 2007, 1622-1626

[19] K.J.Henderson, T.C.Zhou, K.J.Otim & K.R.Shull, Ionically Cross-Linked Triblock Copolymer Hydrogels with High Strength. Macromolecules 43, 2010, 6193-6201

[20] S.Abdurrahmanoglu, M.Cilingir & O.Okay, Dodecyl methacrylate as a crosslinker in the preparation of tough polyacrylamide hydrogels, Polymer 52, 2011, 694-699

[21] J.-Y. Sun, X.H.Zhao, W.R.K.Illeperuma, O.Chaudhuri, K.H.Oh, D.J.Mooney, J.J.Vlassak, Z.Suo, Highly stretchable and tough hydrogels, Nature, 489, 2012, 133-136

[22] R.S. Rivlin, A.G. Thomas, J. Polym. Sci., 1953, 10, 291-313

[23] W.R.K.Illeperuma, J.-Y.Sun, Z.Suo, J.J.Vlassak, Fiber-reinforced tough hydrogels, Extreme Mechanics Letters 1, 2014, 90-96

[24] W.R.K.Illeperuma, Z.Suo, J.J.Vlassak, Tough, fire retarding hydrogels and hydrogel-fabric laminates, Patent application filed 7/7/2014

[25] W.R.K. Illeperuma, J.-Y. Sun, Z. Suo, J.J. Vlassak. Force and stroke of a hydrogel actuator. Soft Matter 9, 8504-8511 (2013)

[26] Y. Okumura, & K. Ito, The polyrotaxane gel: a topological gel by figure-of-eight cross-links, Adv. Mater. 13, 2001, 485-487

[27] K.Haraguchi, K. & T.Takehisa, Nanocomposite hydrogels: a unique organic-inorganic network structure with extraordinary mechanical, optical and swelling/de-swelling properties, Adv. Mater. 14, 2002, 1120-1124

[28] G.J.Lake, & A.G.Thomas, The strength of highly elastic materials, Proc. R. Soc. A 300, 1967, 108-119

[29] N.K.Simha, C.S.Carlson & J.L.Lewis, Evaluation of fracture toughness of cartilage by micropenetration. J. Mater. Sci. Mater. Med. 14, 2003, 631-639

[30] G.J.Lake, Fatigue and fracture of elastomers, Rubber Chem. Tech. 68, 1995, 435-460

[31] T.Sakai, T.Matsunaga, Y.Yamamoto, C.Ito, R.Yoshida, S.Suzuki, N.Sasaki, M.Shibayama and U.Chung, Design and Fabrication of a High-Strength Hydrogel with Ideally Homogeneous Network Structure from Tetrahedron-like Macromonomers. Macromolecules 41,2008, 5379-5384

[32] M.E.Seitz, D.Martina, T.Baumberger, V.R.Krishnan, C.-Y.Hui & K.R.Shull, Fracture and large strain behavior of self-assembled triblock copolymer gels, Soft Matter 5, 2009, 447-456

[33] W.-C. Lin, W.Fan, A.Marcellan, D.Hourdet and C.Creton, Large Strain and Fracture Properties of Poly(dimethylacrylamide)/Silica hybrid hydrogels, Macromolecules 43, 2010, 2554-2563

[34] Q.G.Wang, J.L.Mynar, M.Yoshida, E.J.Lee, M.S.Lee, K.Okuro, K.Kinbara & T.Aida, High-water-content mouldable hydrogels by mixing clay and a dendritic molecular binder. Nature 464, 2010, 339-343

[35] M.A.Haque, T.Kurokawa, G.Kamita & J.P.Gong, Lamellar bilayers as reversible sacrificial bonds to toghen hydrogel: hysteresis, self-recovery, fatigue resistance, and crack blunting, Macromolecules 44, 2011, 8916-8924

[36] D.C.Tuncaboylu, M.Sari, W.Oppermann, O.Okay, Tough and self-healing hydrogels formed via hydrophobic interactions, Macromolecules 44, 2011, 4997-5005

[37] C.-Y.Hui, A.Jagota, S.J.Bennison & J.D.Londono, Crack blunting and the strength of soft elastic solids, Proc. R. Soc. Lond A 459, 2003, 1489-1516

[38] Q.M.Yu, Y.Tanaka, H.Furukawa, T.Kurokawa & J.P.Gong, Direct observation of damage zone around crack tips in double-network gels, Macromolecules 42, 2009,3852-3855

[39] R.E.Webber, C.Creton, H.R.Brown & J.P.Gong, Large strain hysteresis and mullins effect of tough double-network hydrogels, Macromolecules 40, 2007, 2919-2927

[40] K.J.Henderson, T.C.Zhou, K.J.Otim & K.R.Shull, Ionically cross-linked triblock copolymer hydrogels with high strength, Micromolecules 43, 2010, 6193-6201

[41] H.J.Kong, E.Wong & D.J.Mooney, Independent control of rigidity and toughness of polymeric hydrogels, Macromolecules 36, 2003, 4582-4588

[42] T.Baumberger and O.Ronsin, From thermally activated to viscosity controlled fracture of biopolymer hydrogels. J. Chem. Phys. 130, 2009, 061102

[43] A.G.Evans, Perspective on the development of high-toughness ceramics. J. Am. Ceram. Soc. 73, 1990, 187-206

[44] H.R.Brown, A model of fracture of double network gels. Macromolecules 40, 2007, 3815-3818

[45] Y.Tanaka, A local damage model for anomalous high toughness of double-network gels. EPL 78, 2007, 56005

[46] A.P.Jackson, Measurement of the fracture toughness of some contact lens hydrogels. Biomater. 11, 1990, 403-407

[47] R.M.Hernandez, G.Orive, A.Murua, J.L.Pedraz, Microcapsules and microcarriers for in situ cell delivery, Adv. Drug Deliv. Rev. 62, 2010, 711-730

[48] T. Baumberger, C. Caroli, D. Martina, Nature materials, 5, 2006, 552-555

[49] Y. Tanaka, R. Kuwabara, Y. Na, T. Kurokawa, J. P. Gong, Y. Osada, J. Phys. Chem. B,

2005,109, 11559-11562

[50] Y. Tanaka, K. Fukao, Y. Miyamoto,Eur. J. Phys., 2000, E 3, 395-401

[51] S. Kundu, A. J. Crosby, Soft Matter, 2009, 5, 3963-3968

[52] V. R. Krishnan, C.Y. Hui, R. Long, Langmuir, 2008, 24, 14245-14253

[53] B.P. Pereira, P.W. Lucas, T. Swee-Hin, J.Biomechanics, 1997, 30, 91-94.

[54] K. R. Agrawal, P. W. Lucas, Proc. R. Soc. Lond. B, 2003, 270, 1277–1282.

[55] R.F.Ker, The design of soft collagenous load-bearing tissues, J. Exp. Biol., 1999, 202, 3315-3324

[56] C.-D.Young, J.-R.Wu, T.-L.Tsou, High-strength, ultra-thin and fiber-reinforced pHEMA artificial skin, Biomaterials, 19, 1998, 1745-1752

[57] F.T.Moutos, L.E.Freed, F.Guilak, A biomimetic three-dimensional woven composite scaffold for functional tissue engineering of cartilage, Nature materials, 6, 2007, 162-167

[58] A.Agrawal, N.Rahbar, P.D.Calvert, Strong fiber-reinforced hydrogel, Acta Biomateriala, 9, 2013, 5313-5318

[59] I-C. Liao, F.T. Moutos , B.T. Estes , X. Zhao and F. Guilak, Composite three-dimensional woven scaffolds with interpenetrating network hydrogels to create functional synthetic articular cartilage, Adv. Funct. Mater., 2013, 23, 5833-5839

[60] S.Lin, C.Cao, Q.Wang, M.Gonzalez, J.E. Dolbow, X.Zhao, Design of stiff, tough and stretchy hydrogel composites via nanoscale hybrid crosslinking and macroscale fiber

reinforcement, Soft Matter, 2014, 10, 7519-7527

[61] S.N.Bakarich, R.Gorkin III, M. Panhuis, G.M.Spinks, Three-dimensional printing fiber reinforced hydrogel composites, 2014, 6, 15998-16006

[62] C.Gamonpilas, M.N.Charalambides, J.G.Williams, Determination of large deformation and fracture behavior of starch gels from conventional and wire cutting experiments, J.MaterSci, 44, 2009, 4976-4986

[63] F.Baldi, F.Bibnotti, I.Peroni, S.Agnelli, T.Ricco, On the measurement of the fracture resistance of polyacrylamide hydrogels by wire cutting test, Polymer testing, 31, 2012, 455-465

[64] A.Bentur and R.Cree, Cement reinforced with steel wool, Int. J. Cem. Comp. & L Concr., 9, 1987, 217-223

[65] L.Li, D.D.L.Chung, Electrical and mechanical properties of electrically conductive polyethersulfone composites, Composites, 35, 1992, 215-223

[66] N.J.Mills & A.Gilchrist , The Effectiveness of Foams in Bicycle and Motorcycle Helmets, Accid. Anal. and Preview, 23, 1991, 153-163

[67] http://www.grantadesign.com/resources/materials/casestudies/helmet.htm

[68] S.Chaudhury, C.Holland, M.S.Thompson, F.Vollrath, A.J.Carr, Tensile and shear mechanical properties of rotator cuff repair patches, J. Shoulder Elbow Surg., 2012, 21, 1168-1176

[69] B.P.Timko et al., Electrical recording from hearts with flexible nanowire device arrays.

Nano Lett., 9, 2009, 914–918

[70] J.Viventi et al., Flexible, foldable, actively multiplexed, high-density electrode array for mapping brain activity in vivo. Nature Neurosci., 14, 2011, 1599–1605

[71] D-H.Kim et al., Epidermal electronics. Science, 333, 2011, 838–843

[72] N.Lu, C.Lu, S.Yang, J.Rogers, Highly sensitive skin-mountable strain gauges based entirely on elastomers, Adv. Funct. Mater., 2012, 22, 4044-4050

[73] B.Tian, J.Liu, T.Dvir, L.Jin, J.H.Tsui, Q.Qing, Z.Suo, R.Langer, D.S.Kohane, C.M.Lieber, Macroporous nanowire nanoelectronic scaffolds for synthetic tissues, Nat. Mater.,2012, 11, 986–994

[74] M.F.Ashby, The CES EduPack database of natural and man-made materials, 2008, Cambridge, UK: Granta Design

[75] http://www.ameriburn.org/resources_factsheet.php

[76] H.Zhang, Fire-Safe Polymers and Polymer Composites, Federal Aviation Administration technical report; U.S. Department of Transportation: Washington, D.C., 2004

[77] R.D.Peacock, P.A.Reneke, R.W.Bukowski, V.Barauskas, Defining flashover for fire hazard calculations, Fire safety journal, 32, 1999, 331-345, P.Grimwood, Flashover–a firefighter's worst nightmare, 2003

[78] A.R.Horrocks, D.Price, eds, Advances in fire retardant materials, Elsevier, 2008

[79] H.Zhang, Fire-safe Polymers and polymer Composites, Ph.D. Dissertation, University of Massachusetts, 2003

[80] A.R.Horrocks, S.Anand, Handbook of technical textiles, CRC Press, 2000

[81]http://www.dupont.com/products-and-services/personal-protective-equipment/thermal protective/brands/nomex.html

[82] T.J.Huang, J.H.William, M.R.Chapmen, Fire retardant and heat resistant yarns and fabrics made therefrom, U.S. Patent 6, 287, 686B1, 2001

[83] www.chapmaninnovations.com, http://www.chicagoprotective.com/pdf/CarbonX.pdf

[84] J.Krasny, J.A.Rockett, D.Huang, Protecting fire fighters exposed in room fires: Comparison of results of bench scale test for thermal protection and conditions during room flashover, Fire Technology, 1988, 24.1, 5-19

[85] S.Lee, C.Park, D.Kulkarni, S.Tamanna, T.Knox, Heat and mass transfer in a permeable fabric system under hot air jet impingement, Proceedings of the international heat transfer conference, IHTC14, 2010, 1-10

[86] T.M.Tuzcu, Hygro-Thermal Properties of Sheep Wool Insulation, Thesis, Civil Engineering Faculty, Delft University of Technology

[87] W.Toreki, Degradable or reversible fire-blocking gel, U.S. Patent 2007/0001156 A1

[88] R.D.Hicks, J.E.Mills, W.-N.Hsu, A.Agne, Water additive and method for fire prevention and fire extinguishing, U.S. Patent 6, 245, 252 B1, 2001

[89] R.N.Bashaw, Freeport, Harper B.G., Jackson L., Method for controlling the spread of fire, U.S.Patent 3, 229, 769, 1966

[90] W.Steve, The Secret Science Behind Movie Stunts & Special Effects, Saddleback Educational Publ, 2008., http://www.zeller-int.com/categories/fireret/zeljel.htm

[91] W.M.Bridgeman, Fire-resistant blanket, U.S. Patent 6, 102, 128, 2000

[92] J.W.Romaine, Fire blanket, U.S. Patent 4, 624, 320, 1986

[93] W.P.Behnke, Thermal protective performance test for clothing, Fire Technol, 1977, 1,6–12

[94] A.Handermann, Oxidized Polyacrylonitile fiber properties, products and applications, Zoltekcorporation (http://www.zoltek.com/white-paper-oxidized-polyacrylonitrile-fiber-properties-products-and-applications/)

[95] J. Crank, Free and Moving Boundary Problems (2nd ed) Oxford University Press, New York, 1975

[96] Z.F. Jin, Y. Asako, Y. Yamaguchi Y and M.Harada, Fire resistance test for fire protection materials with high water content, Int J Heat Mass Transfer, 43, 2000, 4395–4404

[97] Y.Asako, T.Otaka, Y.Yamaguchi, Fire Resistance Characteristics of Materials with Polymer Gels Which Absorb Aqueous Solution of Calcium Chloride, Numer. Heat Transfer, Part A , 45, 2004, 49–66

[98] W.M.Irvine and J.B.Pollack, Infrared optical properties of water and ice spheres, Icarus 8.1, 1968, 324-360

[99] W.P.Behnke, Predicting flash fire protection of clothing from laboratory tests using second-degree burn to rate performance, Fire and Materials, 1984, 8:2, 57-63

[100] http://www2.dupont.com/Energy_Solutions/en_US/assets/downloads/418_419.pdf

[101] A.M.Stoll and M.A.Chianta, Method and rating system for evaluation of thermal protection, Aerospace Med., 1969, 40, 1232-1238

[102]Y.Hirokawa, T.Tanaka, Volume phase transition in a non ionic gel, J.Chem.Phys. 81(12), Pt. II, 1984, 6379-6380.

[103] H.Shirota, N.Endo, K.Horie, Volume phase transition of polymer gel in water and

heavy water, Chemical Physics, 238, 1998, 487-494.

[104] S.Cai, Z.Suo, Mechanics and chemical thermodynamics of phase transition in temperature –sensitive hydrogels, J.Mech.Phys.Solids, 59, 2011, 2259-2278.

[105] L.B.Peppas, N.A.Peppas, Equilibrium swelling behavior of pH-sensitive hydrogels, Chemical Engineering Science, 46, 1991, 715-722.

[106] L.Zarzar, P.Kim, J.Aizenberg, Bio-inspired design of submerged hydrogel-actuated polymer microstructures operating in response to pH, Adv. Mater., 23, 2011, 1442-1446.

[107] T.Tanaka, I.Nishio, S.T.Sun, S.U.Nishio, Collapse of gels in an electric field, Science, 218, 1982, 467-469.

[108] M.Guenther, D.Kuckling, C.Corten, G.Gerlach, J.Sorber, G.Suchaneck, K.-F.Arndt, Chemical sensors based on multiresponsive block copolymer hydrogels, Sensors and actuators B 126, 2007, 97-106.

[109] R.Bashir, J.Z.Hilt, O.Elibol, A.Gupta, N.A.Peppas, Micromechanical cantilever as an ultrasensitive pH microsensor, Appl.Phys.Lett., 81, 2002, 3091-3093.

[110] M.E.Harmon, M.Tang, C.W.Frank, A microfluidic actuator based on thermoresponsive hydrogels, Polymer, 44, 2003, 4547- 4556.

[111] D.J.Beebe, J.S.Moore, J.M.Bauer, Q.Yu, R.H.Liu, C.Devadoss, B.-H. Jo, Functional hydrogel structures for autonomous flow control inside microfluidic channels, Nature 404, 2000, 588-590.

[112] A.Richter, S.Howitz, D.Kuckling, K.-F. Arndt, Influence of volume phase transition phenomena on the behavior of hydrogel- based valves, Sensors and actuators B 99, 2004, 451-458.

[113] R.Langer, Drug delivery and targeting, Nature 392, 1998, 5-10.

[114] R.Dinarvand, A.D' Emanuele, The use of thermoresponsive hydrogels for on-off release of molecules, Journal of controlled release, 36, 1995, 221-227.

[115] G.M.Spinks, L.Liu, G.G.Wallace, D.Zhou, Strain response from Polypyrrole actuators under load, Adv. Funct. Mater, 12, 2002, 437-440.

[116] R.Kornbluh, R.Pelrine, J.Eckerle, J.Joseph, Electrostrictive polymer artificial muscle actuators, In Proc. IEEE Intl. Conf. Rob. Autom.Leuven, Belgium, 1998, 2147-2154.

[117] F.F.C.Duval, S.A.Wilson, G.Ensell, N.M.P.Evanno, M.G.Cain, R.W.Whatmore, Characterization of PZT thin film micro-actuators using a silicone micro-force sensor, Sensors and actuators A 133, 2006, 35-44.

[118] R.Shankar, T.K.Ghosh, R.J.Spontak, Dielectric elastomers as next generators polymeric actuators, Soft Matter, 3, 2007, 1116-1129.

[119] A.Suzuki, S.Kojima, Phase transition in constrained polymer gels, J.Chem.Phys., 11, 1994, 10003-10007.

[120]H.G.Schild,Poly(N-isopropylacrylamide): Experiment, theory and applications, Prog.Polym.Sci., 17, 1992, 163-249.

[121] C.Wu, X.Wang, Globule-to-coil transition of a single homopolymer chain in solution, Physical Review Letters, 80, 1998, 4092-4094.

[122] S.Cai, Z.Suo, Equations of state for ideal elastomeric gels, EPL, 2012, 34009p1-p6.

[123] J.Li, Y.Hu, J.J.Vlassak, Z.Suo, Experimental determination of equations of state for ideal elastomeric gels, Soft matter, 8, 2012, 8121-8128.

[124] P.J.Flory, J.Rehner, Statistical mechanics of cross-linked polymer networks II.

Swelling, Journal of Chemical Physics, 11(11), 1943, 521-526.

[125] P.J.Flory, Thermodynamics of high polymer solutions, Journal of chemical physics, 10(1), 1942, 51-61.

[126] M.L.Huggins, Solutions of long chain compounds, Journal of chemical physics, 9(5), 1941, 440.

[127]S.Hirotsu,Y.Hirokawa,T.Tanaka,Volume-phase transitions of ionized N isopropylacrylamide gels, J.Chem.Phys. 87(2), 1987, 1392-1395.

[128] W.Hong, X.Zhao, J.Zhou, Z.Suo, A theory of coupled diffusion and large deformation in polymeric gels, J.Mech.Phys.Solids, 56, 2008, 1779-1793.

[129] F.Horkay, I.Tasaki, P.Basser, Effect of monovalent-divalent cation exchange on the swelling of polyacrylate hydrogels in physiological salt solutions, Biomacromolecules, 2, 2001, 195-199.

[130] B.G.Stubbe et al, Tailoring the swelling pressure of degrading Dextran Hydroxyethyl Methacrylate hydrogels, Biomacromolecules, 4, 2003, 691-695.

[131] V.A.Parsegian, R.P.Rand, N.L.Fuller, D.C.Rau, Osmotic stress for the direct measurement of intermolecular forces, Methods in Enzymology, 127, 1986, 400-416.

[132] M.Trunec, Osmotic drying of gelcast bodies in liquid desiccant, Journal of European Ceramic Society, 31, 2011, 2519-2524.

[133] H.Senff, W.Richtering, Influence of crosslink density on rheological properties of temperature sensitive microgel suspensions, Colloid PolymSci, 278, 2000, 830-840.

[134] K.S.Oh, J.S.Oh, H.S.Choi, Y.C.Bae, Effect of crosslinking density on swelling behavior of NIPA gel particles, Macromolecules, 31, 1998, 7328-7335.

[135] C.Sayil, O.Okay, Macroporouspoly(N-isopropyl)acrylamide networks: formation conditions, Polymer, 42, 2001, 7639-7652

[136] Jianyu Li, W.R.K. Illeperuma, Zhigang Suo, Joost, J. Vlassak. Hybrid hydrogels with extremely high stiffness and toughness. ACS Macro Letters 3, 520-523 (2014)

[137] Keplinger, C., Sun, J. Y., Foo, C. C., Rothemund, P., Whitesides, G. M. & Suo, Z. G.Stretchable, Transparent, Ionic Conductors. Science 341, 984-987 (2013)

[138] J. Y. Sun, C. Keplinger, G. M. Whitesides & Z. Suo. Ionic skin. Adv. Mater. **26**, 7608-7614 (2014)

[139] Yang, C. H., Wang, M. X., Haider, H., Yang, J. H., Sun, J. Y., Chen, Y. M., Zhou, J. X. & Suo, Z. G.Strengthening alginate/polyacrylamide hydrogels using various multivalent cations. ACS Applied Materials & Interfaces (2013)

[140] Block, W., 1991. To Freeze or Not to Freeze? Invertebrate Survival of Sub-Zero Temperatures. Functional Ecology, Vol. 5, No. 2, 284-290

[141] Duman, J. G., Wu, D. W., Xu, L., Tursman, D., Olsen, T. M., 1991. Adaptations of Insects to Subzero Temperatures. The Quarterly Review of Biology, vol. 66, no. 4.

[142] W.K.Dunshee, R.W.H.Chang, Instant hot or cold, reusable cold pack, U.S.Patent 4,462,224, 1984

[143] S.A.Lowe, Freezable insert cooler, U.S.Patent 5,570,588, 1996

[144] C.Swenson, L.Sward, J.Karlsson, Cryotherapy in sports medicine, Scand.J.Med.Sci.Sports, 6, 193-200, 1996

[145] J.W.Becker, T.Toro, Insulated container for packaging perishable goods, U.S.Patent

5,820,268,1998

[146] http://www.prog-univers.com/IMG/pdf/CalciumChloridHandbook.pdf,

[147] M.Shazly, V.Prakash, B.A.Lerch, High strain-rate behavior of ice under uniaxial compression, International Journal of Solids and Structures, 46, 1499-1515, 2009

[148] J.W.Glen, The creep of polycrystalline ice, Proceedings of the Royal Society of London. Series A, Mathematical and Physical Sciences, 228, 519-538, 1955

[149]http://www.foodsafetynews.com/2012/01/lunch-box-gel-packs-could-leak/#.VNqA_HbiRLE

[150] http://www.gelcool.com/military_page.html

[151]http://www.mrc-eng.com/Downloads/Aqueous%20LiCl&CaCl2%20Solution%20Props.pdf